

The contribution of the sodium channel subunit $\text{Na}_v1.6$ to neuronal excitability

Dissertation

zur

Erlangung des Doktorgrades (Dr.rer.nat.)

der

Mathematisch-Naturwissenschaftlichen Fakultät

der

Rheinischen-Friedrich-Wilhelms-Universität Bonn

vorgelegt von

Michael Winfried Royeck

aus

Püttlingen

Bonn 2009

Angefertigt mit Genehmigung der
Mathematisch-Naturwissenschaftlichen Fakultät
der Rheinischen Friedrich-Wilhelms-Universität Bonn.
Diese Dissertation ist auf dem Hochschulschriftenserver der ULB
Bonn unter http://hss.ulb.uni-bonn.de/diss_online
elektronisch publiziert.

Erscheinungsjahr: 2010

Erstgutachter: Prof. Dr. Heinz Beck

Zweitgutachter: Prof. Dr. Horst Bleckmann

Tag der Promotion: 23. Februar 2010

There are known knowns. There are things we know that we know. There are known unknowns. That is to say, there are things that we now know we don't know. But there are also unknown unknowns. There are things we do not know we don't know.

Donald Rumsfeld, Former US Defense Secretary on February 12, 2002

Acknowledgements

Ich möchte mich bei Prof. Dr. Heinz Beck bedanken, für die ausgezeichnete Unterstützung, seinen Einsatz und die Möglichkeit in seinem spannenden Labor zu promovieren.

Ich möchte mich bei Prof. Dr. Horst Bleckmann bedanken, dass er meine Promotion naturwissenschaftlich betreut hat.

Ich möchte mich bei Prof. Dr. Susanne Schoch-McGovern bedanken, für ihre Unterstützung, ihren Einsatz und die Zusage als Prüferin zu fungieren.

Ich möchte mich bei Prof. Dr. Walter Witke bedanken, für die Zusage als Prüfer zu fungieren.

Ich möchte mich bei allen jetzigen und ehemaligen Kollegen des Nervenzentrums, insbesondere den Mitgliedern der Arbeitsgruppen Beck, Schoch und Becker, dafür bedanken, dass Ihr die Zeit meiner Promotion zu dem gemacht habt was sie war und mir auf vielseitige Weise geholfen habt.

Zusätzlich möchte ich mich bedanken bei Dr. Julika Pitsch, Marie-Therese Horstmann, Elena Alvarez-Baron Fuentes, Dr. Thoralf Opitz, Roland Krüppel, Boris Chagnaud und Tobias Mittelstaedt für die Korrekturen, Ratschläge und Hilfen während der Promotion.

Zuletzt möchte ich mich bedanken, bei meinen Eltern, meiner Familie, meinen Freunden und Trixy. Ihr habt mich immer unterstützt.

Table of Contents

Acknowledgements	IV
Table of Contents	V
Index of Figures	VIII
Index of Tables	X
Abbreviations	XI
Abstract	XIII
1. Introduction	1
1.1 Action potentials and intrinsic membrane properties.....	1
1.2 Voltage gated Na ⁺ channels	1
1.3 Subcellular distribution of Na ⁺ channel subunits	4
1.4 Types of Na ⁺ currents.....	4
1.5 Initiation of action potentials	6
1.6 Hippocampus	8
1.7 The CA1 pyramidal neuron.....	10
1.8 Mesial temporal lobe epilepsy	12
1.9 Aim of the study.....	13
2. Materials and methods	14
2.1 Experimental animals	14
2.1.1 Functionally Na _v 1.6 deficient mice – the <i>Scn8a</i> ^{med} mutation	14
2.1.2 The pilocarpine model of temporal lobe epilepsy	14
2.2 Preparation of brain tissue.....	15
2.2.1 Preparation of brain tissue from mice and rats for electrophysiological experiments.....	15
2.2.2 Preparation of rat brain tissue and subfield microslices for biochemical analysis	15
2.3 Immunohistochemistry.....	16
2.3.1 Analysis of immunohistochemistry.....	16
2.4 Quantitative real-time RT-PCR.....	17
2.4.1 Preparation of cDNA and probes	17
2.4.2 Analysis of mRNA expression	18
2.5 Western blotting of Na ⁺ channels.....	18
2.5.1 Sample preparation	18
2.5.2 SDS gel electrophoresis and immuno-blotting	18

2.6	Electrophysiology and computational Modelling	19
2.6.1	Shared procedures	19
2.6.2	Voltage clamp recordings	19
2.6.3	Determination of passive membrane properties.....	20
2.6.4	Recording of the transient Na ⁺ current.....	20
2.6.5	Recording of the persistent Na ⁺ current.....	20
2.6.6	Analysis of voltage clamp recordings of Na ⁺ currents	21
2.6.7	Recording of T-type Ca ²⁺ currents	21
2.6.8	Analysis of voltage clamp recordings of T-type Ca ²⁺ currents	21
2.6.9	Current clamp recordings	22
2.6.10	Analysis of current clamp recordings	22
2.7	Cell-attached recordings of discharge behaviour	23
2.8	Computational modelling of a CA1 pyramidal cell.....	23
2.9	Statistical analysis and software	23
3.	Results	24
3.1	Subcellular distribution of Na ⁺ channels in the CA1 region of the hippocampus	24
3.2	Absence of Na _v 1.6 positively shifts I _{NaT} activation.....	26
3.3	Absence of Na _v 1.6 reduces the persistent Na ⁺ current I _{NaP}	28
3.4	Lack of compensatory changes in I _{CaT}	30
3.5	Reduced spontaneous firing in the absence of functional Na _v 1.6 subunits	30
3.6	Na _v 1.6 subunits contribute to setting spike threshold in CA1 pyramidal cells ...	32
3.7	Spike afterdepolarization in CA1 pyramidal cells lacking Na _v 1.6	34
3.8	Na _v 1.6 subunits contribute to spike gain.....	35
3.9	Na _v 1.6 subunits contributes to action potential initiation	36
3.10	Computer simulations of spike initiation at the AIS	39
3.11	Na ⁺ channel mRNA expression following status epilepticus.....	45
3.12	Na ⁺ channel protein expression following status epilepticus	46
3.13	Axonal localization of Na ⁺ channels and Na _v 1.6 following status epilepticus ...	47
3.14	Changes in Na ⁺ currents of CA1 pyramidal neurons following status epilepticus	49
3.15	Discharge behavior of CA1 pyramidal neurons following status epilepticus	51
4.	Discussion	54
4.1	Neuronal expression and subcellular localization of Na _v 1.6.....	54
4.2	The role of axonal Na _v 1.6 channels in action potential initiation	54
4.3	The contribution of Na ⁺ currents to spike gain	57
4.4	The contribution of Na ⁺ currents to the spike afterdepolarization	58
4.5	Compensatory or homeostatic changes in mice lacking functional Na _v 1.6 channels.....	59
4.6	Na ⁺ channels in chronic epilepsy	59

4.7	Modulation of persistent Na ⁺ currents by intracellular spermine.....	61
4.8	Changes in intrinsic firing properties in chronic epilepsy.....	61
5.	References.....	63
6.	Contributions.....	78
7.	Curriculum vitae.....	79
8.	Erklärung.....	80

Index of Figures

<i>Figure 1-1: General structure of voltage gated Na⁺ channel α-subunits.</i>	2
<i>Figure 1-2: The transient, persistent, and resurgent Na⁺ current.</i>	5
<i>Figure 1-3: Morphology of the hippocampal formation.</i>	9
<i>Figure 1-4: Morphology of the CA1 pyramidal neuron.</i>	11
<i>Figure 3-1: Axon initial segment localization of Na⁺ channels in central neurons of Scn8a^{med} and Scn8a^{wt} mice.</i>	25
<i>Figure 3-2: Semi-quantitative analysis of fluorescence intensity of PanNa_v relative to Ankyrin G in slices obtained from Scn8a^{med} and Scn8a^{wt} mice.</i>	26
<i>Figure 3-3: Voltage dependence of activation of I_{NaT} in CA1 pyramidal neurons is shifted in the depolarizing direction in Scn8a^{med} mice.</i>	28
<i>Figure 3-4: Reduction of the persistent Na⁺ current (I_{NaP}) in Scn8a^{wt} and Scn8a^{med} CA1 pyramidal neurons.</i>	29
<i>Figure 3-5: T-type Ca²⁺ (I_{CaT}) current amplitude is unaltered in CA1 pyramidal cells of Scn8a^{med} mice.</i>	30
<i>Figure 3-6: Discharge behavior of Scn8a^{wt} and Scn8a^{med} neurons recorded in cell-attached configuration.</i>	31
<i>Figure 3-7: Spike threshold of CA1 pyramidal neurons recorded in the slice preparation is increased in Scn8a^{med} mice.</i>	33
<i>Figure 3-8: The spike afterdepolarization in Scn8a^{med} and Scn8a^{wt} mice.</i>	34
<i>Figure 3-9: The gain of CA1 neurons is decreased in the absence of Na_v1.6 channels</i>	36
<i>Figure 3-10: Spike initiation in Scn8a^{wt} and Scn8a^{med} mice.</i>	37
<i>Figure 3-11: Altered delay between axonal and somatic components and steepness of spike initiation in Scn8a^{med} and Scn8a^{wt} mice.</i>	38
<i>Figure 3-12: Transient Na⁺ current (i_{NaT}) and its voltage dependence of activation of in the CA1 neuron model.</i>	39
<i>Figure 3-13: Spike parameters of modelled action potentials.</i>	40
<i>Figure 3-14: Influence of transient AIS Na⁺ current density and voltage dependence on spike initiation.</i>	41
<i>Figure 3-15: Influence of transient AIS Na⁺ current density and voltage dependence on spike initiation with a 60% reduction of persistent Na⁺ current.</i>	43
<i>Figure 3-16: Influence of transient AIS Na⁺ current density and voltage dependence on spike initiation with a 60% reduction of persistent Na⁺ current only at the AIS.</i>	44
<i>Figure 3-17: Na⁺ channel α-subunit mRNA expression in the CA1 region after status epilepticus</i>	46
<i>Figure 3-18: Na⁺ channel content in CA1 microslices after experienced status epilepticus.</i>	47
<i>Figure 3-19: Unchanged axonal aggregation of Na⁺ channel α-subunits in the hippocampus proper following status epilepticus.</i>	48
<i>Figure 3-20: Axonal aggregation of Na_v1.6 in the hippocampus proper following status epilepticus.</i>	49
<i>Figure 3-21: Increase in the persistent Na⁺ current 12-20 d after status epilepticus.</i>	50

<i>Figure 3-22: Discharge behavior of intact CA1 pyramidal neurons recorded in the slice preparation in whole-cell configuration in pilocarpine treated rats.</i>	<i>51</i>
<i>Figure 3-23: The spike afterdepolarization is increased in whole-cell recordings of CA1 pyramidal neurons in epileptic rats.</i>	<i>52</i>

Index of Tables

<i>Table 1: Overview of Na⁺ channel α-subunit classification and distribution [modified after Catterall et al.2005].</i>	3
<i>Table 2: RNA probes used in TaqmanTM experiments [modified after Ellerkmann et al., 2003].</i>	17

Abbreviations

ACSF	artificial cerebrospinal fluid
ADP	spike afterdepolarization
AIS	axon initial segment
Ank G	Ankyrin G
BFNIS	Benign Familial Neonatal-Infantile Seizures
CA1	Cornu Ammonis region one
cf	commissural fibre
dNTP	deoxyribonucleosidetriphosphate
DG	dentate gyrus
DRG	dorsal root ganglion
f.p.	forward primer
GEFS+	Generalized Epilepsy with Febrile Seizures plus
HEK293	human embryonic kidney cell line 293
h.p.	hybridization probe
I_{NaP}	persistent Na^+ current
IC	intracellular solution
I_{CaT}	T-type Ca^{2+} current
I_{NaR}	resurgent Na^+ current
I_{NaT}	transient Na^+ current
med	muscle endplate disease
mf	mossy fibre
mRNA	messenger ribonucleic acid
n.s.	not significant
LINE	long interspersed nuclear element
ODC	ornithine decarboxylase
PBS	phosphate buffered saline
PCR	polymerase chain reaction
PP	perforant path
r.p.	reverse primer
SAM-DC	S-adenosylmethionine decarboxylase
SC	Schaffer collaterals
$Scn8a^{med}$	homozygous mutant from the strain C3HeB/FeJ- $Scn8a^{med/J}$
$Scn8a^{wt}$	homozygous wild-type from the strain C3HeB/FeJ- $Scn8a^{med/J}$
SDS	Sodium Dodecyl Sulfate
SMEI	Severe Myoclonic Epilepsy of Infancy

SS	spermine synthase
SSAT	spermidine/spermine N1-acetyltransferase
SUB	subiculum
SYP	synaptophysin
t_{del}	temporal delay in spike initiation
TRIS	tris(hydroxymethyl)aminomethane
Triton/TX-100	4-octylphenol polyethoxylate
TTX	tetrodotoxin

Abstract

The focus of this work was to elucidate the contribution of a single Na⁺ channel α -subunit, namely Na_v1.6, to the discharge properties of CA1 pyramidal neurons. In the first part of this work, we show that Na_v1.6 is strongly aggregated at the axon initial segment. Interestingly, in the absence of Na_v1.6 overall Na⁺ channel density at the axon initial segment remains unchanged, indicating compensation. We find that Na_v1.6 displays a hyperpolarized voltage dependence of activation and contributes to persistent and resurgent Na⁺ currents. As a consequence, loss of Na_v1.6 increases action potential threshold and affects spike initiation at the axon initial segment. Furthermore, the absence of Na_v1.6 significantly reduces spike gain and spontaneous action potential firing. Utilizing a computational model we characterize the interplay between Na⁺ channel density and voltage dependence at the axon initial segment in shaping initiation and threshold of action potentials.

In the second part, we concentrated on the role of Na_v1.6 during status epilepticus induced epileptogenesis in rats. We show that in epileptic CA1 pyramidal neurons the spike afterdepolarization is augmented due to an upregulation of the persistent Na⁺ current. Utilizing mRNA expression analysis, Western blotting, and immunohistochemistry we demonstrate that the increased excitability is not mediated by upregulation of Na⁺ channel α -subunits, including Na_v1.6. Furthermore, our immunolabellings show that Na_v1.6 and total Na⁺ channel density at axon initial segments are unchanged. In additional experiments, we find that the increased persistent Na⁺ current in CA1 pyramidal neurons from pilocarpine treated rats is sensitive to high concentrations of the intracellular polyamine spermine. Therefore, we suggest that the generation of a *de novo* portion of persistent Na⁺ current, which contributes to the augmented excitability in epilepsy, is mediated by altered polyamine modulation instead of increased Na⁺ channel expression.

1. Introduction

1.1 Action potentials and intrinsic membrane properties

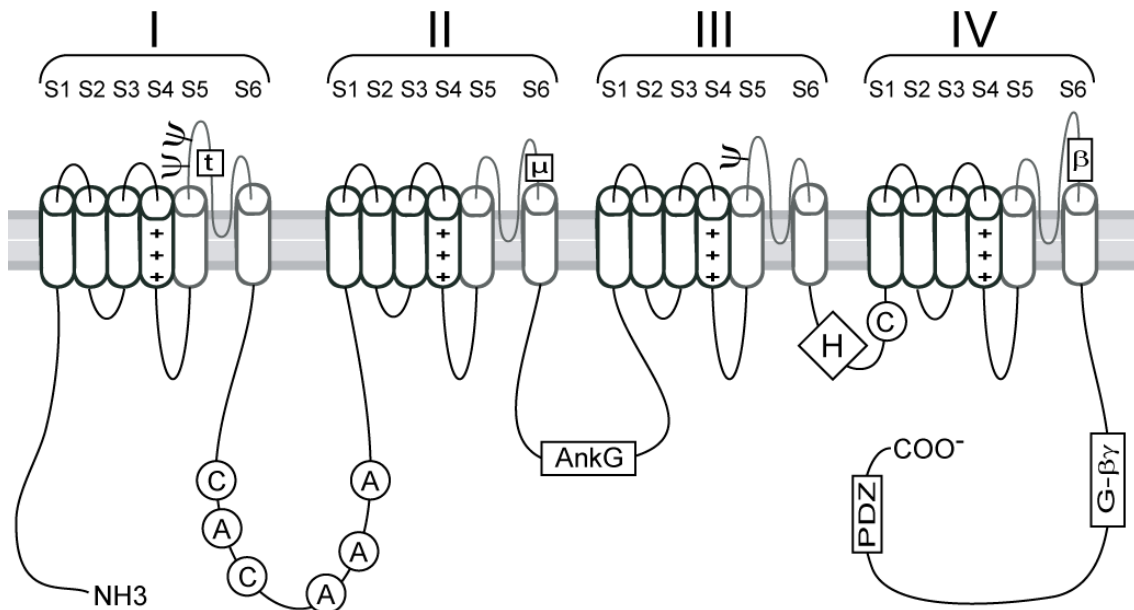
Neurons in the central nervous system integrate excitatory and inhibitory synaptic potentials into an output of action potentials. These rapid discharges propagate along the axon where they trigger transmitter release at synaptic boutons. The number, pattern, and timing of action potentials are important determinants of the synaptic output and therefore crucial for information encoded by the neuron within its network. The shape of action potentials is characterized by a fast overshooting spike that can differ significantly in shape and origin between different neuronal cell types [*for review see* Bean, 2007]. The overshooting spike is followed by hyper- or depolarizing afterpotentials. In some cases the depolarizing afterpotential itself is sufficient to reach action potential threshold thereby generating a burst discharge.

Both, the input/output relation of a neuron and the waveform of an action potential depend on the intrinsic properties of the neuron. These are determined by the neuron's endowment with voltage- and ion-gated ion channels, as well as the geometry of the neuronal processes. The branching pattern of neuronal processes remains rather stable following the neuron's maturation. In contrast, the distribution and expression level of ion channels varies significantly throughout life, and is thought to be actively controlled. It is known that neurons alter their ion channel expression depending on the history of synaptic input and previous activity, both in physiological [Zhang & Linden, 2003] and in pathophysiological contexts [Beck & Yaari, 2008]. Such regulation of ion channels is called intrinsic plasticity [Zhang & Linden, 2003], which is complementary to synaptic plasticity such as long term potentiation [Bliss & Lomo, 1973, Malenka & Bear, 2004]. In some cases the expression of long term potentiation is accompanied by specific changes in membrane excitability [Xu et al. , 2005, Brown & Randall, 2009]. Whereas the homeostatic mechanisms and molecular basis of synaptic plasticity are fairly well understood, the knowledge of the mechanisms underlying plasticity affecting intrinsic properties is far more limited.

1.2 Voltage gated Na⁺ channels

Voltage gated Na⁺ channels are proteins that upon depolarization permit the influx of Na⁺ ions into the cell and are responsible for the rapid upstroke of action potentials [Hille, 2001]. They are integral membrane proteins that are predominantly expressed in excitable cells such as muscle cells and neurons. Expression of voltage gated Na⁺ channels was also reported in other cell types such as glial cells [Chiu et al. , 1984] and endothelial cells [Gordienko & Tsukahara, 1994]. Voltage gated Na⁺ channels consist of one α -subunit that can be associated with accessory β -subunits. The α -subunit contains the Na⁺ selective pore, the voltage sensor, and the channels activation and inactivation gate. It has been shown that α -subunits alone are sufficient to give rise to a voltage sensitive Na⁺ current when expressed in various expression systems [Catterall, 2000].

The general structure of a functional voltage gated Na⁺ channel α -subunit is depicted in *figure 1-1*. It contains four homologous domains (I-IV), each of them consisting of six transmembrane α -helices (S1-S6). Within each domain the S4 segment forms a part of the Na⁺ channel's voltage sensor [Terlau & Stühmer, 1998], which consists of a repeating motif of a positively charged amino acid followed by two hydrophobic residues [Catterall, 1986, Guy & Seetharamulu, 1986]. This α -helical



transmembrane structure undergoes a conformational change upon depolarization that mediates the voltage dependent opening of the Na^+ permeable pore.

Figure 1-1: General structure of voltage gated Na^+ channel α -subunits.

Each α -subunit consists of four domains (I-IV) that contain six transmembrane segments (S1-S6). S4 segments contain the voltage sensor, S5 and S6 including their linker domain (dark grey) form the Na^+ selective pore. The inactivation gate (H) resides in the linker domain III-IV. Proposed sites for N-glycosylation are marked by (Ψ). Phosphorylation sites for PKC (C) and PKA (A) are shown as circles. Boxes illustrate the locations of bindings sites of TTX (t) and μ -conotoxin (μ), as well as interaction domains with other proteins namely the accessory Na^+ channel β -subunits (β), G-protein $\beta\gamma$ -subunits (G- $\beta\gamma$) and the PDZ domain (PDZ) at the c-terminus. The site of the binding motif for the cytoskeletal protein Ankyrin G (Ank G) present in $\text{Na}_v1.1$, $\text{Na}_v1.2$, $\text{Na}_v1.3$, and $\text{Na}_v1.6$ is also shown [modified after Yu & Catterall, 2003, Diss *et al.*, 2004].

The inner part of the ion channel pore is formed by the transmembrane α -helices S5 and S6. The linker region between these two segments reaches into the outer leaflet of the membrane's lipid bilayer and forms the outer part of the ion channel pore. The intracellular loop between domain III and IV serves as an inactivation gate that blocks the open channel upon prolonged depolarization [Stühmer *et al.*, 1989, Catterall *et al.*, 2005]. Within the linker regions between the Na^+ channel segments are sites for protein modification through glycosylation or phosphorylation, as well as the binding sites for the toxins tetrodotoxin (TTX) or μ -conotoxin. Interactions with other proteins also take place within these linker domains. Such interactions are either intracellularly, as the binding to cytoskeleton associated proteins (*see chapter 1.3*), or extracellularly, as binding to Na^+ channel β -subunits.

In native tissue, Na^+ channel α -subunits can be associated with accessory β -subunits. Structurally, β -subunits consist of a single transmembrane domain and larger extracellular than intracellular domains. In total, five β -subunits ($\beta1-4$ and $\beta1a$) have been described so far; all of them are expressed in the mammalian brain. It has been shown that $\beta1$ -subunit expression increases the surface density of $\text{Na}_v1.2$ α -subunits four-fold [Isom *et al.*, 1995]. Association of β -subunits modulates Na^+ channel kinetics and voltage dependence of activation and inactivation [Isom, 2001, Isom, 2002, Qu *et al.*, 2001]. A more specialized function was reported for the $\beta4$ -subunit that serves as a secondary inactivation gate [Yu *et al.*, 2003, Grieco *et al.*, 2005]. However,

knowledge about the extent of α -subunits functioning alone or in conjunction with β -subunits in the mammalian brain is still limited.

In mammals there are nine different genes encoding the nine monomeric α -subunits of voltage gated Na^+ channels (*Scn1a* to *Scn11a*), which share about 80% of their sequence. The proteins are named $\text{Na}_v1.1$ to $\text{Na}_v1.9$ [Catterall et al. , 2005]. The numbers in the gene and in the protein name are not necessarily the same (see table 1). For example, the *Scn8a* gene encodes the Na^+ channel α -subunit $\text{Na}_v1.6$. In addition, several proteins resembling Na^+ channels are expressed in several cells. These are termed Na_x and are about 50% homologous in their underlying nucleotide sequence. Whether these Na_x genes give rise to functional voltage gated Na^+ selective ion channels is still unknown [for review see Diss et al., 2004].

Table 1: Overview of Na^+ channel α -subunit classification and distribution [modified after Catterall et al.2005].

protein name	gene name	localization
$\text{Na}_v1.1$	SCN1A	central neurons, cardiac myocytes
$\text{Na}_v1.2$	SCN2A	central neurons
$\text{Na}_v1.3$	SCN3A	central neurons, cardiac myocytes
$\text{Na}_v1.4$	SCN4A	skeletal muscle
$\text{Na}_v1.5$	SCN5A	cardiac myocytes, skeletal muscle, some central neurons
$\text{Na}_v1.6$	SCN8A	central and peripheral neurons
$\text{Na}_v1.7$	SCN9A	DRG neurons, sympathetic neurons, Schwann cells, and neuroendo-
$\text{Na}_v1.8$	SCN10A	small and medium DRG neurons
$\text{Na}_v1.9$	SCN11A	c-type DRG neurons, trigeminal neurons
Na_x	SCN6A, SCN7A	cardiac myocytes, smooth muscle, astrocytes, central and peripheral

mRNAs encoding Na^+ channels are subject to alternative splicing. Alternative splice variants were discovered first for $\text{Na}_v1.2$ and $\text{Na}_v1.3$ [Gustafson et al. , 1993, Sarao et al. , 1991]. These were shown to be developmentally regulated and deviate in their biophysical properties [Auld et al. , 1990] even though they differ only in a single amino acid. Alternative splicing was described for all Na^+ channel α -subunits [for review see Diss et al., 2004], including *Scn8a* [Drews et al. , 2005, Plummer et al. , 1997], and for the $\beta 1$ -subunit [Kazen-Gillespie et al. , 2000, Qin et al. , 2003]. All voltage gated Na^+ channel α -subunits undergo extensive posttranslational modification such as glycosylation and phosphorylation. N-glycosylation takes place at the extracellular loop between S5 and S6 of the domains I, II, and III in a subtype specific manner [Bennett, 2001, Bennett, 2002] and is thought to influence channel function and subcellular targeting. Furthermore, it has been shown that Na^+ channels are substrates for many protein kinases. The protein kinases A and C, but also the tyrosine kinase, the p38 mitogen activated kinase, and the calcium calmodulin kinase II were demonstrated to phosphorylate the channel protein at the large intracellular loops between the domains I, II, III, and IV (see figure 1-1) [Bevan & Storey, 2002, Cantrell & Catterall, 2001, Carr et al. , 2003].

Another mechanism known to modulate Na^+ current amplitude in neurons is a blockade of the Na^+ channel by the polyamine spermine, which is present in the cytosol

of all cells [Huang & Moczydlowski, 2001]. Spermine is a metabolic derivative of the amino acid ornithine and was recently shown to potently block persistent Na^+ currents (see *chapter 1.4*) in cortical layer 5 pyramidal neurons [Fleidervish et al. , 2008].

Finally, a series of other proteins was shown to influence the Na^+ channel's properties and targeting such as members of the cytoskeleton and associated proteins (see *chapter 1.3*) [Garrido et al. , 2003b, Herzog et al. , 2003], the β -site amyloid precursor protein cleaving enzyme 1 [Kim et al. , 2007], and the G-protein $\beta\gamma$ -subunit [Ma et al. , 1997].

The many possibilities to control excitability via Na^+ channel subunit expression and posttranslational modification suggest that intrinsic membrane properties are regulated extensively and that they are important in neuronal network behaviour and generation of brain functions.

1.3 Subcellular distribution of Na^+ channel subunits

Voltage gated Na^+ channels and currents have been detected in somatic, dendritic, and axonal compartment of neurons. Interestingly, individual Na^+ channel subunits show distinct subcellular patterns of expression suggesting functional specialization [for review see Vacher et al., 2008]. Without a doubt the highest concentrations of Na^+ channels are found within axonal membranes. A particularly strong aggregation occurs at the proximal region of the axon, termed axon initial segment (AIS), the nodes of ranvier in myelinated fibres, and unmyelinated zones of retinal ganglion cells [Catterall, 1981, Boiko et al. , 2001, Boiko et al. , 2003, Pan et al. , 2006]. The axon initial segment is a specialized subcellular region found in a wide range of excitatory and inhibitory neurons. In glutamatergic neurons the Na^+ channel subunit that is most strongly associated with the AIS is $\text{Na}_v1.6$ [Jenkins & Bennett, 2001, Boiko et al. , 2003, Hossain et al. , 2005, Wart & Matthews, 2006b, Royeck et al. , 2008, Lorincz & Nusser, 2008], while in inhibitory neurons $\text{Na}_v1.1$ seems to be of particular importance [Yu et al. , 2006, Ogiwara et al. , 2007, Lorincz & Nusser, 2008]. Apart from Na^+ channels, the K^+ channels $\text{K}_v1.1$ and $\text{K}_v1.2$ [Inda et al. , 2006, Lorincz & Nusser, 2008] as well as $\text{K}_v7.2$ and $\text{K}_v7.3$ [Devaux et al. , 2004, Pan et al. , 2006] have been found in high concentrations at the AIS. Recently, clustering of T-type Ca^{2+} channels has been reported at the axon initial segment of cochlear interneurons [Bender & Trussell, 2009]

The subcellular trafficking and localization of Na^+ channels seems to involve proteins associated to the cytoskeleton such as β -actin, compact myelin, dynein [Malik-Hall et al. , 2003], neurofascin [Koticha et al. , 2006], and Ankyrin G (Ank G) [Garrido et al. , 2003a]. In particular, Ank G was shown to be necessary and sufficient to confer targeting of $\text{Na}_v1.2$ to the axon initial segment of cultured hippocampal neurons. This localization of Na^+ channels is mediated by a consensus motif in the DII-DII linker region that is conserved in $\text{Na}_v1.1$, $\text{Na}_v1.2$, $\text{Na}_v1.3$ and $\text{Na}_v1.6$ [Garrido et al. , 2003a, Garrido et al. , 2003b, Pan et al. , 2006]. Direct interaction with cytoskeleton associated proteins such as neurofascin was additionally reported for Na^+ channel β -subunits [Ratcliffe et al. , 2001]. However, if this interaction also plays a role in subcellular localization of Na^+ channels is still unknown.

1.4 Types of Na^+ currents

The voltage gated Na^+ channels discussed above give rise to a prominent transient Na^+ current (I_{NaT}) and to two smaller Na^+ currents, namely the persistent Na^+ current (I_{NaP}) [French et al. , 1990] and the resurgent Na^+ current (I_{NaR}) [Raman & Bean, 1997]. These currents are illustrated in *figure 1-2* and have been thoroughly studied in a wide range of neurons, both in whole-cell and cell-attached configuration utilizing voltage clamp (see *methods 2.6.4, 2.6.5, and 2.6.6*).

The transient Na^+ current initiates and mediates the fast rising phase of the action potential. The sequence of events underlying the gating of this current was first described in the squid giant axon [Hodgkin & Huxley, 1952] without knowledge of the underlying ion channel. It was many years later that the first voltage-dependent Na^+ channel was described [Kado & Baud, 1981]. Today understanding of the structural correlates of the voltage dependent activation and inactivation is very detailed (see *chapter 1.2*).

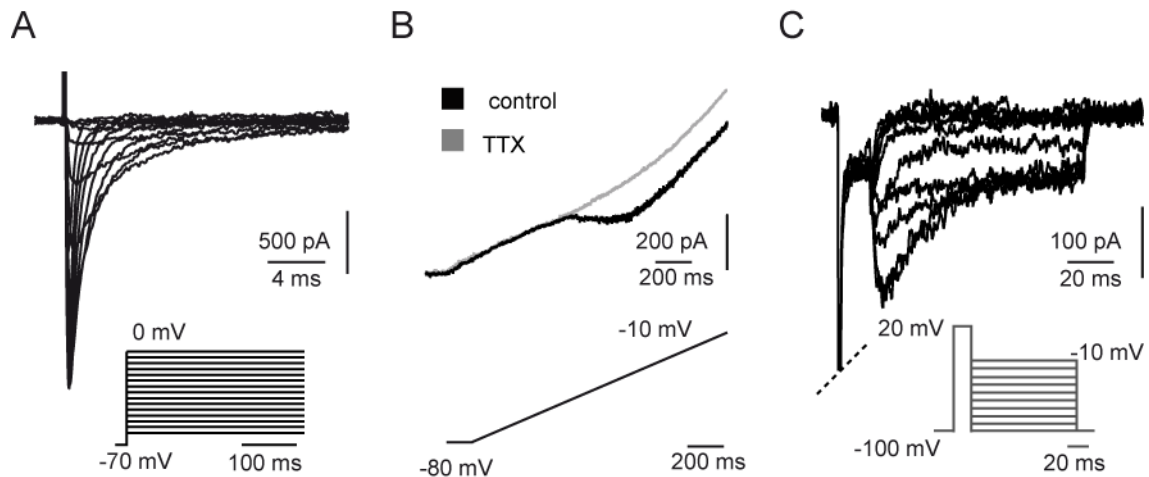


Figure 1-2: The transient, persistent, and resurgent Na^+ current.

(A) Overlay of traces that illustrates activation and fast inactivation of the transient Na^+ current (I_{NaT}). Whole-cell currents were recorded in an acutely isolated CA1 pyramidal cell under conditions designed to reduce contribution of other conductances (see methods 2.6.4). **(B)** Example traces illustrating the persistent Na^+ current (I_{NaP}) recorded in the slice preparation (see methods 2.6.5). The current is recorded using a slow ramp (50 mV/s) that leads to inactivation of I_{NaT} and selectively reveals I_{NaP} (black trace). Voltage gated Na^+ channel mediated portion of the recorded current is then unveiled by application of TTX (grey trace). **(C)** Example of a Na^+ currents recorded in a cell containing a prominent resurgent Na^+ current (I_{NaR}). Voltage dependence of I_{NaR} is obtained by stepping to different potentials following the full-blown activation of I_{NaT} . Transient current responses preceding I_{NaR} are truncated [Royeck et al. , 2008]. Voltage paradigms to elicit the different Na^+ currents are shown as insets.

At hyperpolarized membrane potentials Na^+ channels are in their closed state. Depolarization of the membrane triggers a conformational change leading to the opening of the Na^+ channel. Influx of Na^+ through the channel pore depolarizes the membrane further causing even more Na^+ channels to open. The prolonged depolarization caused by the Na^+ influx then promotes closing of the pore by the inactivation gate (see *figure 1-1*), a process called fast inactivation. The conformational changes underlying Na^+ channel activation and inactivation differ in time and voltage dependence. In addition to fast inactivation, Na^+ channels also undergo slow inactivation, which does not primarily depend on the fast inactivation gate. Recovery from fast as well as slow inactivation is time dependent. This leads to a refractory period during which depolarization fails to open the channel pore. Recovery from activation and inactivation is also voltage dependent, thus leading to a complex dependence of Na^+ channel availability on previous activity and membrane potential. Finally, repolarization of the membrane potential induces closing of the channel's activation gate. This process is called deactivation.

In many neurons fast inactivation of Na^+ channels is not complete and a persistent Na^+ (I_{NaP}) current can be recorded [French et al. , 1990, Crill, 1996, Magistretti & Alonso, 1999]. There are three reasons why this non- or slowly inactivating Na^+ current cannot be completely attributed to the window current that flows due to overlap of the voltage dependence of activation and inactivation of the transient Na^+ current. First, the

window current amplitude that can be measured in a single cell is not sufficient to underly the complete non-inactivating Na^+ current observed in the same cell [French et al. , 1990]. Second, I_{NaP} appears prominently at subthreshold potentials, further distinguishing it from the transient Na^+ current that mediates the window current. Third, the occurrence of persistent Na^+ current was analyzed in single channel recordings and attributed to a different gating mode [French et al. , 1990, Alzheimer et al. , 1993, Crill, 1996, Magistretti et al. , 1999].

In *Xenopus laevis* oocytes, human embryonic kidney cells line 293 (HEK293), and primary cultures from dorsal root ganglion (DRG) neurons recombinant Na^+ channel subunit $\text{Na}_V1.6$ produced larger amplitudes of I_{NaP} compared to other subunits [Smith et al. , 1998, Rush et al. , 2005, Chen et al. , 2008]. However, I_{NaP} cannot be exclusively attributed to this subunit. To what extent I_{NaP} is affected by posttranslational modifications or associations of the Na^+ channels with other proteins is still poorly understood. In expression systems, the co-expression of $\text{Na}_V1.2$ with the G-protein $\beta\gamma$ -subunit leads to a significant upregulation of I_{NaP} [Ma et al. , 1997]. More recently, co-expression of $\text{Na}_V1.1$ with the $\beta 4$ -subunit was also shown to increase I_{NaP} amplitude in hippocampal cultures [Aman et al. , 2009]. Regarding the subcellular location of I_{NaP} it has been shown that the persistent Na^+ current is efficiently blocked by tetrodotoxin (TTX) puff applications to the soma and proximal axon [Yue et al. , 2005, Astman et al. , 2006]. Apart from this axo-somatic preference, studies utilizing cell-attached recordings [Magistretti & Alonso, 1999] and imaging experiments [Mittmann et al. , 1997] also reported I_{NaP} at dendritic locations.

In many recordings an intermediate inactivating component of the transient Na^+ current is observed [Yue et al. , 2005]. This current fraction is very poorly understood, but might depend on posttranslational modifications such as phosphorylation [Ratcliffe et al. , 2000] and changes in voltage dependence of activation or inactivation which are caused by the association with β -subunits that are often absent in experiments that analyze recombinant Na^+ channels [*for review see* Isom, 2002].

Additionally, the existence of a resurgent Na^+ current (I_{NaR}) has been reported in several brain regions including subfields of the hippocampus [Raman & Bean, 1997, Castelli et al. , 2007]. The resurgent Na^+ current is generated by a recovery from channel inactivation while the activation gate is still open. The inactivation released upon repolarization is thought not to depend on the inactivation gate of the Na^+ channel α -subunit itself. It was shown that the intracellular C-terminus of the $\beta 4$ -subunit is able to serve as an additional inactivation gate [Grieco et al., 2005, *but see* Chen et al., 2008 *and* Aman et al., 2009]. If the full length $\beta 4$ -subunit also subserves this function has recently been questioned [Aman et al. , 2009]. The resurgent Na^+ current seems to be modulated by Na^+ channel phosphorylation [Grieco et al. , 2002]. In *Scn8a^{med}* CA1 pyramidal neurons lacking $\text{Na}_V1.6$ the amplitude of I_{NaR} is reduced [Royeck et al. , 2008].

1.5 Initiation of action potentials

One important factor that defines the discharge properties of a neuron is the threshold for the generation of an action potential. It is important to know, which factors determine the voltage that has to be reached in a given condition in order to trigger an action potential, and whether there is a specific site within the neuron where this occurs first.

A large number of experiments utilizing imaging or simultaneous electrophysiological recordings have shown that in most cases action potentials are initiated at an axonal location close to the soma. This principle holds true for subicular neurons [Colbert & Johnston, 1996], cortical pyramidal neurons [Stuart & Sakmann, 1994, Stuart et al. , 1997, Palmer & Stuart, 2006, Meeks & Mennerick, 2007], as well

as Purkinje cells [Stuart & Häusser, 1994, Khaliq & Raman, 2005, Khaliq & Raman, 2006]. Recently, this region was located even more precisely to the most distal portion of the axon initial segment (AIS) in cortical neurons [Palmer & Stuart, 2006].

What are the properties of the axon initial segment that endow this subcellular site with the important function of action potential initiation?

It is well known that passive properties influence the propagation of membrane potential changes along neuronal processes. Passive properties are dictated by the geometry of the neuronal compartments, their membrane resistance and capacitance. Compared to the soma and most dendritic processes the axon initial segment has a small diameter accounting for a very small capacitance. Several modelling and physiological studies suggest that depolarization of the membrane potential occurs first at the axon initial segment, while depolarization of the soma is delayed due to the charging of its larger capacitance. Therefore passive properties alone already support initiation of the action potential at the axon initial segment [McCormick et al. , 2007, Meeks & Mennerick, 2007, Shu et al. , 2007].

A pronounced aggregation of various ion channels at the axon initial segment has been reported. Very interesting regarding action potential initiation is the conspicuously high density of voltage gated Na^+ channels (see *chapter 1.3*). Furthermore, various K^+ channels have been shown to be aggregated at the AIS, namely $\text{K}_v7.2$ and $\text{K}_v7.3$ [Pan et al. , 2006] and K_v1 D-type K^+ channels [Kole et al. , 2007, Goldberg et al. , 2008, Lorincz & Nusser, 2008]. If the high density of channel protein gives rise to increased current densities is matter of debate. Cell-attached recordings performed at the axon suggested a uniform Na^+ current density between the axon and soma [Colbert & Johnston, 1996, Colbert & Pan, 2002]. In contrast, a recent study also utilizing Na^+ imaging reported that I_{NaT} density at the axon initial segment is increased [Kole et al. , 2008]. Regardless of this discrepancy, reduction of axonal Na^+ channel availability by focal application of TTX was shown to increase spike threshold and affect action potential initiation [Meeks & Mennerick, 2007].

In addition, the biophysical properties of these axonal ion channels are proposed to be different than elsewhere in the neuron. Recently, cooperative Na^+ channel opening was suggested to account for the initiation at the axon initial segment and the rapid rise (termed 'kink') at the onset of the spike in cortical neurons [Naundorf et al. , 2006]. Using cell-attached recordings, Colbert & Pan [2002] found that in cortical neurons the voltage dependence of I_{NaT} activation was shifted by 8 mV in the hyperpolarized direction. Considering this, it is a tempting hypothesis that the voltage dependence of activation of ion channels at the axon initial segment determines the threshold for action potentials generation and localizes initiation to this compartment.

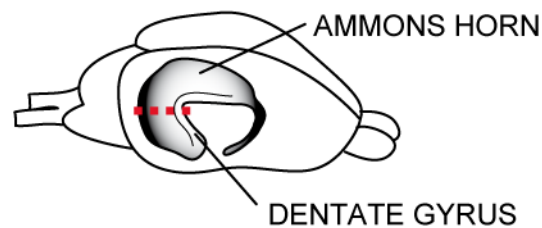
Interestingly, there are various subthreshold currents that are mediated by channels located at the axon initial segment. These are the T-Type Ca^{2+} current, [Bender & Trussell, 2009], the persistent Na^+ current (I_{NaP}) [Yue et al. , 2005, Astman et al. , 2006], as well as two K^+ currents, the M-type current mediated by K_v7 channels [Pan et al. , 2006, Vervaeke et al. , 2006b], and D-type current mediated by K_v1 channels [Kole et al. , 2007]. Blocking axonal D-type currents with dendrotoxin, increased spike halfwidth in axons significantly, while somatic action potential duration and threshold remained unaffected [Kole et al. , 2007]. Of more importance in determining the action potential threshold is the slowly activating M-current. Application of the K_v7 antagonist XE991 lowered action potential threshold following injection of a ramp current into the cell [Hu et al. , 2007] and increased spike gain significantly [Shah et al. , 2008]. However, the contribution of the M-current in setting the spike threshold for single action potentials is controversial [*compare* Chen & Yaari, 2007, *and* Peters et al., 2005, Otto et al., 2006, *with* Shah et al., 2008]. The subthreshold activated T-type Ca^{2+} current is also a slowly activating current and therefore it is rather unlikely that it strongly influences the threshold for single action potentials but also might be of greater importance during periods of prolonged depolarization and firing. In contrast to this, the

persistent Na^+ current activates almost instantly upon depolarization [Alzheimer et al. , 1993, Magistretti et al. , 1999]. Complete dynamic clamp subtraction of I_{NaP} increased the action potential threshold by 3 mV during steady state firing that was triggered by constant current injection in CA1 pyramidal neurons [Vervaeke et al. , 2006b].

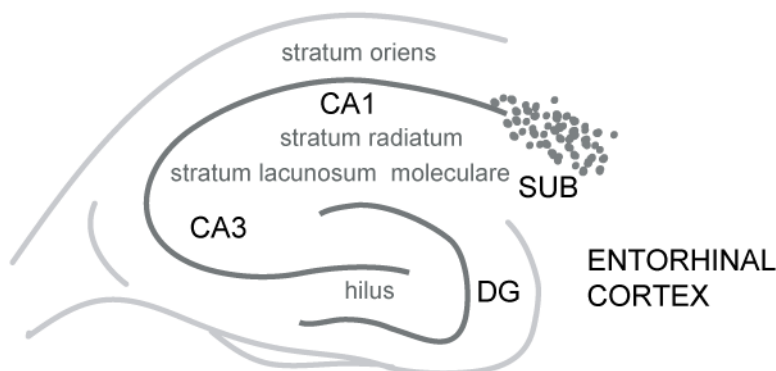
1.6 Hippocampus

The hippocampal formation in the rodent brain bends from the septal nuclei over the diencephalon towards the medial temporal lobe. It consists of the dentate gyrus, the Cornu Ammonis, the subiculum, the presubiculum, and ends with the parasubiculum next to the entorhinal cortex. Here, the dentate gyrus and the Cornu Ammonis are referred to as the hippocampus. The name hippocampus (as the seahorse) and the name Cornu Ammonis (meaning 'horn of Ammon' after the ancient Egyptian god) acknowledge the curved shape of the hippocampus. Both parts contain a single prominent cellular layer. In the dentate gyrus the cell layer is formed mainly by unipolar granule neurons and in the Cornu Ammonis by multipolar pyramidal cells. The Cornu Ammonis has originally been divided into four regions CA1 to CA4 [Lorente de No, 1934]. The region CA4 however, that resides within a polymorphic layer of the dentate gyrus named hilus (see figure 1-3 B) is now considered to be part of CA3. The CA2 region is a small band between CA3 and CA1 that contains neurons that share their morphology with CA3 and connectivity with CA1 pyramidal neurons [Lorente de No, 1934]. The CA1 region itself is bordered by the subiculum recognisable by the broadening and dispersion of the pyramidal cell layer (see figure 1-3 B).

A



B



C

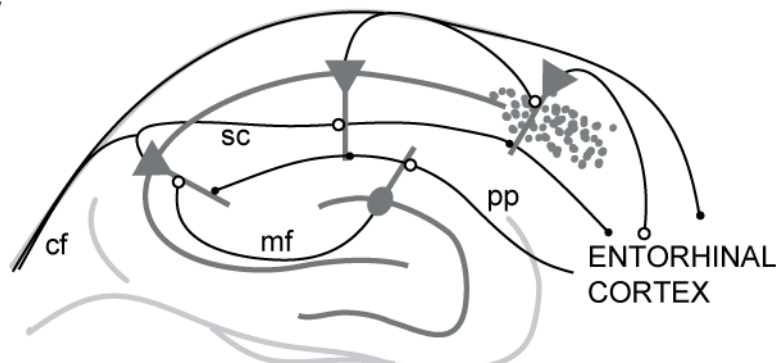


Figure 1-3: Morphology of the hippocampal formation.

(A) Position of the hippocampal formation in one hemisphere of the rodent brain showing the Cornu Ammonis enveloping the dentate gyrus. The dashed red line indicates the level from which sections with the appearance of (B) and (C) can be obtained. (B) Section illustrating the laminar structure of the hippocampus. The principal cell layers are shown in dark grey and are the dentate granule cell layer (DG) of the dentate gyrus; the CA3 and CA1 pyramidal cell layers of the Cornu Ammonis with the adjacent subiculum (SUB). The layer above the CA1 pyramidal cell layer is called stratum oriens; below are the stratum radiatum and the stratum lacunosum moleculare. (C) The classic excitatory synaptic pathway of the hippocampal formation (*open circles*) and additional excitatory synapses (*closed circles*). The classic pathway begins with the perforant path (pp), followed by the mossy fibre tract (mf) and the Schaffer collaterals (sc). The CA1 pyramidal cells project onto the subicular neurons that project onto the entorhinal cortex. Both CA3 and CA1 also project to the contralateral hippocampus through the commissural fibres (cf).

The hippocampus receives input from and projects to many brain regions, like septum, hypothalamus, thalamus, amygdala, olfactory cortex, associational cortex, and brainstem. It also is strongly connected to the contralateral hippocampus [Amaral & Witter, 1989, Squire et al. , 2004]. The highly regular neuronal connections inside the hippocampal formation of one hemisphere make the hippocampus a tempting study object. These main excitatory circuits in the hippocampal formation were already described by Ramon y Cajal [1893]. In the simplified laminar neuronal network described in his studies, the entorhinal cortex serves as the main in- and output structure of the hippocampus and is starting point for the well-known '*trisynaptic pathway*' [Andersen et al. , 1971]. This is formed by three consecutive fibre tracts, namely the perforant path (pp), the mossy fibres (mf) and the Schaffer collaterals (sc, see figure 1-3 C). The perforant path mainly projects onto the dendrites of the dentate gyrus granule cells in the stratum lacunosum moleculare. The axons of the perforant path initiate in layer II and III of the entorhinal cortex, transverse or *perforate* the subiculum and reach as far as CA1 [Johnston & Amaral, 2003]. The dentate gyrus granule cells give rise to the mossy fibres that innervate the CA3 pyramidal neurons close to their cell bodies in the stratum lucidum. These synaptic connections show some remarkable features such as their presynaptically expressed short- and long term plasticity [Harris & Cotman, 1986, Zalutsky & Nicoll, 1990, Salin et al. , 1996]. The mossy fibre synapses are among the largest synaptic bodies found in the mammalian brain [Hamlyn, 1962]. Finally, the CA3 pyramidal cells provide excitatory input onto the apical and basal dendrites of CA1 pyramidal cells with their Schaffer collaterals crossing the stratum radiatum in a parallel manner.

The CA1 pyramidal neurons project onto the neurons of the adjacent subicular complex and the entorhinal cortex. Both CA3 and CA1 are also connected to the contralateral hippocampus via the commissural fibres. Additionally to these are the inhibitory inputs provided by the various types of interneurons that reside in the different strata or are interspersed between the pyramidal cells in stratum pyramidale [Freund & Buzsáki, 1996]

The involvement of the hippocampus in memory formation becomes impressively apparent considering the pathology of the patient H.M.. This recently deceased man suffered from severe epilepsy and underwent bilateral surgical removal of the hippocampus. Following the operation H.M. suffered from retrograde amnesia but more dramatically completely lost the ability to add new information to his long term memory [Scoville & Milner, 1957]. This anterograde memory loss was also found in other patients with bilateral hippocampal damage [Rempel-Clower et al. , 1996]. Apart from its role in the generation and consolidation of explicit memories [*for review see* Martin & Morris, 2002, Bird & Burgess, 2008] the hippocampus also has an important role in spatial navigation. *In vivo* single unit recordings in the CA1 region of the rat led to the identification of so called place cells. These cells display an increased propensity to fire

if the rat is at a specific location in space [O'Keefe & Dostrovsky, 1971, Wilson & McNaughton, 1993, Neves et al. , 2008].

1.7 The CA1 pyramidal neuron

Since all electrophysiological experiments of this study were performed on principal cells of the CA1 region of the hippocampus, they are introduced here in more detail. The CA1 pyramidal neuron is one of the most intensely studied cells in the mammalian brain. This is probably due to their good viability in the slice preparation, the convenient access of the CA3 to CA1 synapses for field potential studies of synaptic plasticity, and the possibility to obtain direct dendritic recordings. In the rat, CA1 pyramidal neurons extend their dendritic trees up to 600 μm towards the hippocampal fissure and 250 μm towards the alveus (*see figure 1-4*). The total dendritic length of a single CA1 pyramidal neuron is approximately 12 to 13.5 mm [Bannister & Larkman, 1995a]. All CA1 pyramidal cells follow largely the same construction scheme. From the soma a large apical dendrite protrudes and bifurcates in the stratum radiatum or in the stratum lacunosum moleculare [Bannister & Larkman, 1995a]. Two to eight basal dendrites extend into the stratum oriens. The CA1 pyramidal cell axons also cross the stratum oriens and project towards the alveus [Bannister & Larkman, 1995a, Pyapali et al. , 1998]. Both, basal and apical dendrites, give rise to many smaller branches that are covered with small membrane protrusions, called dendritic spines. These spines form the postsynaptic part of most excitatory synapses [Ramon y Cajal, 1893, Lorente de No, 1934, Bannister & Larkman, 1995b]. Therefore the number of spines is considered a reasonably good measure for the amount of excitatory input that a CA1 pyramidal neuron receives [Gray, 1959, Gulyás et al. , 1999, Megias et al. , 2001].

CA1 pyramidal cells receive excitatory input through the Schaffer collaterals, the commissural fibres, as well as through the temporal ammonic pathway from the layer three of the entorhinal cortex [Ramon y Cajal, 1893]. The latter input is restricted to the distal part of the CA1 pyramidal cell dendrite in the stratum lacunosum [Blackstad, 1958]. CA1 pyramidal neurons furthermore receive excitatory input from the basolateral nucleus of the amygdala, the nucleus reuniens of the thalamus [Krettek & Price, 1977, Wouterlood et al. , 1990, der Weel et al. , 1997, Kempainen et al. , 2002] and other CA1 pyramidal cells [van Groen & Wyss, 1990, Deuchars & Thomson, 1996]. In addition, several types of inhibitory interneurons contact CA1 pyramidal cells, thereby forming distinct microcircuits [for review see [Freund & Buzsáki, 1996, Maglóczy & Freund, 2005].

The axons of CA1 pyramidal neurons project onto subicular pyramidal neurons [Amaral et al. , 1991] and mainly layer neurons in layer five of the entorhinal cortex [Swanson & Cowan, 1977, Finch & Babb, 1981]. The axons of the CA1 neurons cross through the stratum oriens into the alveus where they bend towards the subiculum onto which they project in a columnar fashion [Tamamaki et al. , 1987, Amaral et al. , 1991].

Intrinsic firing properties of CA1 pyramidal neurons

CA1 pyramidal neurons have been extensively studied in the slice preparation where they are at a resting membrane potential between -60 and -70 mV. Typically, a CA1 pyramidal cell responds with multiple spikes to prolonged depolarisations. A linear increase in the amplitude of the current injection usually results in a linear increase in the number of action potentials fired [Madison & Nicoll, 1984]. Spikes within such a spike train display a strong frequency accommodation attributed to the gradual activation of M current and Ca^{2+} dependent K^+ currents [Lancaster & Adams, 1986, Lancaster & Nicoll, 1987]. Spike trains are followed by a prolonged afterhyperpolarization thought to be mediated by Ca^{2+} activated SK K^+ channels (*Kcnn*) [Marrion & Tavalin, 1998, Bowden et al. , 2001].

A short depolarization of sufficient size usually elicits a single spike that is followed by a pronounced afterdepolarization (ADP; see *figure 1-4 B*) [Kandel & Spencer, 1961, Storm, 1987a, Storm, 1989, Jensen et al. , 1994]. Extensive effort has already been put into the identification and classification of the conductances underlying the action potential wave form of CA1 pyramidal neurons. For instance pharmacological block of voltage gated K^+ channels, as well as Ca^{2+} gated K^+ channels was shown to delay the repolarization of the somatic action potential [Zhang & McBain, 1995]. In the latter case *Kcnma1* (BK) channels are thought to contribute to action potential repolarization [Storm, 1987b, Gu et al. , 2007, Matthews et al. , 2008]. The afterdepolarization following the fast spike was shown to be driven by the axo-somatic I_{NaP} [Yue et al. , 2005] as well as Ni^{2+} sensitive Ca^{2+} currents [Metz et al. , 2005]. The size of the ADP can also be increased by pharmacological block of dendritic D-type K^+ currents [Metz et al. , 2007] or axo-somatic M-type K^+ currents [Yue & Yaari, 2004]. The interplay between I_{NaP} and the M-type current in the determination of CA1 action potential firing was analyzed in more detail in a combined electrophysiological and computational study [Golomb et al. , 2006]. More recently, an intracellular block of M-type K^+ channels by Ca^{2+} ions was shown to influence ADP size [Chen & Yaari, 2008].

Another feature of CA1 pyramidal neurons is a prominent expression of the hyperpolarization activated unspecific cation current (I_H) that mediates the pronounced voltage sag that follows hyperpolarization or leads to a rebound depolarization following the end of a hyperpolarization.

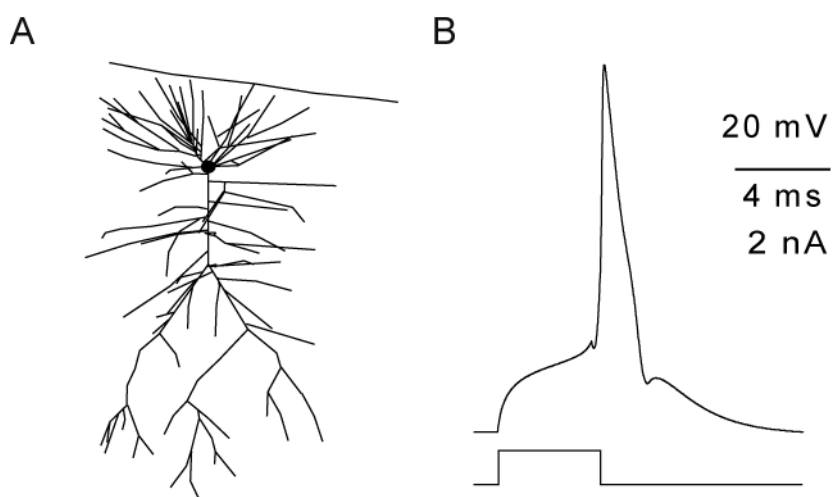


Figure 1-4: Morphology of the CA1 pyramidal neuron.

(A) Branching schematic of the neuron utilized in the computational model (see *methods 2.8*). The morphology of the neuron is based on [Bannister & Larkman, 1995a]. **(B)** Action potential elicited in the model by simulation of a brief 4 ms current injection [*modified after* Royeck et al., 2008].

In some cases the size of the ADP amplitude is sufficient to reach spike threshold again, thus triggering additional spikes or burst discharges. Such a burst firing of CA1 pyramidal neurons is frequently observed during *in vivo* recordings [Kandel et al. , 1961, Suzuki & Smith, 1985, Frank et al. , 2001]. Under these conditions, however, the contribution of synaptic drive and specific intrinsic membrane properties to the generation of the burst discharge are unclear. Nevertheless, burst discharges also occur in the CA1 region *in vitro* in the absence of synaptic inputs [Jensen et al. , 1996, Masukawa et al. , 1982]. The probability of burst discharges was shown to depend on several factors. Recordings of CA1 pyramidal neurons with pharmacologically reduced dendritic A-type K^+ currents display intrinsic burst firing due to enhanced Na^+ channel

mediated backpropagation of the action potential into the dendrite. In this case, the backpropagating action potential activates Ni^{2+} sensitive Ca^{2+} currents that trigger the subsequent spikes of the discharge [Magee & Carruth, 1999]. Furthermore, several alterations of the composition the extracellular milieu, such as cation contents and osmolarity were shown to affect burst propensity [for review see Yaari & Beck, 2002]. For instance, increasing the K^+ concentration or occluding Ca^{2+} from the bath solution was shown to facilitate burst firing of CA1 pyramidal neurons [Jensen et al. , 1994, Jensen et al. , 1996]. The latter phenomenon is caused by a Ca^{2+} dependent increase in I_{NaP} that enhances the ADP and thereby promotes bursting [Su et al. , 2001].

Changes in intrinsic properties of CA1 pyramidal neurons that affect discharge behaviour are observed in neurological diseases [for review see Yaari & Beck, 2002, Beck & Yaari, 2008]. The changes in firing behavior following pilocarpine induced status epilepticus were thoroughly studied utilizing sharp microelectrodes [Sanabria et al. , 2001, Yaari et al. , 2007, Becker et al. , 2008, Chen et al. , 2009]. These studies found that a large percentage of CA1 pyramidal neurons turn from regular spike accommodating pyramidal neurons into burst firing neurons.

Burst firing neurons are classified into low threshold bursters if they respond to a just supra-threshold current injection with a high frequency burst of action potentials. They are called high threshold bursters if they respond to a stronger more prolonged depolarization with an initial burst of spikes followed by a pronounced hyperpolarized interspike potential [Su et al. , 2002, Chen et al. , 2009]. These pathophysiological changes might be due to alterations in protein expression. The abovementioned low threshold bursting is mediated by increased T-type Ca^{2+} currents associated with a strong upregulation of the $\text{Ca}_v3.2$ Ca^{2+} channel subunits [Becker et al. , 2008]. Additionally, the A-type K^+ potassium channel $\text{K}_v4.2$ [Bernard et al. , 2004] or the H-current mediating channel HCN1 and HCN2 [Jung et al. , 2007, Marcelin et al. , 2008] show changes in expression in epilepsy.

1.8 Mesial temporal lobe epilepsy

Epilepsy is a severe chronic neurological disease that affects 0.4 to 1% of the human population [Sander & Shorvon, 1996, Bell & Sander, 2001]. The World Health Organization (WHO) defines epilepsy as a disorder characterized by the occurrence of recurrent seizures. Epileptic seizures are correlates of sudden, usually brief, excessive electrical discharges of large neuronal ensembles. The severity of seizures varies from brief lapses of attention or muscle jerks, to severe and prolonged convulsions. A very strong enduring seizure is the so called status epilepticus that, if untreated or even with treatment, sometimes results in the death of the patient. The experience of a single status epilepticus in patients without seizure history can lead to the development of chronic epilepsy [DeLorenzo et al. , 1996, Hesdorffer et al. , 1998]. There are many causes that can facilitate the development of epilepsy, such as head trauma, intoxication, encephalitis, or genetic mutations. However, in many cases the reason underlying the development of chronic epilepsy cannot be identified.

The most common form of epilepsy is mesial temporal lobe epilepsy [Engel, 2001]. Electrodes implanted into the hippocampus of patients suffering from temporal lobe epilepsy revealed that pathological electric activity of the hippocampus often precedes the manifestation of an epileptic seizure [Engel, 1996]. In such a case, hippocampal neurons probably act as a trigger for the subsequent seizure. A structural disorder found in the hippocampus of 65% of patients that suffer from temporal lobe epilepsy is Ammon's horn sclerosis [Blümcke et al. , 1999, Blümcke et al. , 2002]. This stereotypic hippocampal injury is characterized by neuronal cell death in the hilus, CA3 and CA1 regions, granule cell dispersion, pathological proliferation of astrocytes (astrogliosis), and a reorganization of synaptic connectivity. Prominent among the synaptic reorganizations that take place in Ammon's horn sclerosis are mossy fibre sprouting

[Scheibel et al. , 1974] and reorganizations of the inhibitory interneuron network [Bekenstein & Lothman, 1993].

Mesial temporal lobe epilepsy is treated pharmacologically with a variety of antiepileptic drugs. The pharmacological control of seizures in temporal lobe epilepsy is considered successful in approximately two thirds of patients [Regesta & Tanganelli, 1999]. In patients with pharmaco-resistant epilepsy the surgical resection of the affected portion of the hippocampus is an additional treatment option.

1.9 Aim of the study

The voltage threshold that has to be reached to trigger the discharge is a feature of great importance in the generation of an action potential. The goal of this work was to determine the contribution of the Na⁺ channel subunit Na_v1.6 in setting the action potential threshold, as well as in defining the subcellular localization of action potential initiation. Furthermore, we aimed to investigate the influence Na_v1.6 has on other discharge properties of CA1 pyramidal neurons. In the first part of this work, we have used the *Scn8a^{med}* mutant mouse line, which is deficient in functional expression of the Na_v1.6 protein, to assess the functional role of this subunit [Duchen, 1970, Duchen & Stefani, 1971]. In the second part, we sought to determine possible changes in Na_v1.6 expression and potential functional consequences during epileptogenesis in the pilocarpine model of epilepsy in rats [Turski et al. , 1984, Cavalheiro, 1995].

2. Materials and methods

2.1 Experimental animals

2.1.1 Functionally Na_v1.6 deficient mice – the *Scn8a*^{med} mutation

In the first part of this study we used mice lacking expression of the pore forming Na⁺ channel α -subunit Na_v1.6. The mice were taken from the inbred laboratory mice strain C3HeB/FeJ-*Scn8a*^{med}/J, Stock Nr. 003798. These *Scn8a*^{med} mice, which are homozygous for the *med* mutation, arose in 1958 in Edinburgh [Searle, 1962]. The name *med* derives from the recessive muscle endplate disease [Duchen, 1970, Duchen & Stefani, 1971]. This mutation disrupts the *Scn8a* Na⁺ channel subunit gene by insertion of a LINE (long interspersed nuclear element) into exon two of the *Scn8a* gene that leads to the expression of a non-functional truncated protein [Burgess et al. , 1995, Kohrman et al. , 1996]. We acquired a total of 6 heterozygous breeding pairs of these mice from Jackson Laboratories (The Jackson Laboratories, Bar Harbor, Maine 04609, USA) and established a colony at our animal facility by mating only heterozygous animals. For experiments we took male and female offspring between postnatal day 17 and 21 (p17 - p21) that were either homozygous (*Scn8a*^{med}) for the mutation or not carrying the mutated allele at all (*Scn8a*^{wt}). The genotype of the animals was determined by PCR (polymerase chain reaction) following the protocol provided by Jackson Laboratories.

2.1.2 The pilocarpine model of temporal lobe epilepsy

Experiments assessing the changes of Na⁺ channels and currents in epilepsy were performed on male Wistar rats (Charles River, Sulzfeld, Germany) using the pilocarpine model of epilepsy [Turski et al. , 1984, Cavalheiro, 1995, Curia et al. , 2008]. Animals were acquired with a weight of approximately 150-180 g corresponding to ~30 d of age and kept in the animal facility for at least 48 h before the pilocarpine treatment. At the day of the pilocarpine treatment all animals were weighed, marked with a number on their tails, and placed into empty cages (5-8 animals per cage). Animals were then injected intraperitoneally with 1 mg/kg body weight scopolamine-methylnitrate diluted in Ringer solution. Scopolamine-methylnitrate acts as a M3 muscarinic acetylcholine receptor antagonist with a reduced tendency to cross the blood brain barrier. Therefore scopolamine attenuates the peripheral actions of the subsequently injected pilocarpine-hydrochloride diluted in aqua ad injectabilia. Pilocarpine (340 mg/kg body weight) was injected intraperitoneally 30 min later in order to induce epileptic seizures. During the following hour rats showed strong salivation, rigid posture, and eventually repetitive limb movements. In most rats this aberrant behaviour eventually develops into a generalized tonic clonic seizure that usually appears 15-30 min after the injection. When the generalized seizure persisted for 5-10 min rats were considered to have fallen into self-sustained status epilepticus starting from the onset of the seizure. These rats were then placed into a separate cage. Observation of this cage was continued to ensure the rats did not recover from the status epilepticus. Rats that did not enter status epilepticus one hour after the first injections were injected a second time with the same dose of pilocarpine. After 40 min in self sustained status epilepticus the animals were injected subcutaneously with 1 ml Diazepam and 1 ml 5% glucose, in order to attenuate the severity of the status epilepticus. Rats that did not enter status epilepticus two hours after the first injection were killed. The surviving pilocarpine treated rats were then housed into single cages with a layer of paper-towels covering the sawdust and a Petri dish with food pellets.

The experience of status epilepticus is followed by a silent period of 7 to 14 days without seizures. During this time reorganizations of the hippocampus take place and eventually the animals begin to suffer from the occurrence of spontaneous generalized epileptic seizures. Pilocarpinized rats were video monitored for the occurrence of spontaneous epileptic seizures. In all experiments, pilocarpine treated or epileptic rats were compared to sham control rats. These controls animals were also weighed and injected with appropriate doses of scopolamine-methylnitrate, diazepam, and 5% glucose. All animal experiments were conducted in accordance with the guidelines of the Animal Care and Use Committee of the University of Bonn.

2.2 Preparation of brain tissue

2.2.1 Preparation of brain tissue from mice and rats for electrophysiological experiments

Anaesthesia was induced by subcutaneous injection of ketamine (100 mg/kg bodyweight, Pfizer, Germany) and xylazine (15 mg/kg bodyweight, Bayer, Germany). Until pain reflexes could no longer be observed saturation of the blood with oxygen was supported by putting the animals into a flow of carbogen (95% O₂ / 5% CO₂, Linde, Germany). As soon as deep anaesthesia was reached the chest was opened and the animal's right atrium was cut. Next the animals were killed by perfusion of the heart through the left ventricle with 1-3°C cold sucrose-based artificial cerebrospinal fluid (ACSF) containing [mM]: 56 NaCl, 100 sucrose, 2.5 KCl, 1.25 NaH₂PO₄, 30 NaHCO₃, 1 CaCl₂, 5 MgCl₂, and 20 glucose (95% O₂ / 5% CO₂) for approximately five to 20 s (3-5 ml for mice, 10-15 ml for rats). The animals were decapitated and the brain quickly dissected out. After removal of the cerebellum the brain was glued with the dorsal cortex onto the stage of a vibratome (MICROM, Germany) and submerged in the same ice-cold ACSF. As required for electrophysiological studies 300 µm thick or for immunohistochemistry 600 µm thick transverse hippocampal slices were cut. The slices destined for electrophysiology were placed into a storage chamber with room temperature (20°C) sucrose-based ACSF containing [mM]: 60 NaCl, 100 sucrose, 2.5 KCl, 1.25 NaH₂PO₄, 26 NaHCO₃, 1 CaCl₂, 5 MgCl₂, 1 kynurenic acid, 20 glucose (95% O₂ / 5% CO₂), that was gradually warmed to 36°C over a period of 30 min. Subsequently, slices were equilibrated in a chamber with ACSF [mM]: 125 NaCl, 3.5 KCl, 1.25 NaH₂PO₄, 26 NaHCO₃, 2 CaCl₂, 2 MgCl₂, and 15 glucose (95% O₂ / 5% CO₂) for at least 30 minutes at 20°C. The 600 µm thick slices prepared for immunohistochemistry were carefully placed in a tissue boat (Sakura, Netherlands). After removal of surplus ACSF the slices were submerged under Tissue-Tec (Sakura, Netherlands), equilibrated for two to five min and carefully frozen over liquid nitrogen (Linde, Germany) before being stored at -80°C.

2.2.2 Preparation of rat brain tissue and subfield microslices for biochemical analysis

Rat brains slices destined for immunohistochemical analysis of Na⁺ channel expression were acquired similar to the abovementioned tissue of *Scn8a*^{med} mice, only differing in the used Vibratome (Leica, Nussloch, Germany) and the thickness of the slices, namely 700 µm.

Tissue samples destined for the analysis of Na⁺ channel expression using Taqman™ mRNA expression analysis or Western blot were acquired as follows: Rats were decapitated following a deep anaesthesia using Isoflurane and the brain was quickly dissected out. After removal of the cerebellum and bulbi olfactori brains were glued with the dorsal cortex onto a chamber of a Leica 1000S Vibratome (Leica, Germany). Using Integraslice blades (Campden Instruments, UK) 700 µm thick

horizontal slices were cut. Hippocampal tissue was then further processed in a Petri dish under visual control using an illuminated 5x magnifying loupe LTS120 (Conelek, Germany). Each hippocampal slice was microdissected into CA3, CA1, and dentate gyrus (DG). More precisely, the CA3 microslices were acquired by cutting along the two ends of the granule cell layer. Then a cut parallel to the first one along the tip of the DG was placed to remove the subiculum. Finally CA1 and DG were separated by cutting along the hippocampal fissure (*compare figure 3-17 A*). Samples were frozen in liquid N₂ prior storage at -80°C

2.3 Immunohistochemistry

From the slices stored at -80°C 12 µm thick tissue sections were cut with a cryostat (MICROM, Germany) and mounted to either DAKO-slides (DAKO, Germany) or Superfrost™-plus-slides (Menzel, Germany) on which they were allowed to rest for 15 min at 20°C. Then the tissue was fixed by submerging the slides for 2 min into a 1:1 mixture of ethanol and acetone (Merck, Germany) and left to dry overnight at 20°C. Finally the slides were stored in a -20°C freezer until the staining experiments were conducted.

Slides were thawed for 30 min at room temperature and afterwards briefly washed in PBS (Biochrom AG, Germany). To avoid unspecific antibody binding the slices were incubated for 2 h at 20°C in a blocking solution consisting of PBS, Triton-X100 (0.1%), fetal calf serum (10%) (PAA laboratories Ltd., Austria), and normal goat serum (5%) (Vector, Burlingame, Ca.). All primary and secondary antibodies were dissolved and stored according to the protocols provided by their suppliers. Primary antibodies were diluted 1:200 in blocking solution and the binding reaction was allowed to take place at 4°C for 12-16 h. For double immunofluorescence, primary antibodies were applied together. The primary antibodies used were a monoclonal mouse anti-Ankyrin G (Ank G) antibody (Zymed, San Francisco, Ca.) directed against the spectrin binding domain of Ank G, a polyclonal rabbit anti-Na_v1.6 directed against amino acids 1042-1061 of the rat Na_v1.6 protein (Alomone Labs Ltd, Israel), a monoclonal mouse anti-PanNa_v antibody, and a polyclonal rabbit anti-PanNa_v antibody (Sigma-Aldrich, Germany). Both antibodies were raised against amino acids 1491-1508 of the rat Na_v1.1 protein, a sequence identical in all mammalian Na_v α-subunits. The antigen for the polyclonal antibody contained an additional cystein [Noda et al. , 1986]. It should be noted that the polyclonal antibody also produced robust immunolabelling of neuronal somata in the hippocampus, which was absent in labellings with the monoclonal antibody (*compare figure 3-1 with figure 3-2*). Labelling of axon initial segments, however, was similar with both antibodies. Excessive unbound primary antibodies were washed away three times at 20°C for 5 min with PBS. Subsequently, slices were incubated for 2 h at 20°C in darkness with FITC- and CY3-conjugated secondary antibodies (Dianova, Germany). Secondary antibodies were diluted 1:200 in blocking solution and incubated together. Finally the slides were washed again 3 times in PBS for 5 min at 20°C and furnished with cover slips using a 1:1 mixture of Vectashield™ -Harding and Vectashield™ -Harding-with-DAPI cover media (Vector, Burlingame, Ca.). The slides were stored light protected at 4°C.

2.3.1 Analysis of immunohistochemistry

Imaging and quantification of the immunolabeled tissue sections was performed using a Leica (TSC NT) confocal microscope and the LCS software (Leica, Germany) for evaluation of staining intensity. The following laser lines of an argon-krypton laser and filters were used sequentially for each fluorophor. For FITC-coupled antibodies 488 nm, DD 488/568 nm double dichroic, emission bandpass 530 ±30 nm and for CY3-labeled antibodies 568 nm, DD 488/568 nm double dichroic and emission longpass 590 nm. All images were acquired with a PL APO 40.0, 0.75 N.A. objective. For semi-quantitative analysis of immunofluorescence special care was taken to minimize

variability. First, labellings intended for the semi-quantitative assay were always done in one batch incorporating *Scn8a^{wt}* and *Scn8a^{med}* specimens. Secondly, laser power was allowed to settle for at least 1 h prior to the imaging session. All images were taken in one continuous imaging session, where apart from the focal plane all laser and microscope settings remained untouched. The pinhole was set to 0.83 Airy unit and the detector gain to ~60%. To determine mean Na⁺ channel density at axon initial segments, we first defined regions of interest (ROI) corresponding to individual axon initial segments based on the Ank G staining. The mean staining intensity for both the Ank G and the PanNav_v or Nav_v1.6 specific signal was then calculated for this ROI. From each section values for ten axon initial segments were determined. We calculated the intensity of PanNav_v or Nav_v1.6 staining as a ratio of the average intensity in the PanNav_v or Nav_v1.6 channel divided by the corresponding average intensity of the Ank G signal.

2.4 Quantitative real-time RT-PCR

2.4.1 Preparation of cDNA and probes

mRNA was isolated from hippocampal microslices using the Dynabeads mRNA Direct Micro Kit (Dyna, Oslo, Norway) following the manufacturers instruction. Quantification of rat Na⁺ channel transcripts was performed by semi-quantitative real-time RT-PCR (PRISM 7700 SDS, PE Biosystems, Foster City, USA) using specific primers designed with Primer Express Software (PE Biosystems). Sequences of the primers and probes used to determine rat mRNA expression are listed in *table 2* as forward primer (f.p.), reverse primer (r.p.), and hybridization probe (h.p.). The PCRs were performed with the Taqman™ system (*see below*) in a 396 well microtiter plate (Braun, Germany) and each reaction contained the Taqman™ EZ RT-PCR Kit (PE Biosystems, Foster City, CA, USA) and was used for a one-tube, single-enzyme RT-PCR according to the manufacturer's protocol, but in a total reaction volume of 12.5 µl. mRNA isolated and aliquoted as described served as template for RT-PCR. Reaction conditions were optimized for manganese (II) acetate (Mn(OAc)₂) concentration (*see table 2*) and contained 300 µM of each deoxyribonucleosidetriphosphate (dNTP), 100 nM of fluorogenic probe, 1 volume of Taqman™ EZbuffer, 0.1 U/µl rTth DNA polymerase and 0.01 U/µl AmpEraseUNG. Cycling conditions were 50°C (2 min), 60°C (20 min) for the reverse step, followed by 95°C (5 min) and a two-step PCR with 60 cycles of 94°C (15 sec) and 59°C (1 min).

Table 2: RNA probes used in Taqman™ experiments [modified after Ellerkmann et al., 2003].

Gene/ Protein	Probe	[nM]	Mn(OAc) ₂ [mM]
<i>Syp</i> /	f.p. 5'-TCAGGACTCAACACCTCAGTGG-3'	50	5
Synapto- physin	r.p. 5'-AACACGAACCATAAGTTGCCAA-3'	300	
	h.p. FAM-5'-TTTGGCTTCCTGAACCTGGTGCTCTG-3'-TAMRA	100	
<i>Scn1a</i> /	f.p. 5'-AGAAACCCTTGAGCCCGAAG-3'	90	5
Nav _v 1.1	r.p. 5'-CACACTGATTTGACAGCACTTGAA-3'	900	
	h.p. FAM-5'-TTGCTTACTGAAGGCTGTGCAGAG-3'-TAMRA	100	
<i>Scn2a</i> /	f.p. 5'-TCGTTGATGTCTCCTTGGTTAGC-3'	300	3
Nav _v 1.2	r.p. 5'-GGGACTTGATGGCACCAAGT-3'	900	
	h.p. FAM-5'-AACTGCAAATGCCTTGGGCTATTCGG-3'-TAMRA	100	

Scn3a /	f.p.	5'-GCCGCTCCGAGCCTTATC-3'	50	5
Nav1.3	r.p.	5'-GATGGAGGGAATTGCACCAA-3'	300	
	h.p.	FAM-5'-CGCTTTGAAGGCATGAGGGCTATTTCGG-3'-TAMRA	100	
Scn8a /	f.p.	5'-CATCTTTGACTTTGTGGTGGTCAT-3'	300	3
Nav1.6	r.p.	5'-CGGATAACTCGGAATAGGGTTG-3'	100	
	h.p.	FAM-5'-CCATTGTGGGAATGTTCTGGCTG-3'-TAMRA	100	

2.4.2 Analysis of mRNA expression

Relative quantification of starting mRNA copy numbers was achieved through the $\Delta\Delta C_T$ -method [Fink et al. , 1998]. Synaptophysin was used as endogenous reference gene, as it lacks significant expression changes following pilocarpine-induced status epilepticus [Chen et al. , 2001]. The Taqman™ system uses the BE Biosystems PRISM 7700 detection system. The fluorogenic probes [Lee et al. , 1993] are excited with an argon laser (488 nm). Attached to the 5'-end of the probe is a fluorescent dye 6-carboxy-fluorescein (FAM, emission maximum 520 nm) and to the 3'-end a strong quenching substance 6-carboxy-tetramethylrodamine (TAMRA). Utilizing the 5'-endonuclease activity of the *Taq* polymerase the quencher TAMRA is cleaved during the elongation phase and the now free FAM dye emits light. This fluorescence is monitored at the end of the elongation phase of each PCR-cycle. During the first (baseline) PCR cycles fluorescence differs little. As soon as the exponential phase of the amplification is reached the fluorescence starts to rapidly increase. The threshold for detection was set to 10x standard deviation of baseline fluorescence and values for each reaction were measured as triplicates. Fluorescent data was stored within the system. Statistical analysis of mRNA expression was done using a Mann-Whitney U-test with a Bonferroni correction of the significance level to $p < 0.0125$.

2.5 Western blotting of Na⁺ channels

2.5.1 Sample preparation

Frozen CA1 microslices (see *chapter 2.2.2*) were homogenized on ice for 10 s with a labsonic-2000 (B.Braun, Melsungen, Germany) in 30 μ l of buffer A containing 10 mM NaCl, 25 mM 4-(2-hydroxyethyl)-1-piperazineethanesulfonic acid pH 7.5 (HEPES), 2 mM ethylene-diamine-tetra-acetic acid (EDTA), 1 mg/ml PEFA-Block (Roche, Mannheim, Germany), and 2% Sodium Dodecyl Sulfate (SDS). To prevent frothing the homogenator was only switched on and off while submerged in the buffer. Homogenates were centrifugated for 30 min at 18.250xg and 4°C. Protein concentrations of the Triton X-100- and SDS-soluble fractions were determined using the ND-1000 (Nanodrop, Wilmington, DE, USA). According to the protein concentration a portion of the supernatant, buffer A, and 8 μ l loading buffer were mixed to create 40 μ l aliquots with a protein concentration of 1 mg/ml. The loading buffer contained: 700 mM tris(hydroxymethyl)aminomethane-HCL (Tris-HCl), 30% glycerol, 290 mM SDS, 0.012% bromphenol blue and 5% β -mercaptoethanol. Samples were stored at -80°C.

2.5.2 SDS gel electrophoresis and immuno-blotting

SDS gel electrophoresis was performed using the Biorad™ Mini-Chamber system. Each gel consisted of a 4.5 ml resolving gel (10%) below a 2 ml stacking gel (5%) The

resolving gel containing: 1.9 ml Aqua dest., 1.7 ml 30% Acrylamide-mix (Roth), 1.5 ml 1.5 M Tris-HCl (pH 8.8), 50 μ l 10% sodium dodecyl sulfate (SDS), 50 μ l 10% Ammonium-persulfat, and 2 μ l TEMED. The stacking gel (2 ml) containing: 1.4 ml Aqua dest., 330 μ l Acrylamide-mix (Roth), 250 μ l 1 M Tris-HCl (pH 6.8), 20 μ l 10% SDS, 20 μ l 10% Ammonium-persulfat, and 2 μ l TEMED. After casting 10% polyacrylamide gels samples were thawed at RT and resolved on 10% polyacrylamide gels. Following transfer onto nitrocellulose membranes the blots were blocked with 5% non-fat milk (Biorad), 5% horse serum, 0.1% TWEEN-20 in phosphate buffered saline pH 7.4 (PBS-T) for 1-2 h at 20°C, and subsequently incubated with primary antibodies (see below) overnight at 4°C on a Rotator in PBS-T. After three 5-min washes with PBS, the membranes were incubated in the dark for 2 h with the appropriate secondary antibody (1:5000) conjugated to IRDye[®]680 or to IRDye[®]800CW (LI-COR, Lincoln, NE, USA) dissolved in PBS-T containing 0.01% SDS. Excessive antibodies were then washed away three times (5 min) with PBS-T and blots stored protected from light in PBS. After rinsing the blots with distilled water protein bands were visualized using the Odyssey[®] Infrared Imaging System (LI-COR, Lincoln, NE, USA). Primary antibodies used were: a monoclonal Synaptophysin antibody (1:20000; SYSY, Göttingen); a monoclonal Na_v1.2 (1:250; 75-024, Neuromab, CA, USA), a polyclonal rabbit anti-Na_v1.6 directed against amino acids 1042-1061 of the rat Na_v1.6 protein (1:250; ASC-009; Alomone Labs Ltd., Israel), a monoclonal mouse anti-PanNa_v antibody (1:500; 8809, Sigma, Germany) and a polyclonal rabbit anti-PanNa_v antibody (1:500; ASC-003, Alomone Labs Ltd., Israel), both raised against amino acids 1491-1508 of the rat Na_v1.1 protein with the antigen for the polyclonal antibody containing an additional cystein [Noda et al. , 1986], a sequence identical in all mammalian Na⁺ channel α -subunits (Sigma-Aldrich, Germany). Immunoblots were quantified using the AIDA software program (German Resource Center for Genomics, Berlin, Germany). Quantitative analysis was performed by calculating the ratio between the background subtracted Na⁺ channel signal and the background subtracted synaptophysin signal. All signals compared were compared to control protein signals of the same lane from the same gel. Statistical analysis was done using a nonparametric Mann Whitney U-Test with the significance level set to (p<0.05).

2.6 Electrophysiology and computational Modelling

2.6.1 Shared procedures

Patch pipettes with a resistance of 3-5 M Ω were pulled from borosilicate glass capillaries (outer diameter: 1.5 mm, inner diameter: 1 mm; Science Products, Germany) on a Narishige PP-830 puller (Narishige, Tokyo, Japan) and filled with the appropriate intracellular solution (IC). Voltage clamp and current clamp recordings were conducted at 20°C and 30°C, respectively. Data were recorded and stored by a personal computer using a data acquisition system (Digidata 1322A) and the pClamp9.0 software (Molecular Devices, CA). Unless indicated otherwise data were filtered at 10 kHz and digitized at 100 kHz. All command and measured voltages shown were corrected for their liquid junction potentials.

2.6.2 Voltage clamp recordings

Tight seal whole-cell recordings were obtained with a seal resistance >1 G Ω in all recordings using an Axopatch 200B amplifier (Molecular Devices; Ca.). Series resistance was 6 \pm 2 M Ω . To improve voltage control, the prediction and compensation dials of the amplifier's series resistance compensation circuit were set between 70 and 90% to achieve a maximal residual voltage error below 2 mV (<0.5 mV for recordings of I_{NaP} , I_{NaR} and I_{CaT}). All other recordings were discarded. Currents were recorded with the pClamp acquisition and analysis program, sampled at 100 kHz, and filtered at

10 kHz (20 kHz and 1 kHz for I_{NaP}). All potentials shown were corrected for liquid junction potentials. Recording temperature was 20°C for all voltage clamp recordings. Unless otherwise indicated, all chemicals or drugs were obtained from Sigma, Germany.

2.6.3 Determination of passive membrane properties

Passive membrane properties were quantified as follows. The input resistance was determined in voltage clamp mode according to Ohm's law from the steady state current response to 5 or 10 mV voltage steps (200 ms) from a -85 mV holding potential and was not significantly different between the mice from both genotypes ($Scn8a^{med}$ 342.52 ± 79.00 M Ω , $Scn8a^{wt}$ 300.60 ± 25.28 M Ω). Cell capacitance was determined by quantifying the charge (Qc) required to fully charge the membrane. Qc was measured as the total area under the current response to the abovementioned voltage steps, minus the charge flowing across the membrane resistance. Cell capacitance was then calculated as Qc/V, where V is the size of the voltage step ($Scn8a^{med}$ 111.55 ± 15.22 pF, $Scn8a^{wt}$ 100.99 ± 8.23 pF) (n = 12 and n = 22, respectively).

2.6.4 Recording of the transient Na⁺ current

For preparation of dissociated neurons, 400 μ m slices were placed in 5 ml of triturating solution containing [mM]: 145 Na-methanesulphonate, 3 KCl, 10 N-2-hydroxy-ethylpiperazine-N'-2-ethanesulfonic acid (HEPES), 0.5 CaCl₂, 1 MgCl₂, and 15 glucose. Solution pH was adjusted to 7.4 with NaOH. Pronase (protease type XIV; 2 mg/ml) (SIGMA, St. Louis, MO) was added to the oxygenated buffer (100% O₂). After two incubation periods, 10 min at 35°C followed by 10 min at 20°C, slices were washed with pronase-free buffer saline of identical composition and transferred to a Petri dish containing 5 poly-L-lysine coated cover slips. The CA1 region was microdissected under a binocular and triturated with fire-polished glass pipettes of decreasing aperture. Cells were allowed to settle for at least 10 min before removing cover slips and placing them into a submerged chamber mounted on the stage of an upright microscope (Axioskop F-2, Zeiss, Germany). Cells were equilibrated for further 10 min before recordings were attempted. Whole-cell recordings of dissociated neurons were performed only on pyramidal-shaped neurons with a smooth surface and a three dimensional contour. All cells possessed a clearly identifiable apical dendrite and remnants of basal dendrites and the axon.

Voltage clamp recordings of transient Na⁺ current (I_{NaT}) were carried out in dissociated CA1 neurons to obtain a reliable voltage control and to minimize space clamp problems. Even in dissociated neurons the large amplitude of I_{NaT} necessitated a reduction of the Na⁺ gradient between bath and IC solutions. The following solutions were used: IC [mM]: 110 CsF, 10 HEPES-Na, 11 EGTA, 20 tetraethylammonium-Cl, 2 MgCl₂, 0.5 guanosine 5'-triphosphate-tris(hydroxyl-methyl)-aminomethane (GTP-TRIS), and 5 ATP-Na₂. Osmolality was adjusted with sucrose to 295 mOsm; pH to 7.25 with CsOH. The oxygenated bath consisted of [mM]: 30 Na-methanesulphonate, 120 tetraethylammonium-Cl, 10 HEPES, 1.6 CaCl₂, 2 MgCl₂, 0.2 CdCl₂, 5 4-aminopyridine (Acros organics, Belgium), and 15 glucose. The pH was adjusted to 7.4 with HCl. Osmolality was adjusted to 310 mOsm with sucrose, and temperature was maintained at 20 \pm 1°C. The liquid junction potential between intra- and extracellular solution was +10 mV and all values and figures were corrected accordingly.

2.6.5 Recording of the persistent Na⁺ current

Recordings of the persistent Na⁺ current (I_{NaP}) were carried out in intact neurons in the slice preparation with intracellular solution containing [in mM]: 110 CsF, 10 HEPES-Na, 11 EGTA, 2 MgCl₂, 0.5 GTP-TRIS, and 2 ATP-Na₂. Osmolality was adjusted with

mannitol to 295 mOsm; pH was adjusted to 7.25 (CsOH). The bath solution for mice recordings consisted of [in mM]: 100 Na-methanesulphonate, 40 tetraethylammonium-Cl, 10 HEPES, 2 CaCl₂, 3 MgCl₂, 0.2 CdCl₂, 5 4-aminopyridine, and 15 glucose. pH 7.4, NaOH; osmolality was adjusted to 305 mOsm with sucrose. For I_{NaP} recordings performed in rat, bath solution consisted of [in mM]: 50 NaCl, 90 tetraethylammonium-Cl, 3 CsCl, 4 4-aminopyridine, 10 HEPES, 25 glucose, 3.5 KCl, 2 MgCl₂, 2 CaCl₂, and 0.1 CdCl₂. The bath had pH 7.4 and osmolality was 305 mOsm. The liquid junction potential between intra- and extracellular solution was +10 mV and all values and figures were corrected accordingly.

2.6.6 Analysis of voltage clamp recordings of Na⁺ currents

The voltage dependent activation of I_{NaT} was determined using standard protocols (see *figure. 3-3 A*, inset). Peak current amplitude were fitted to the following Boltzmann function:

$$\text{equation 1 } I_{(V)} = G_{\max} / (1 + \exp((V_{1/2} - V)/k_m)) (V - V_{Na}),$$

where $I_{(V)}$ is the current amplitude, G_{\max} is the maximal Na⁺ conductance, $V_{1/2}$ is the membrane potential at which $G_{(V)}$ is half of G_{\max} , V is the command potential, k_m is the slope at $V_{1/2}$, and V_{Na} is the Na⁺ reversal potential.

Peak currents were then converted to conductance $G_{(V)}$ using:

$$\text{equation 2 } G_{(V)} = I_{(V)} / (V - V_{Na})$$

with V_{Na} being the Na⁺ reversal potential, V the command potential and $I_{(V)}$ the current amplitude.

The voltage dependence of steady-state inactivation was determined using standard procedures with prepulses (500 ms) to various voltages, followed by a 10 ms test pulse to 0 mV (see *figure. 3-3 C*, inset). The peak currents were fitted using:

$$\text{equation 3 } I_{(V)} = G_{\max} / (1 + \exp((V_{1/2} - V)/k_m))$$

where G_{\max} is the maximal Na⁺ conductance, $V_{1/2}$ is membrane potential at which $G_{(V)}$ is half of G_{\max} and k_m is the slope at $V_{1/2}$.

To determine the voltage dependent activation of I_{NaP} , the TTX subtracted current responses to the voltage ramp (*figure 3-4 A and figure 3-21 A*) were converted to conductance using *equation 2* and subsequently fitted using *equation 3* (*figure 3-4 C and figure 3-21 C*). In all cases, fitting was done using a Levenberg-Marquardt algorithm.

2.6.7 Recording of T-type Ca²⁺ currents

Recordings of T-type Ca²⁺ currents (I_{CaT}) were carried out in slices which had been preincubated for 1 h in 5 ml oxygenated bath containing: omega-CgTx GVIA (2 μM), omega-CgTx MVIIC (3 μM), omega-AgaTx IVA (0.2 μM) (Biotrend, Germany) and cytochrome C (2 mg/ml) to block N- and P/Q-type Ca²⁺ channels. Following transfer of the slices to the recording chamber, recordings were carried out with intracellular solution containing [in mM]: 105 Cs-methanesulphonate, 25 tetraethylammonium-Cl, 10 HEPES, 5 EGTA, 2 MgCl₂, 2 CaCl₂, 25 sucrose, 4 ATP-Na₂ and 0.3 GTP-TRIS; pH was adjusted to 7.2 with CsOH; osmolality with sucrose to 295 mOsm. The bath solution contained [in mM]: 115 Na-methanesulphonate, 25 tetraethylammonium-Cl, 3.5 KCl, 2 MgCl₂, 2 CaCl₂, 4 4-aminopyridine, 10 HEPES, 25 glucose, 0.005 tetrodotoxin (Biotrend, Germany) and 0.01 nifedipine (pH 7.4, NaOH; osmolality was adjusted to 310 mOsm with sucrose). Liquid junction potential was -5.0 mV.

2.6.8 Analysis of voltage clamp recordings of T-type Ca²⁺ currents

The amplitude of the T-type Ca²⁺ current was determined by fitting the tail current following a 20 ms depolarization with a biexponential function using a Levenberg-Marquardt algorithm (*figure 3-5 A*, inset). Under our recording conditions, the faster deactivating current component represents R-type Ca²⁺ currents, while the slower component is due to deactivation of T-type Ca²⁺ currents [Sochivko et al. , 2002]. The

amplitude corresponding to the slower deactivating component was derived by extrapolation of the fitted curve to the end of the depolarizing voltage step.

2.6.9 Current clamp recordings

For current clamp recordings in intact CA1 neurons in the slice preparation, we used a Multiclamp 700B amplifier (Molecular Devices, CA). Whole-cell configuration was obtained in voltage clamp mode before switching to current clamp mode, where pipette capacitance and bridge balance were monitored and carefully compensated. Cells with naive membrane potential more positive than -60 mV were excluded. Subsequently, membrane potential was clamped to the appropriate level using the slow voltage clamp circuit of the amplifier set to 5 s. The IC solution used was [mM]: 130 K-gluconate, 20 KCl, 10 HEPES, 0.16 ethylene glycol-bis(2-aminoethylether)-N,N,N',N'-tetraacetic acid (EGTA), 2 Mg-adenosine 5'-triphosphate (ATP), and 2 Na₂-ATP; pH was titrated to 7.25 with KOH; osmolality was adjusted to 295 mOsm using sucrose. For bath solution a modified ACSF was used [mM]: 124 NaCl, 3.5 KCl, 26 NaHCO₃, 1.6 CaCl₂, 2 MgCl₂, and 10 glucose (95% O₂ / 5% CO₂). Temperature was maintained at 30 ± 1°C. The liquid junction potential determined for these solutions was -15 mV and all values and figures were corrected accordingly.

2.6.10 Analysis of current clamp recordings

The measured resting membrane potential was not different between *Scn8a^{med}* (-72.80 ± 1.25 mV) and *Scn8a^{wt}* mice (-73.98 ± 0.66 mV). Spike thresholds were determined by measuring the voltage at which the increase in slope of the voltage trace is maximal. This time-point corresponds to the maximum of the second derivation of the voltage trace (d^2V/dt^2) and was determined as the time at which the third derivation of the voltage trace became zero. Spike amplitude was measured as the difference between resting membrane potential and the peak of the spike. The maximal rates of rise and decay were determined as the peak and antipeak of the second derivation of the voltage trace. Spikes during prolonged (600 ms) current injections vary systematically, depending on the time of occurrence during the current injection and the number of prior spikes. We analyzed the first, second and subsequent spikes in an action potential train separately. Analysis of spike parameters for spikes elicited by 4 ms current injection was done using Clampfit 9.0. Repetitive firing was analyzed using an IGOR routine that detected spikes automatically and determined spike properties, such as amplitude, halfwidth, threshold and maximum slopes of rise and decay.

In addition to these parameters, we determined the axo-somatic delay by assessing the delay between the two peaks observed in the second derivation of the voltage trace. This assessment was also carried out with the automated IGOR detection routine. Each automatically analysed spike was subsequently inspected. In some cases, the automated IGOR detection routine failed to detect two peaks because of overlap between the two peaks. In these cases, an estimate of the axo-somatic delay had to be obtained by a manual determination.

The size of the spike afterdepolarization (ADP) was determined by measuring the area under the ADP starting from the beginning of the fast afterhyperpolarization to the time when membrane voltage returned to the holding potential. This delivers a value that incorporates both active and passive portions of the ADP. In order to evaluate the magnitude of the active portion of the ADP, we first estimated the contribution of passive components by obtaining voltage responses to subthreshold current injections of identical duration. These passive voltage responses were scaled so that the peak of the passive response was superimposed to the action potential threshold. The corresponding area approximates the passive response of the neuron and was subtracted from the total ADP area, yielding the active component of the ADP. This analysis could not be applied in current clamp recordings in the rat, since the

subthreshold passive responses recorded are sometimes larger than the ADP [compare Brown & Randall, 2009]. In these recordings the peak voltage of the ADP was chosen as a measure of the ADP.

2.7 Cell-attached recordings of discharge behaviour

To analyze action potentials without perturbation of the intracellular milieu unavoidable in whole-cell patch clamp recordings we investigated action potential firing in the cell-attached configuration [Perkins, 2006]. Acute 300 μm slices (see 2.6.1) were placed in a submerged chamber and perfused with ACSF complemented with the GABA_A antagonist 100 μM picrotoxin (in EtOH final concentration 2‰) and increased extracellular $[\text{K}^+]$ to 3.5 mM. Blocking of synaptic inhibition and change of the K^+ equilibrium potential were done to facilitate the frequency of spontaneous discharges. Borosilicate recording pipettes were pulled with a horizontal microelectrode puller (Sutter instruments, UK) to yield 9-11 M Ω pipettes that were filled with the modified ACSF. Pipettes were then moved to close proximity of the soma and a small suction was applied to form a close contact with the plasma membrane resulting in seal resistances of 80-500 M Ω . Validity of recordings was verified by placing a bipolar tungsten electrode in the stratum radiatum and orthodromically evoking action potential through injection of a charge neutral biphasic 0.5 ms current pulses with a stimulus isolator (AM-Systems, USA).

2.8 Computational modelling of a CA1 pyramidal cell

There are several computational models that mimic the discharge behaviour of CA1 pyramidal cells. In order to investigate the role of Na^+ channels in action potential initiation we used a computational model created by Marie-Therese Horstmann and Dr. Heinz Beck (University of Bonn). The model is based on a pre-existing model of a CA1 pyramidal neuron from which it also derives the neuron's passive properties [Varona *et al.*, 2000]. Both models draw on the exemplary cytoarchitecture proposed by Bannister & Larkmann [1995] (see figure 1-4 A) and utilize the java based program NEURON [Carnevale & Hines, 2006]. It includes three different voltage gated Na^+ currents, five different K^+ currents, four Ca^{2+} currents, the cation unselective hyperpolarization activated H current (I_h), and Ca^{2+} dynamics to account for release of Ca^{2+} from intracellular Ca^{2+} stores [Royeck *et al.*, 2008]. Simulation of a 4 ms current injection of sufficient amplitude into the model cell resulted in the generation of a single action potential of realistic shape typical for CA1 pyramidal neurons (see figure 1-4 B). A more elaborate description of the model can be found in the publication Royeck *et al.* [2008]. The model is available for download at the homepage of the NEURON database in the internet (senselab.med.yale.edu/odordb/eavData.asp?o=115356).

2.9 Statistical analysis and software

All data are presented as average \pm standard error of the mean (SEM). For comparison of means, a two-tailed Student's t-test was performed as appropriate. Differences between axo-somatic spike delay and input-output relations between *Scn8a*^{wt} and *Scn8a*^{med} mice were analyzed by mANOVA. Analysis of changes in protein concentration and mRNA expression was done using a Mann-Whitney U-Test. Comparison of the four groups of I_{NaP} recordings was done using ANOVA. For all tests, the significance level was set at $p < 0.05$. Data analyses were done with the Clampfit 9.0 software (Molecular Devices, CA), Origin 7 (OriginLab, Northampton, MA), IGOR (Wavemetrics Inc., Lake Oswego, OR), SPSS 14.0 (SPSS Inc., USA), Graphpad Prism (Graphpad Software, San Diego, CA), and Excel 2003 on a Windows™ based PC-system (Microsoft, Redmond, WA).

3. Results

3.1 Subcellular distribution of Na⁺ channels in the CA1 region of the hippocampus

The aggregation of Na⁺ channels at the axon hillock and axon initial segment in central nervous system neurons was first described in both the frog and rat retina [Wollner & Catterall 1986]. Later it was shown that Na_v1.6 α -subunits strongly contribute to the observed aggregation of Na⁺ channels at the AIS in different types of neurons of the CNS [Boiko et al. , 2003, Hossain et al. , 2005, Wart & Matthews, 2006b, Van Wart et al. , 2007]. We examined the localization of Na_v1.6 α -subunits in horizontal hippocampal sections of mouse brains using fluorescent double immunolabelling for Ankyrin G (Ank G) and for Na_v1.6. Ankyrin G is a well established marker for AIS that is involved in the targeting of ion channel subunits to the AIS [see for instance Garrido et al., 2003]. In the CA1 region, Na_v1.6 subunits were strongly colocalized with Ankyrin G whereas labelling intensity is much weaker surrounding the AIS (see figure 3-1 A, panel a). This shows that Na_v1.6 is present in high concentration at AIS in the CA1 region of the hippocampus. Additional double immunolabellings with a monoclonal PanNa_v antibody sensitive to all Na⁺ channel α -subunits and the Na_v1.6 antibody revealed the colocalization of both immunolabels at AIS with a strong intensity (see figure 3-1 A, panel b). Hippocampal sections of *Scn8a^{med}* mice were devoid of Na_v1.6 immunoreactivity, but PanNa_v immunoreactive AIS were still present (see figure 3-1 B). To correctly interpret this result it should be noted that the epitope of the polyclonal Na_v1.6 antibody is located in the intracellular linker region between S5 and S6 of domain III and the epitope of the PanNa_v antibodies used resides in the C-terminal region of Na⁺ channel α -subunits. Therefore all observed labelling cannot be attributed to the residual expressed N-terminal part of Na_v1.6 in *Scn8a^{med}* mice.

Na⁺ channel aggregation at AIS persisted in *Scn8a^{med}* mice, as apparent from immunolabellings with the PanNa_v antibody, that produced a robust signal at AIS of *Scn8a^{med}* mice (see figure 3-2 A, compare rightmost micrographs, see also figure 3-1 A b and B). In order to assess Na⁺ channel aggregation at the AIS in more detail, we analyzed the AIS by double immunolabellings with antibodies directed against Ank G and PanNa_v. AIS were present in undiminished numbers in mice of both genotypes and did not appear altered in Ank G immunolabellings (see figure 3-2 A, compare leftmost micrographs). We analyzed the density of Na⁺ channel proteins at *Scn8a^{wt}* and *Scn8a^{med}* mice AIS in a semi-quantitative manner. Double immunolabellings for Ank G and PanNa_v allowed us to demarcate individual AIS in the Ank G channel (see figure 3-2 A leftmost panels, see insets for larger magnification) and to determine the intensity of the PanNa_v immunolabelling within this region of interest (for detailed description see methods chapter 2.3.1, *Scn8a^{wt}*: 8 slices from 5 mice, *Scn8a^{med}*: 10 slices from 5 mice; 10 AIS were analyzed in each slice). Indeed, the ratios of PanNa_v to Ankyrin G immunolabelling intensities at *Scn8a^{wt}* and *Scn8a^{med}* mice AIS were not different (1.5 ± 0.1 and 1.3 ± 0.04 , respectively, *n.s.*; see figure 3-2 B). The lack of a significant reduction in PanNa_v staining at AIS of *Scn8a^{med}* mice suggests that the absence of Na_v1.6 subunits allows other Na_v subunits to accumulate at the AIS.

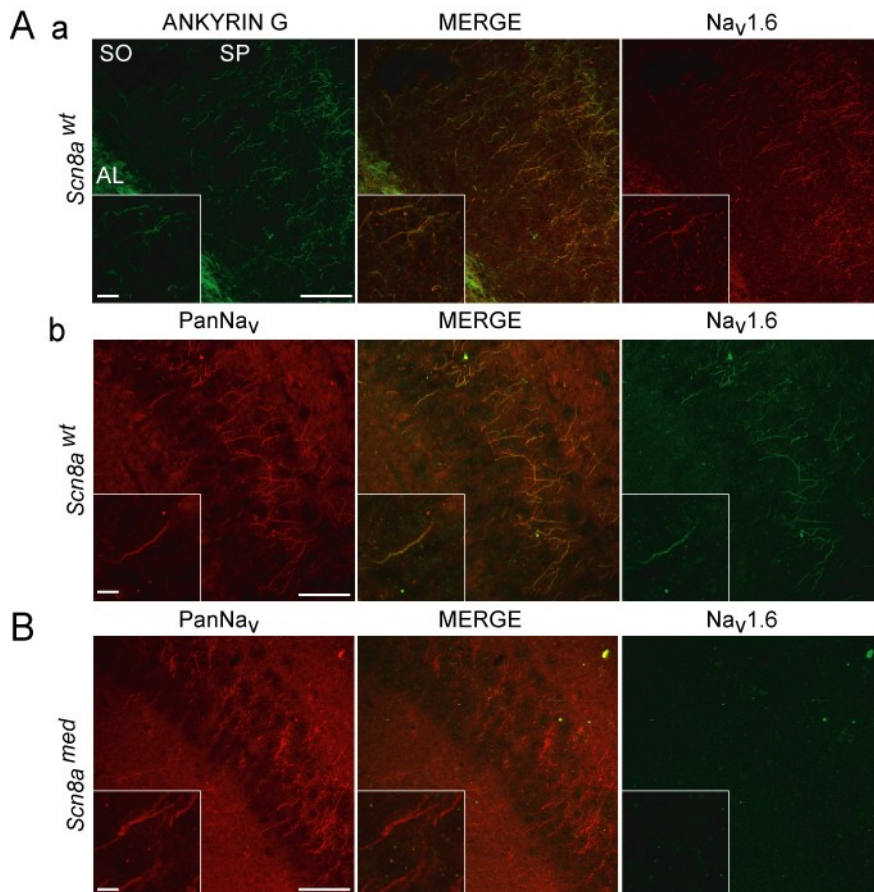


Figure 3-1: Axon initial segment localization of Na⁺ channels in central neurons of *Scn8a*^{med} and *Scn8a*^{wt} mice.

(A), panel a, In *Scn8a*^{wt} animals a monoclonal Ankyrin G (Ank G) antibody, a marker for AIS (green, leftmost panel), colocalizes with a polyclonal antibody directed against Na_v1.6 (red, rightmost panel, merged in the middle panel). The insets (bottom left) in this and the panels (B) and (C) correspond to higher magnifications of individual AIS. Stratum pyramidale (SP), stratum oriens (SO), alveus (AL). **panel b**, Na_v1.6 also colocalizes with the immunolabelling obtained with a monoclonal PanNa_v antibody. **(B)**, Staining pattern for Na_v1.6 and PanNa_v in *Scn8a*^{med} mice. No detectable staining is observed for Na_v1.6, while the PanNa_v antibody yields a pronounced staining of AIS.

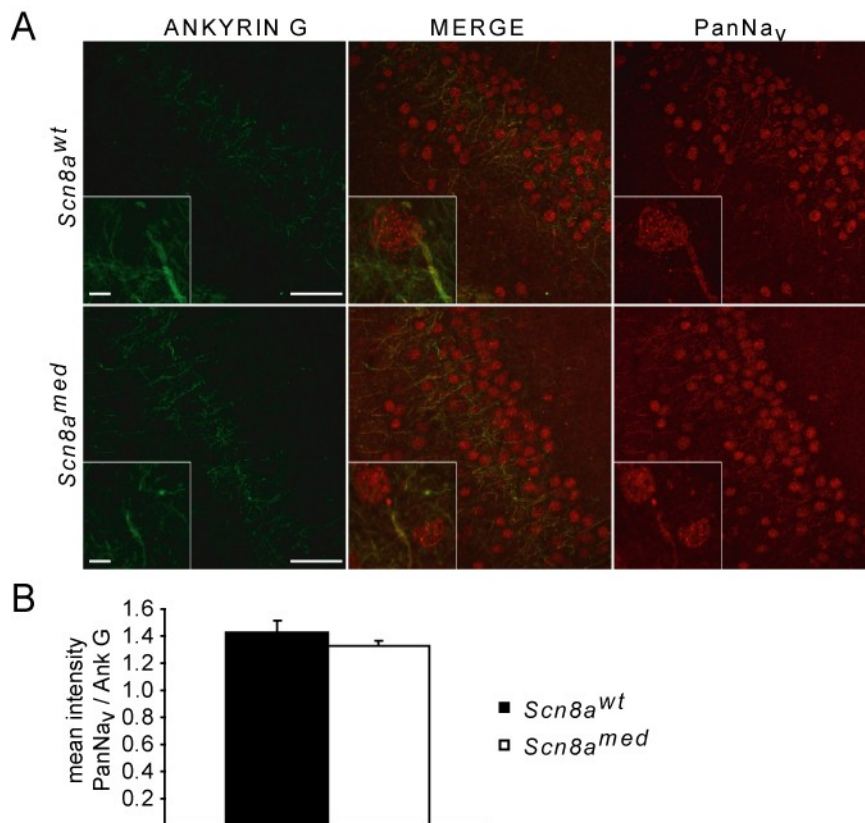


Figure 3-2: Semi-quantitative analysis of fluorescence intensity of PanNav_v relative to Ankyrin G in slices obtained from *Scn8a^{med}* and *Scn8a^{wt}* mice.

(A), Representative examples of double immunofluorescence labelling with the monoclonal Ank G antibody (green) and a polyclonal PanNav_v antibody (red) used for quantification of PanNav_v staining at AIS, in *Scn8a^{wt}* mice (upper panels) and *Scn8a^{med}* mice (lower panels). (B), Average AIS fluorescence intensity of PanNav_v relative to Ank G in *Scn8a^{wt}* mice (black bar, 10 AIS analyzed in each of 8 slices obtained from 5 animals) and *Scn8a^{med}* mice (white bar, 10 AIS analyzed in each of 10 slices obtained from 5 animals, *n.s.*), for a detailed description of the semi quantitative analysis of PanNav_v staining at AIS see methods. Scale bars correspond to 50 μm in main panels and 5 μm in the insets.

3.2 Absence of Nav1.6 positively shifts I_{NaT} activation

It has been hypothesized previously that I_{NaT} at the AIS activates at more negative voltages than I_{NaT} at the soma, causing spikes to commence at or close to the AIS [Colbert & Pan, 2002]. This peculiarity may be due to the selective accumulation of Nav1.6 channels at the AIS. Nav1.6 was shown to activate at more negative voltages than other Na⁺ channels [Rush et al. , 2005]. In these experiments recombinant Nav1.2 or Nav1.6 subunits were expressed in cultured dorsal root ganglion neurons prepared from Nav1.9 deficient mice. The TTX binding site in both recombinant subunits was mutated to render them insensitive to TTX. Since Nav1.9 is the only TTX resistant subunit in DRG neurons, this model allows the characterization of Nav1.2 and Nav1.6 mediated Na⁺ currents in isolation in presence of TTX. Because of these results we hypothesized that the absence of axonal Nav1.6 channels in CA1 neurons would lead to a depolarizing shift in the I_{NaT} activation curve. To test this, we performed whole-cell recordings of I_{NaT} in dissociated CA1 pyramidal neurons of *Scn8a^{wt}* and *Scn8a^{med}* mice (*n* = 6 and *n* = 7, respectively). Cells were held at -70 mV and subjected to depolarizing voltage steps of increasing potentials. Even though we recorded I_{NaT} in dissociated neurons with a reduced Na⁺ concentration gradient to clamp the transient Na⁺ current

sufficiently we still had to exclude approximately 50% of the recordings from analysis due to insufficient voltage clamp. Representative traces of I_{NaT} evoked by increasing voltage steps in $Scn8a^{wt}$ (topmost traces) and $Scn8a^{med}$ (lower traces) neurons are shown in *figure 3-3 A*. From this data we constructed the I_{NaT} activation curve for each of the tested neurons by fitting it with a Boltzmann function (see *methods chapter 2.6.6*). The average peak conductance of I_{NaT} was not significantly different between the groups ($Scn8a^{wt}$: $69.2 \text{ nS} \pm 10.5$, $n = 8$; $Scn8a^{med}$: $59.8 \text{ nS} \pm 6.5$ *n.s.*, $n = 11$). The averaged normalized data and activation curve for each group of neurons is provided in *figure 3-3 B*. We found that the I_{NaT} activation curve was ~ 5 mV more positive in mutant neurons ($V_{1/2} = -25.00 \pm 1.18$ mV) than in wild-type neurons ($V_{1/2} = -29.77 \pm 1.00$ mV, $p = 0.008$; see *figure 3-3 B*). The steepness of the activation curve was not significantly different between the two experimental groups (slope factor $k_m = 5.87 \pm 0.48$ mV for $Scn8a^{wt}$ and $k_m = 5.37 \pm 0.39$ mV for $Scn8a^{med}$ neurons; *n.s.*). Similar results were obtained depolarizing the cells from a holding potential of -80 mV (*data not shown*).

We also compared the two groups of neurons with respect to steady-state inactivation of I_{NaT} . Representative families of I_{NaT} traces evoked by a depolarizing step to 0 mV preceded by 500 ms long prepulses to various potentials in neurons from a $Scn8a^{wt}$ (topmost) and $Scn8a^{med}$ (lower) mouse are shown in *figure 3-3 C* (voltage protocols shown in the inset). From these data we constructed the I_{NaT} steady-state inactivation curve for each of the tested neurons by fitting with a Boltzmann function (see *methods chapter 2.6.6*). The averaged data for each group of neurons is provided in *figure 3-3 D*. In contrast to the marked difference in I_{NaT} activation, steady-state inactivation was similar in the two groups of neurons.

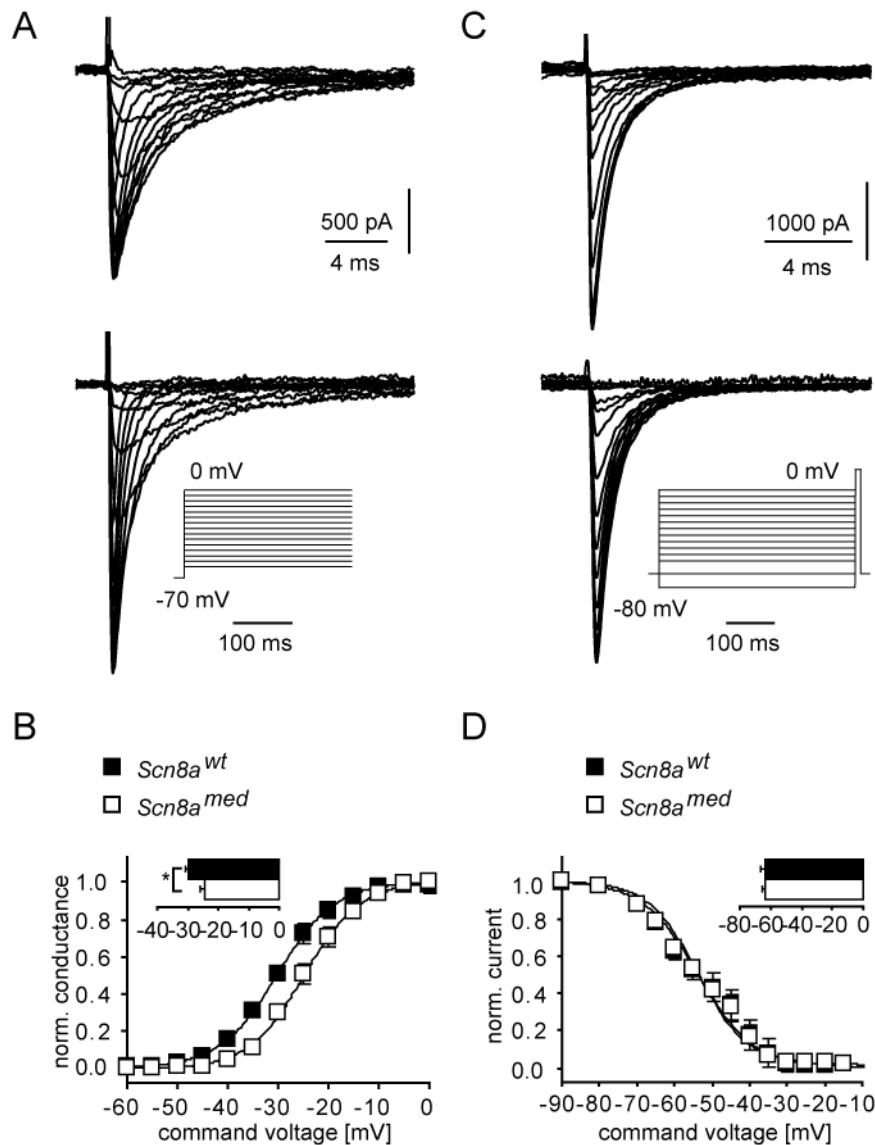


Figure 3-3: Voltage dependence of activation of I_{NaT} in CA1 pyramidal neurons is shifted in the depolarizing direction in $Scn8a^{med}$ mice.

(A), Representative examples of I_{NaT} elicited in dissociated CA1 neurons from a $Scn8a^{wt}$ (top) and a $Scn8a^{med}$ mouse (lower). The voltage paradigm is shown in the inset. (B), Voltage dependent activation of I_{NaT} for $Scn8a^{med}$ mice (open symbols, $n = 7$) and $Scn8a^{wt}$ littermates (closed symbols, $n = 6$). Data from individual cells were fitted with a Boltzmann function (see methods 2.6.6). Boltzmann functions constructed from the average values of $V_{1/2}$ and k_m are superimposed on the depicted data points. The voltage of half-maximal activation $V_{1/2}$ of I_{NaT} was significantly shifted to a more depolarized voltage in $Scn8a^{med}$ mice (see inset). (C), Voltage dependence of inactivation of I_{NaT} . Representative examples of I_{NaT} elicited in dissociated CA1 neurons from a $Scn8a^{wt}$ (top) and a $Scn8a^{med}$ mouse (lower). Voltage paradigm is shown in the inset. (D), Voltage dependence of inactivation was unchanged in $Scn8a^{med}$ mice ($V_{1/2}$ in $Scn8a^{wt}$ and $Scn8a^{med}$ mice indicated in the inset). Boltzmann functions superimposed on the data points as for panel B.

3.3 Absence of $Na_v1.6$ reduces the persistent Na^+ current I_{NaP}

Recombinant $Na_v1.6$ channels expressed in cultured dorsal root ganglion neurons generate a conspicuous persistent Na^+ current (I_{NaP}) component [Rush et al. , 2005],

and published data suggest that these subunits carry a significant proportion of I_{NaP} in different native cell types [Do & Bean, 2004, Maurice et al. , 2001]. Furthermore a large proportion of I_{NaP} was shown to be localized at the proximal axonal or perisomatic region of cortical and CA1 pyramidal neurons using imaging and focal application of TTX [Astman et al. , 2006, Yue et al. , 2005]. I_{NaP} was recorded by applying ramp commands (50 mV/s) to CA1 pyramidal neurons held at -80 mV in acute hippocampal slices (see figure 3-4 Aa). This voltage ramp revealed a prominent inward current corresponding to I_{NaP} that was blocked by application of 0.5 μ M TTX (see figure 3-4 Ab). I_{NaP} was isolated by subtracting recordings in the presence of TTX from control recordings (see figure 3-4 Ac and Ad for $Scn8a^{wt}$ and $Scn8a^{med}$ mice, respectively). Average current parameters, such as maximal I_{NaP} conductance, voltage of half maximal activation and slope factor were determined by fitting the TTX subtracted current trace from each cell to a Boltzmann function (see methods 2.6.6). The maximal conductance determined was 1.9 ± 0.1 nS in $Scn8a^{wt}$ neurons ($n = 11$) and 1.1 ± 0.2 nS in $Scn8a^{med}$ neurons ($n = 16$), corresponding to a reduction of I_{NaP} in the latter group to 58.1% of wild-type levels (see figure 3-4 B). At the same time, the voltage dependence of I_{NaP} was similar in the two groups (see figure 3-4 C; $Scn8a^{wt}$ neurons: $V_{1/2} = -38.6 \pm 2.4$ mV and $k_m = 4.1 \pm 0.3$ mV, $n = 11$; $Scn8a^{med}$ neurons: $V_{1/2} = -39.8 \pm 1.3$ mV and $k_m = 3.4 \pm 0.3$ mV, $n = 16$, n.s.).

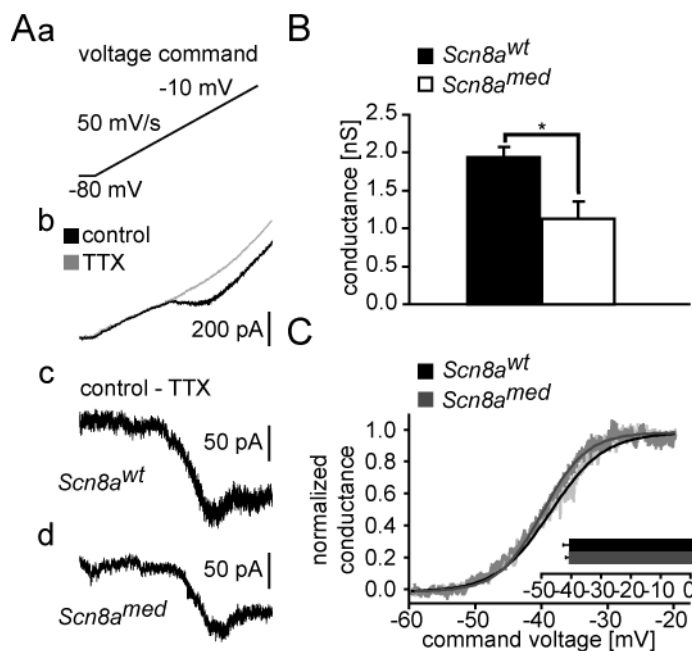


Figure 3-4: Reduction of the persistent Na^+ current (I_{NaP}) in $Scn8a^{wt}$ and $Scn8a^{med}$ CA1 pyramidal neurons.

(A), In recording solutions designed to reduce other types of inward and outward currents (see methods 2.6.5), voltage ramps (50 mV/s, panel a) were applied to elicit I_{NaP} . Panel b depicts current traces elicited under control conditions in an intact CA1 neuron in the slice preparation in a $Scn8a^{wt}$ mouse in the absence (black trace) and presence of 0.5 μ M TTX (grey trace). The TTX-sensitive I_{NaP} was isolated by subtraction (subtracted trace in panel c). A representative TTX subtracted I_{NaP} current trace recorded in a $Scn8a^{med}$ neuron is depicted in panel d. (B), Averaged peak conductances (see methods) obtained from neurons of $Scn8a^{wt}$ and $Scn8a^{med}$ mice ($n = 11$ and $n = 16$, respectively). I_{NaP} amplitude was reduced to 58.1% of wild-type littermate I_{NaP} amplitude in mutant mice. (C), Voltage dependence of activation of I_{NaP} was derived from individual current traces converted to conductance (see methods 2.6.6), and averaged for $Scn8a^{wt}$ (grey, $n = 11$) and $Scn8a^{med}$ neurons (light grey, $n = 16$). Superimposed fit curves were constructed from the averaged fit parameters derived for $Scn8a^{med}$ (dark grey) and $Scn8a^{wt}$

mice (*black*). Neither the voltage of half-maximal activation $V_{1/2}$ nor the slope factor k_m of I_{NaP} is significantly affected by the absence of functional $Na_V1.6$ channels.

3.4 Lack of compensatory changes in I_{CaT}

Homeostatic or compensatory changes can occur following the ablation of a protein. For example a downregulation of $Na_V1.1$ and an upregulation of $Na_V1.3$ are observed in the Na^+ channel β_1 -subunit knockout mouse [Chen et al. , 2004]. The absence of $Na_V1.6$ in $Scn8a^{med}$ mice has been shown to lead to upregulation of $Na_V1.2$ [Vega et al. , 2008]. Furthermore, compensatory regulation can also include less related proteins. In $Scn8a^{med}$ mice a compensatory increase of another subthreshold inward current was reported in Purkinje neurons of the cerebellum. In these cells upregulation of T-type Ca^{2+} currents (I_{CaT}) was found by analyzing the currents active between two spikes during repetitive firing [Swensen & Bean, 2005]. To test if such a regulation of Ca^{2+} currents also occurs in CA1 pyramidal neurons we isolated I_{CaT} current pharmacologically in intact CA1 neurons in the slice preparation using a cocktail of Ca^{2+} channel blockers and TTX (see *methods* 2.6.7). T-type currents were discriminated by analyzing the tail currents following different conditioning pulses back to -95 mV. On the basis of their slow deactivation kinetics in these Ca^{2+} tail current recordings T-type Ca^{2+} currents can be discriminated from the fast deactivating R-type currents (*compare figure 3-5 A*)[Sochivko et al. , 2002]. T-type current amplitudes in CA1 were not different at all tested conditioning pulse voltages (see *figure 3-5 B*). For instance, average maximal current amplitudes were -388.51 ± 55.9 pA in $Scn8a^{med}$ ($n = 8$) and -373.30 ± 106.7 pA in $Scn8a^{wt}$ neurons ($n = 7$).

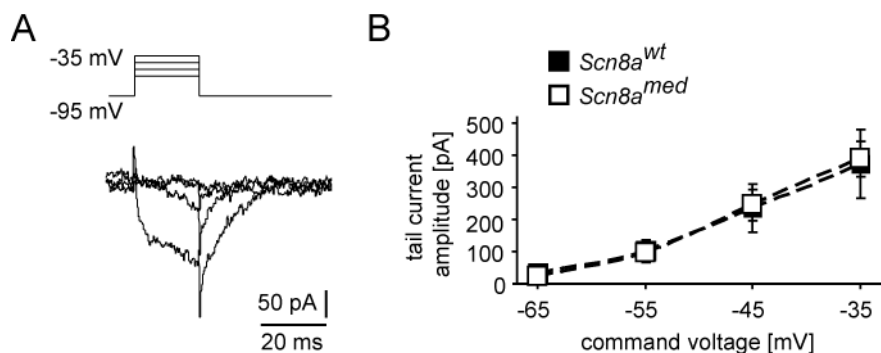


Figure 3-5: T-type Ca^{2+} (I_{CaT}) current amplitude is unaltered in CA1 pyramidal cells of $Scn8a^{med}$ mice.

(A), Ca^{2+} currents were elicited under recording conditions designed to block Na^+ and K^+ currents, and to maximize the contribution of I_{CaT} to the inward currents (see *methods chapter 2.6.7 for exact description*). Under these conditions, compound Ca^{2+} tail currents consisting mainly of R-type and T-type currents were elicited following brief (20 ms) depolarizations, with the slow component reflecting I_{CaT} (*voltage protocol see inset*). (B), Amplitude of I_{CaT} was not different in $Scn8a^{med}$ ($n = 8$) compared to $Scn8a^{wt}$ ($n = 7$) mice at any of the conditioning pulse voltages.

3.5 Reduced spontaneous firing in the absence of functional $Na_V1.6$ subunits

What influence has the lack of functional $Na_V1.6$ subunits causing a 40% reduction in I_{NaP} and a ~ 5 mV depolarized shift in the voltage dependence of activation on the discharge behavior of CA1 pyramidal cells? In a first set of experiments we performed cell-attached recordings on CA1 pyramidal cells in the acute slice preparation. In this configuration action potentials can be reliably recorded without perturbation of the

intracellular milieu [Perkins, 2006]. Spontaneous action potential firing is sparse in the acute slice preparation, an observation we also made in both wild-type and mutant animals (*data not shown*). To enhance the frequency of spontaneous discharges, we blocked synaptic inhibition by including the GABA_A-receptor-antagonist picrotoxin into the recording solution. Since this was not sufficient to evoke spontaneous spiking in *Scn8a^{med}* neurons we furthermore elevated the extracellular K⁺ levels, thereby depolarizing the resting potential of neurons throughout the slice. Under these conditions firing frequency in *Scn8a^{med}* neurons was still dramatically decreased (0.2 ± 0.1 Hz; $n = 12$) compared to neurons recorded from *Scn8a^{wt}* mice (1.8 ± 0.2 Hz, $n = 14$, $p < 0.01$). Quality of the recordings and propensity of the cell to fire action potentials was verified using synaptic stimulation through an electrode placed in the stratum radiatum. The shape of the recorded spikes (see figure 3-6 A, B, E, and F) is influenced by the resistance between the ACSF filled pipette and the neuron's plasma membrane as well as by the shape and capacitance of the recording pipette. Because of this variability we refrained from quantitative analysis of the shape of individual action potential currents. However, in both genotypes the down stroke of the spikes displays a clear biphasic shape caused by the back-propagation of the axonal spike into the soma (see figure 3-6 A and B) [Coombs et al. , 1957, Yu et al. , 2008]. From this attribute seen in all recordings we concluded that in pyramidal cells of *Scn8a^{med}* and *Scn8a^{wt}* mice an action potential initiation zone must exist.

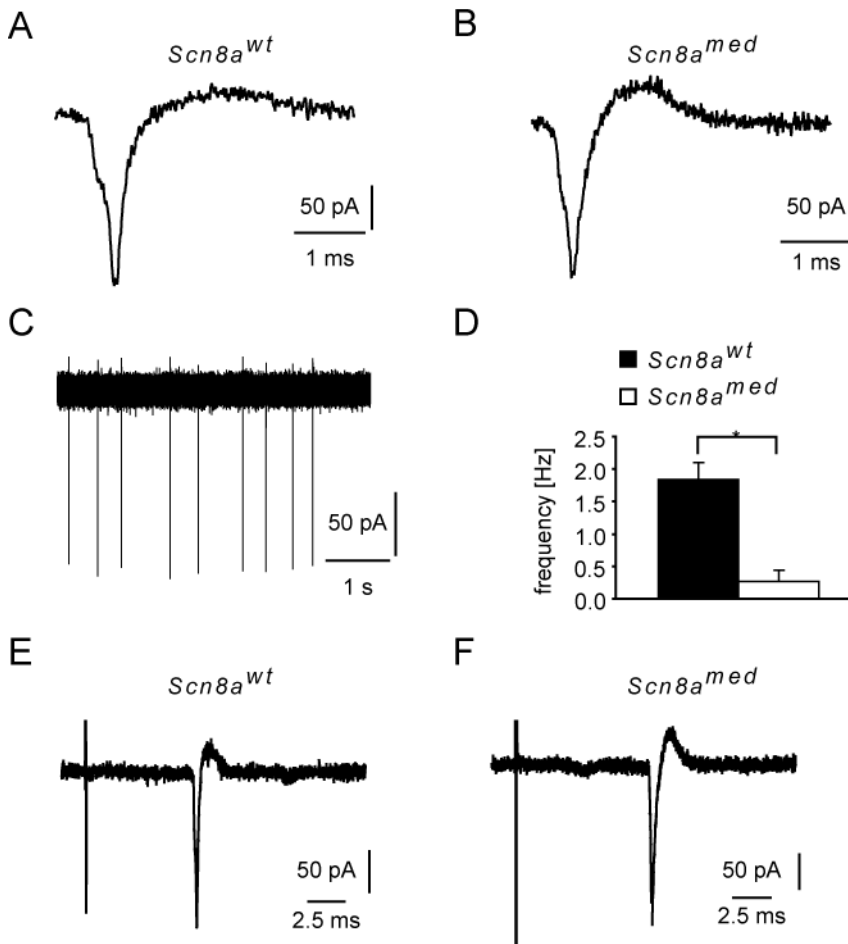


Figure 3-6: Discharge behavior of *Scn8a^{wt}* and *Scn8a^{med}* neurons recorded in cell-attached configuration

(A) and (B), Representative cell-attached recordings of spontaneous occurring spikes in *Scn8a^{wt}* and *Scn8a^{med}*, respectively. In these recordings extracellular K⁺ was elevated to 5 mM and synaptic inhibition was blocked by 100 μ M picrotoxin. (C), Example of continuous sponta-

neous firing in a *Scn8a^{wt}* neuron. **(D)**, Average spontaneous firing frequency is strongly reduced in CA1 neurons lacking Na_v1.6 (1.8 ± 0.2 Hz in *Scn8a^{wt}*, closed symbols, $n = 14$ and 0.2 ± 0.1 Hz in *Scn8a^{med}* open symbols $n = 12$ $p < 0.01$). **(E) and (F)**, Synaptically triggered spikes could be reliably evoked by current injections through a bipolar stimulation electrode placed in stratum radiatum in all recordings of *Scn8a^{wt}* and *Scn8a^{med}* neurons, respectively.

3.6 Na_v1.6 subunits contribute to setting spike threshold in CA1 pyramidal cells

To analyze how the changes in the active intrinsic membrane properties influence the discharge patterns of CA1 pyramidal cells in more detail we performed whole-cell current clamp recordings in the slice preparation. From the pronounced depolarizing shift in the voltage dependence of the transient Na⁺ current (I_{NaT}) and the strong reduction in the spontaneous firing frequency we hypothesized to find a depolarized spike threshold in *Scn8a^{med}* mice. To test this we elicited spikes by intracellular injection of brief (4 ms) depolarizing square current pulses from a membrane potential of -80 mV imposed with slow voltage clamp (see *methods and figure 3-7 A and B*). Spike thresholds were significantly more depolarized in *Scn8a^{med}* (-56.7 ± 1.0 mV, $n = 14$) compared to *Scn8a^{wt}* (-60.4 ± 0.9 mV $n = 22$). This corresponds to a statistically significant +3.7 mV shift (see *figure 3-7 C*; $p = 0.011$). Changes of similar magnitude were also observed when spikes were elicited from other holding potentials in the range of -65 to -80 mV (see *figure 3-7 D*), and for instance, amounted to +4.9 mV for spikes elicited from -70 mV. In contrast, spike amplitude and the maximal rate of depolarization during spike upstroke were the same in the two groups of neurons (118.5 ± 0.4 mV and 419.6 ± 5.1 mV/ms in *Scn8a^{wt}* and 117.7 ± 0.7 mV and 405.9 ± 5.8 mV/ms in *Scn8a^{med}* neurons, *n.s.*), as expected from the lack of difference in maximal Na⁺ conductance (see *results 3.2*). However, we did find a statistically significant increase in the maximal rate of spike repolarization in *Scn8a^{med}* versus *Scn8a^{wt}* neurons (-86.2 ± 1.9 mV/ms versus -78.2 ± 2.0 mV/ms, respectively, for spikes evoked from a holding potential of -80 mV; $p = 0.007$).

The increase of the spike threshold was also found during repetitive neuronal firing elicited by prolonged (600 ms) depolarizing current pulses (see *figure 3-7 E and F*). We analyzed the threshold of the first nine spikes separately (see *figure 3-7 G*). This analysis also revealed a significantly more depolarized spike threshold for all spikes in *Scn8a^{med}* mice. A potential confounding factor in this analysis is that the time of occurrence of spikes after onset of the current injection could be different between *Scn8a^{wt}* and *Scn8a^{med}* mice. However, except for the first spike in a train which occurred significantly earlier after the onset of the current injection, the time-points at which subsequent spikes occurred were not significantly different (see *figure 3-7 H*). Thus, the spike history was well comparable between *Scn8a^{wt}* and *Scn8a^{med}* mice using this form of analysis. Additional analysis in which spikes were binned according to the time of their occurrence after the onset of current injection (*bin width 100 ms*) also yielded comparable results: spike thresholds in *Scn8a^{med}* neurons were significantly more positive than those of *Scn8a^{wt}* for all bins (*data not shown*). Collectively, these results support the notion that the high density of Na_v1.6 channels at the AIS contributes to its low spike threshold.

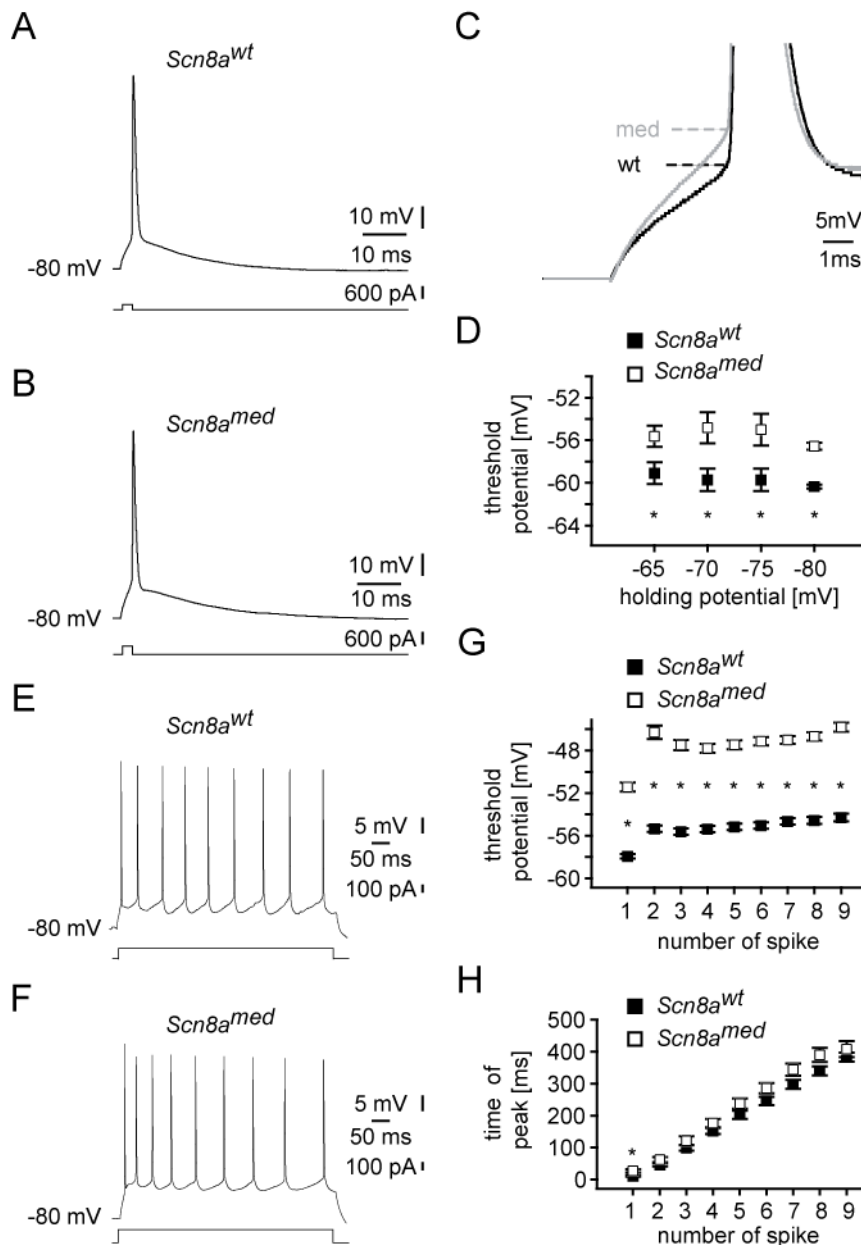


Figure 3-7: Spike threshold of CA1 pyramidal neurons recorded in the slice preparation is increased in *Scn8a^{med}* mice.

(A) and (B), Example traces of spikes elicited by brief (4 ms), just suprathreshold current injection recorded in a *Scn8a^{wt}* (panel A) or *Scn8a^{med}* mouse (panel B). Lower traces depict the corresponding current injection. Slow current clamp was used to set the membrane potential to -80 mV. **(C)**, Overlay of the two representative traces shown in panels A and B at higher magnification to illustrate the difference in spike threshold more clearly (grey trace: *Scn8a^{med}*). **(D)**, Average values obtained for the spike threshold with short current injections (cf. panels A and B) in *Scn8a^{med}* (open symbols, $n = 14$) and *Scn8a^{wt}* mice (closed symbols, $n = 22$). The difference in threshold was significant at all membrane potentials given (asterisks). **(E) and (F)**, Example traces of spikes elicited with prolonged current injection (600 ms). **(G)**, Average values for spike thresholds obtained during prolonged current injections (c.f. panels E and F). The first nine spikes were analyzed binned according to their spike history. As for brief current injections, the spike thresholds were significantly different between genotypes within all bins. **(H)**, Average values for the time of spike occurrence following the current injection according spike history. Only the first spikes elicited occurred significantly later in *Scn8a^{med}* neurons.

3.7 Spike afterdepolarization in CA1 pyramidal cells lacking $\text{Na}_v1.6$

In both developing and adult rat CA1 pyramidal cells, action potentials actively repolarize to a potential about 10 mV positive to their resting potential. From this potential, referred to as the fast afterhyperpolarization (fAHP), the membrane potential increases, thus creating an afterdepolarization (ADP) [Jensen et al. , 1996]. The ADP is normally "boosted" by low threshold activated inward currents, namely I_{NaP} and the I_{CaT} . Subsequently, the cell returns to its resting membrane potential over the course of tens to hundreds of milliseconds [Chen et al. , 2005, Yue et al. , 2005]. Since we found a reduction in I_{NaP} , in $\text{Scn8a}^{\text{med}}$ neurons, we expected a reduction of the size of the spike ADP, which we measured as the area under the curve (see methods 2.6.10). To evaluate the contribution of I_{NaP} and I_{CaT} to the somatic spike ADP (the active ADP component), we subtracted from the native ADP the putative passive component, obtained by evoking in the same neuron a subthreshold voltage response and scaling its amplitude so that its initial peak coincides with the spike threshold (see methods chapter 2.6.10; figure 3-8 A and B, see overlay of scaled subthreshold trace and spike ADP in figure 3-8 C). Intriguingly, this analysis revealed that the active ADP component in Scn8a^{wt} ($168.3 \pm 6.8 \text{ mV}\cdot\text{ms}$, $n = 22$) and $\text{Scn8a}^{\text{med}}$ neurons ($149.3 \pm 11.3 \text{ mV}\cdot\text{ms}$, $n = 14$) was the same (*n.s.*; action potentials elicited from -80 mV).

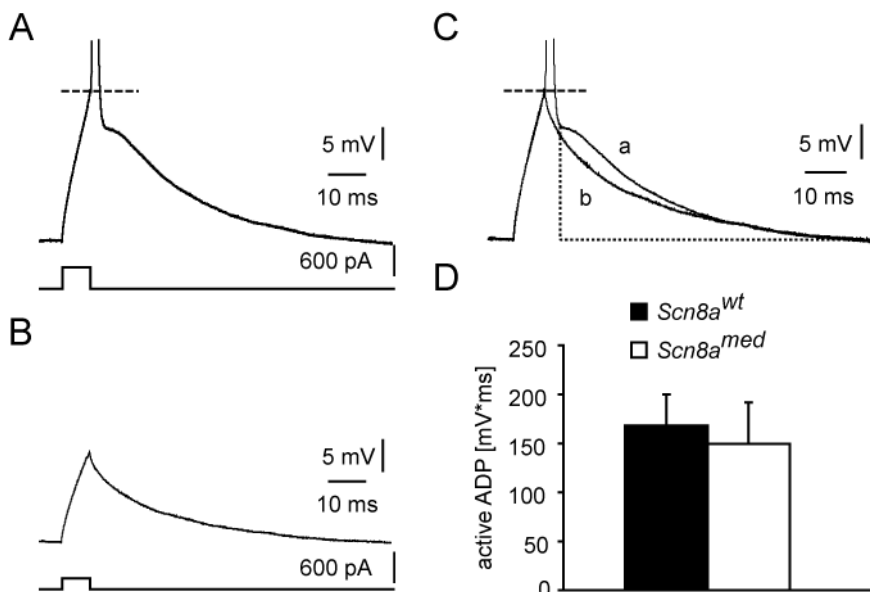


Figure 3-8: The spike afterdepolarization in $\text{Scn8a}^{\text{med}}$ and Scn8a^{wt} mice.

The active portion of the spike afterdepolarization (ADP) is not significantly reduced in $\text{Scn8a}^{\text{med}}$ mice. (A), Action potential recorded from a $\text{Scn8a}^{\text{med}}$ mouse displaying a pronounced ADP. Lower trace depicts the corresponding current injection. The dashed line indicates the voltage of the spike threshold. (B), Response to a subthreshold current injection used to determine the passive component of the ADP. (C), In order to quantify the active part of the ADP the subthreshold response (depicted in panel B) was scaled that the peak of the subthreshold response corresponds to the spike threshold (trace b). The area of the active component of the ADP was determined by subtracting the area under trace b from the total area of the ADP under trace a. Areas were measured starting from the maximum of the fast afterhyperpolarization to the time-point at which the membrane voltage returned to holding potential (indicated by dotted lines). (D), Magnitude of the active ADP was not significantly altered in $\text{Scn8a}^{\text{med}}$ mice ($n = 14$) compared to Scn8a^{wt} littermate controls ($n = 22$, *n.s.*).

3.8 Na_v1.6 subunits contribute to spike gain

In the cell-attached recordings (see figure 3-6 D) *Scn8a^{med}* spontaneous firing frequency was significantly reduced. This could be attributed to the depolarizing shift in the spike threshold and the diminished resurgent Na⁺ current [Raman & Bean, 1997, Raman et al. , 1997, Royeck et al. , 2008]. Both factors would be expected to conspire in order to reduce spike gain of CA1 neurons in *Scn8a^{med}* mice. In contradiction to this a reduced I_{NaP} was also reported to attenuate spike gain [Vervaeke et al. , 2006b]. Using dynamic clamp Vervaeke et al. [2006b] described an increase in spike gain following a dynamic clamp subtraction of I_{NaP} . The authors attributed this finding to an increase in Na⁺ channel inactivation due to the additional depolarization mediated by I_{NaP} . To elucidate which influence the lack of functional Na_v1.6 subunits has on spike gain, we elicited spikes in *Scn8a^{med}* ($n = 5$) and *Scn8a^{wt}* ($n = 7$) neurons by applying prolonged (600 ms) depolarizing current pulses of increasing magnitude (from 20 to 120 pA) in whole-cell current clamp recordings (see figure 3-9 A and B, respectively). In this context it should be mentioned, that the average passive membrane properties do not differ between both genotypes (see methods 2.6.1). Examination of the relation of current injection to the corresponding number of spikes yielded a significantly shallower increase in spike rate in *Scn8a^{med}* compared to *Scn8a^{wt}* neurons ($p < 0.01$; see figure 3-9 C).

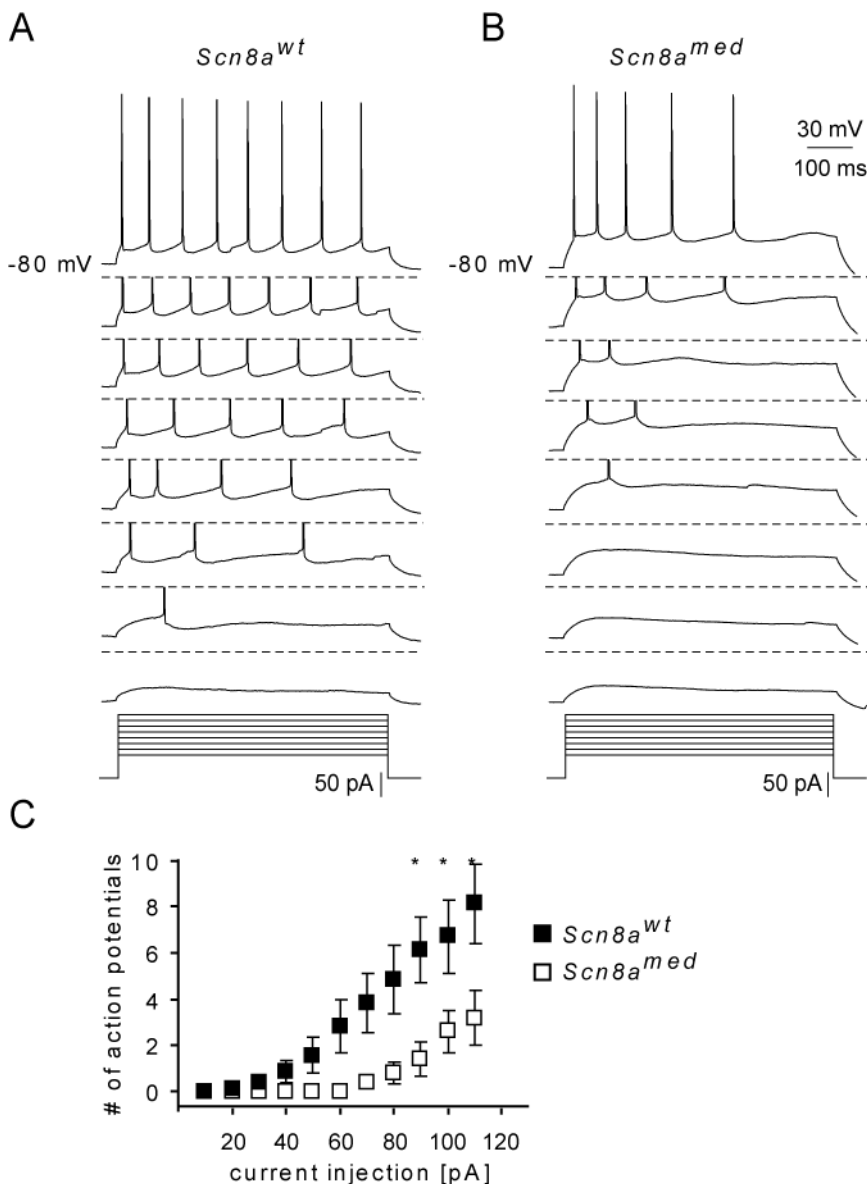


Figure 3-9: The gain of CA1 neurons is decreased in the absence of $Na_v1.6$ channels

(A) and (B), Example traces of spikes elicited by current injections (600 ms) of increasing magnitude from a holding potential of -80 mV. Some traces are truncated at -45mV (*dashed line*). Spike frequencies increase in both $Scn8a^{wt}$ and $Scn8a^{med}$ mice, but the increase is considerably less pronounced in $Scn8a^{med}$ mutant mice. **(C)**, Quantification of the average spike gain of CA1 neurons by plotting the number of spikes during the 600 ms current injection versus the magnitude of the current injection ($Scn8a^{wt}$, $n = 7$ and $Scn8a^{med}$, $n = 5$, $p < 0.01$).

3.9 $Na_v1.6$ subunits contributes to action potential initiation

Spike initiation occurs within the axon in most types of cortical neurons [Colbert & Pan, 2002, Khaliq & Raman, 2006, Palmer & Stuart, 2006, Stuart et al. , 1997, Stuart & Häusser, 1994, Stuart & Sakmann, 1994], and more precise attempts of localization have revealed an initiation site at the most distal portion of the AIS in layer 5 cortical pyramidal neurons [Palmer & Stuart, 2006] and CA3 pyramidal neurons [Meeks & Mennerick, 2007]. In action potentials elicited by prolonged current injection, phase plots (dV/dt versus V) allowed to distinguish a first phase of spike upstroke due to spike propagation from the AIS into the soma [McCormick et al. , 2007, Shu et al. , 2007], and a second phase, caused by the somatic spike (*see figure 3-10 A and B*). This phenomenon was observed both for the first spike as well as for later spikes (*see figure 3-10 Aa: 1st spike in train and figure 3-10 Ba, 5th spike in train, multiple spikes from individual cells are shown*). The initiation of spikes in $Scn8a^{wt}$ neurons ($n = 7$; *see figure 3-10 Ab and Bb, upper panels*) appeared more abrupt than in $Scn8a^{med}$ mice ($n = 5$; *see figure 3-10 Ab and Bb, lower panels*). This abrupt initiation was previously described in neocortical neurons as ‘kink’ and is a consequence of the invasion of the soma by the axonal spikes [McCormick et al. , 2007, Shu et al. , 2007]. The abruptness of the voltage change at the onset of a spike can be quantified as a maximum of the second derivation of the voltage trace. We calculated the second derivation of the voltage traces as described by Coombs *et al.* [1957]. Representative results are depicted in *figure 3-11*. Panel *Aa* and *Ba* show the voltage trace, first derivation (*black trace*) and second derivation (*grey trace*) are shown in panels *Ab* and *Bb*. The two peaks in the second derivation, corresponding to the rate of change of (dV/dt), are due to a first (*axonal*) and a second (*somatic*) component. Amplitude of the first peak in the second derivation was significantly smaller in $Scn8a^{med}$ neurons, regardless of which spike in a train was evaluated (*see figure 3-11 C*). Comparable results were obtained when action potentials were binned into 100 ms bins according to the time of occurrence after onset of the current injection (*data not shown*).

The two consecutive peaks in the second derivation of the voltage trace reflect axonal and somatic spike initiation. The temporal delay between them (t_{del}) is a measure for the time from the initiation of the action potential at the AIS to its arrival at the soma. We examined how t_{del} varied during repetitive spiking evoked by prolonged (600 ms) depolarizing current pulses. For this analysis we again analyzed the 1st, 2nd, and subsequent spikes separately. We found that t_{del} was significantly larger in $Scn8a^{med}$ compared to $Scn8a^{wt}$ mice ($p < 0.01$, *comparisons of individual data points with t-test indicated by asterisks in figure 3-11 D*). The lack of difference for the 1st spike in a train may be related to the different latency of occurrence after onset of the current injection for the first spike only (*see figure 3-7 H*). Comparable results were obtained when spikes were binned into 100 ms bins according to the time of occurrence after onset of the current injection (*significantly longer t_{del} for all except the initial bin, data not shown*). This type of analysis was not performed for single spikes elicited with 4 ms current injections because the spike upstroke was strongly

contaminated to different degrees in different cells by the voltage transient induced by the current injection step.

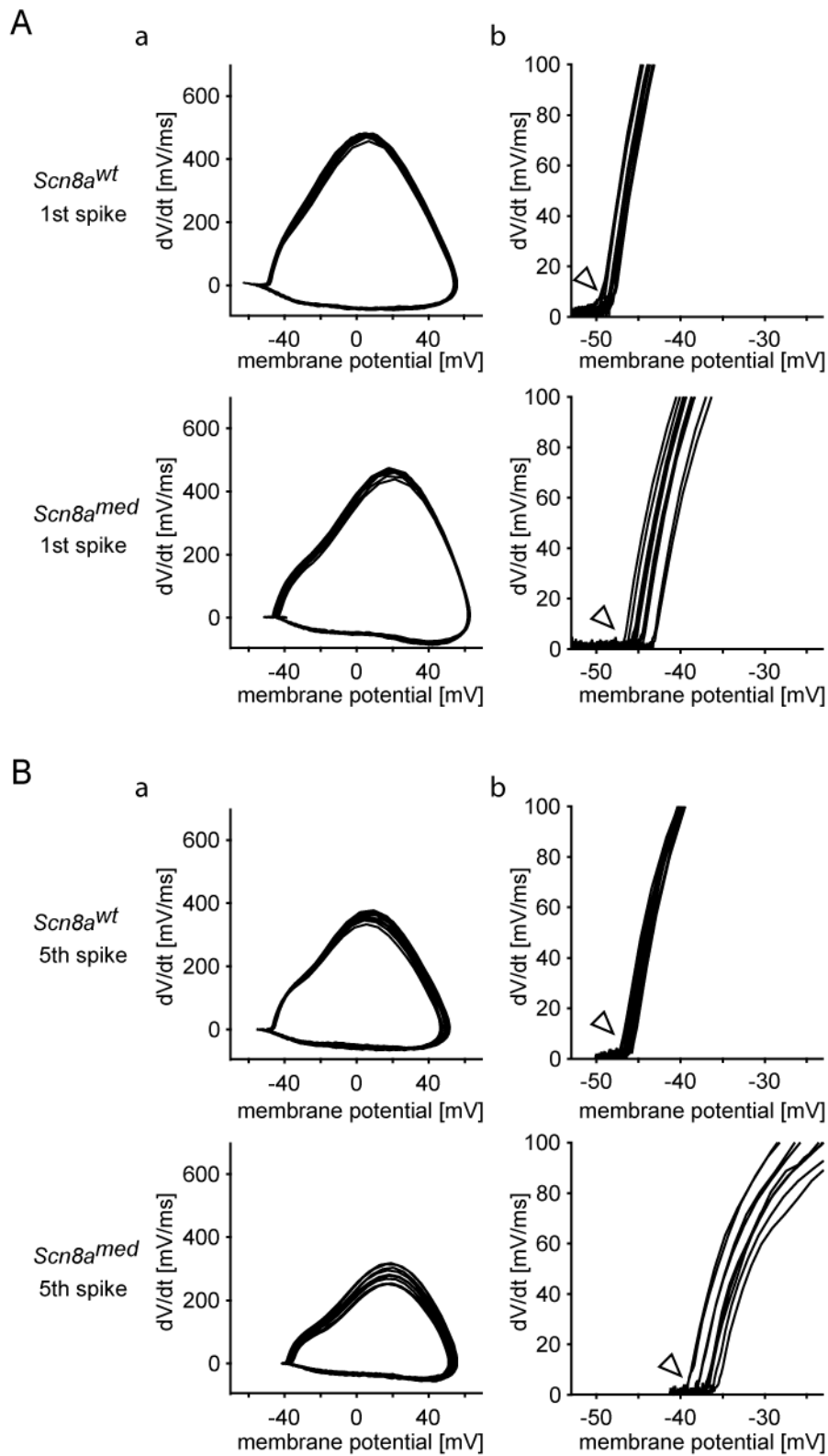


Figure 3-10: Spike initiation in *Scn8a^{wt}* and *Scn8a^{med}* mice.

Phase plots of dV/dt versus V for all the 1st (Aa) and 5th (Ba) spikes generated in a *Scn8a^{wt}* (top panel) and a *Scn8a^{med}* neuron (lower panel). Note the nonmonotonous ascending phase of the spikes, suggestive of two underlying components. (Ab) and (Bb), Sections of the corresponding phase plots representing spike initiation shown with higher resolution. Note the abrupt

rise of dV/dt in $Scn8a^{wt}$ ('kink' indicated by arrowheads, *Ab* and *Bb* top panels) that appears much less pronounced in $Scn8a^{med}$ mice (*Ab* and *Bb* lower panels).

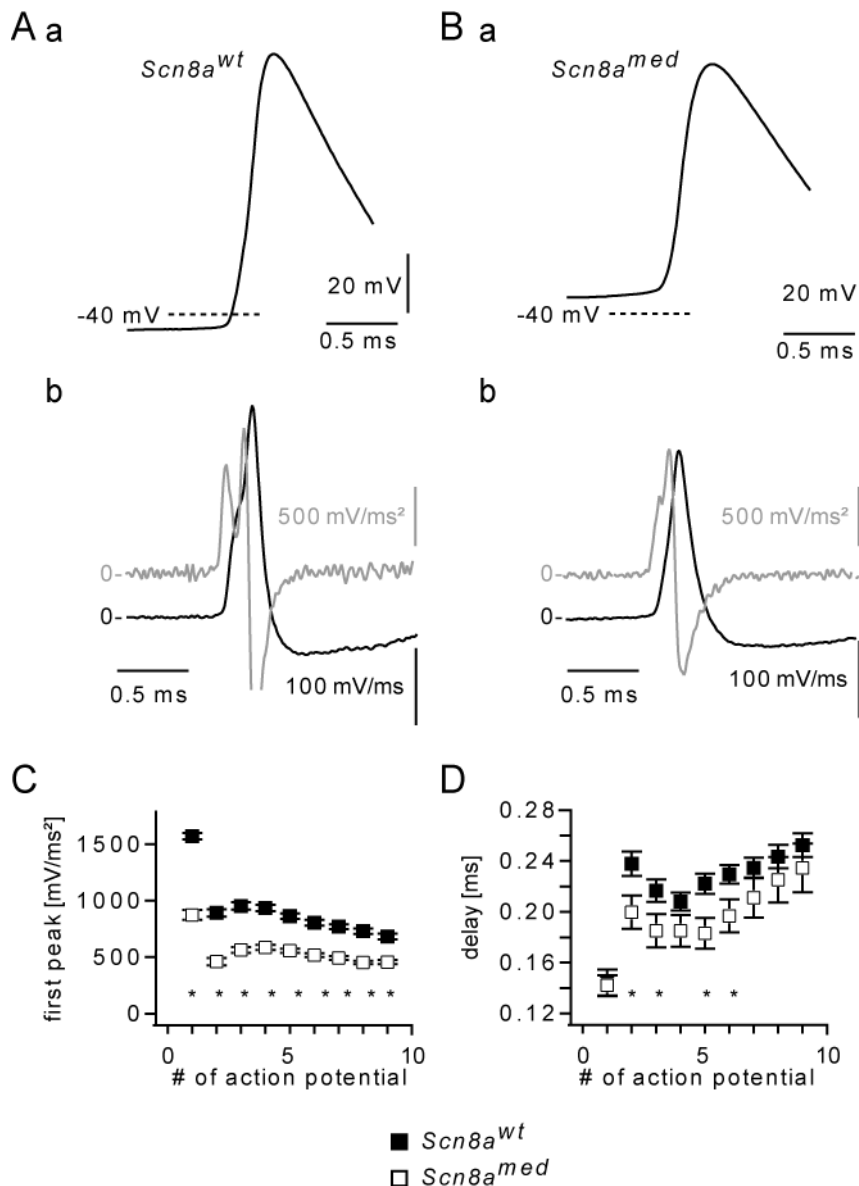


Figure 3-11: Altered delay between axonal and somatic components and steepness of spike initiation in $Scn8a^{med}$ and $Scn8a^{wt}$ mice.

(Aa) and (Ba), representative traces of a fifth spike from a $Scn8a^{wt}$ (A) and $Scn8a^{med}$ mouse (B). **(Ab) and (Bb)**, First and second derivation of the voltage traces shown in panels *Aa* and *Ba*. The second derivation is depicted in grey. Note the occurrence of two consecutive peaks in both cases, with a smaller temporal delay in the CA1 neuron from a $Scn8a^{med}$ mouse. **(C)**, The amplitude of the first (axonal) peak in the second derivation of the voltage trace is significantly decreased in $Scn8a^{med}$ mice (compare figure 3-11 *Ab* and *Bb*), as expected from the less abrupt rise of the initial phase of the spike in $Scn8a^{med}$ mutant compared to $Scn8a^{wt}$ neurons. **(D)**, Quantitative analysis of the delay (t_{del}) between axonal and somatic component in $Scn8a^{wt}$ and $Scn8a^{med}$ mice. t_{del} was determined as the latency between the 1st and 2nd peak of the second derivation of the voltage traces. Spikes were binned depending on their spike history. The latency t_{del} was significantly shorter for the second, third, fifth, and sixth spike analyzed in the spike train.

3.10 Computer simulations of spike initiation at the AIS

Our electrophysiological results described above strongly suggest that in CA1 pyramidal cells the high density of $\text{Na}_v1.6$ channels imposes a low spike threshold at the AIS and thereby localizes spikes initiation to this region. Another factor influencing spike threshold and spike trigger zone is the overall Na^+ current density at the AIS and at the soma. Studies using cell-attached patch-clamp recordings to compare I_{NaT} densities at AIS *versus* somatic membranes have reported either equal [Colbert & Johnston, 1996, Colbert & Pan, 2002] or a much higher [Kole et al. , 2008] Na^+ current densities at the AIS.

We performed simulations in a realistic computer model of a CA1 neuron in order to systematically explore the consequences of altering transient Na^+ current density and / or voltage dependence upon spike threshold and trigger zone (see figure 1-4 for morphology and for detailed description of included conductances Royeck et al. [2008]). This approach also allowed us to directly compare voltage traces at axonal and somatic sites. The i_{NaT} incorporated in axonal and somatic compartments in this model is shown in figure 3-12 A. We varied the voltage of half-maximal activation ($V_{1/2}$) systematically at the AIS from 0 to -7 mV more hyperpolarized compared to the soma ($\Delta V_{1/2}$: shift of $V_{1/2}$ of activation relative to somatic i_{NaT} , activation curves are depicted for $\Delta V_{1/2}$ of 0, -4 and -7 mV in figure 3-12 B). As a second parameter we varied i_{NaT} density at the AIS. Figure 1-4 B shows an exemplary somatic spike elicited by a brief current injection at the soma of the model neuron. i_{NaT} densities at the AIS and at the soma were equal; $\Delta V_{1/2}$ was 0 and -7 mV, as indicated, detailed description of spike properties for different i_{NaT} densities and $\Delta V_{1/2}$ in figure 3-13.

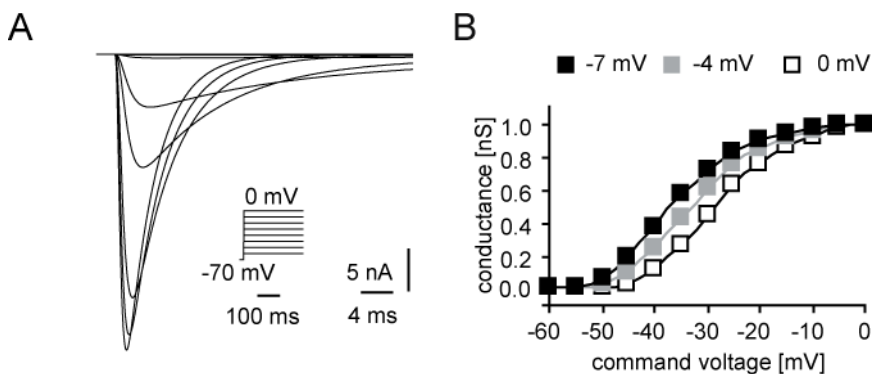


Figure 3-12: Transient Na^+ current (i_{NaT}) and its voltage dependence of activation of in the CA1 neuron model.

(A), Characterization of i_{NaT} incorporated in the model. Na^+ currents were simulated in an isopotential compartment and elicited with the voltage paradigm shown in the inset with $\Delta V_{1/2}$ set to 0 mV. (B), Voltage dependence of activation of i_{NaT} for different values of $\Delta V_{1/2}$. Activation curves were constructed as described in the methods section (see chapter 2.6.4).

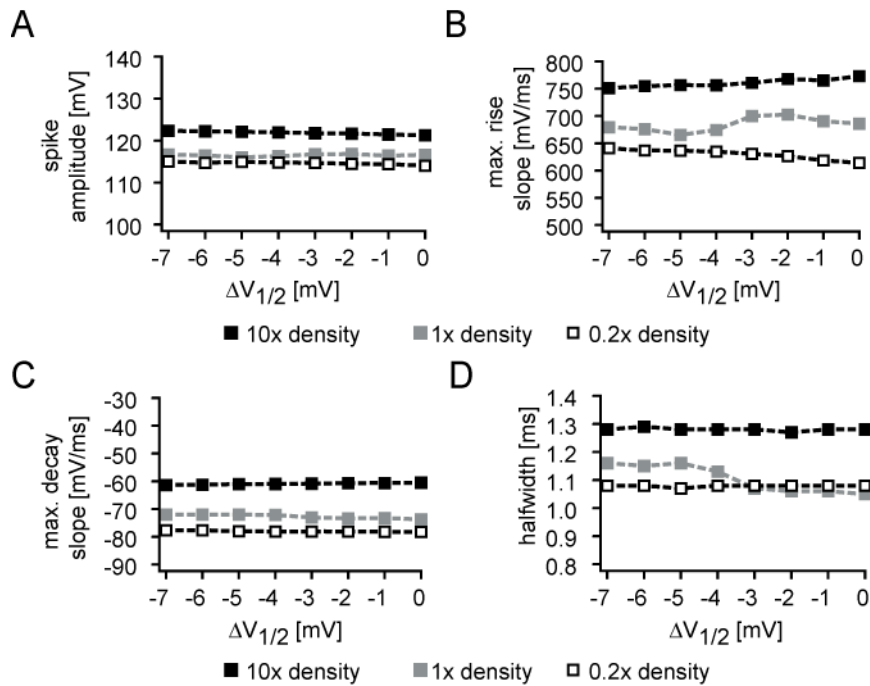


Figure 3-13: Spike parameters of modelled action potentials.

(A), Spike amplitude measured from resting membrane potential to the peak of the spike. (B) and (C), Peak dV/dt of the rising (B) and falling phases (C) of the spike. (D), Width of spikes measured at the half-maximal amplitude (*halfwidth*). All parameters are depicted for different relations of somatic vs. AIS i_{NaT} density (*light gray, gray and black, see legend*). $\Delta V_{1/2}$ values on the x-axis correspond to the shift in the voltage dependence of activation of i_{NaT} at the AIS relative to the soma.

We then stimulated the model neuron with brief current injections and recorded the voltage responses in both the AIS (*grey*) and the soma (*black*) of the model neuron (see figure 3-14 A). These simulations were carried out for different values of $\Delta V_{1/2}$ (0 to -7 mV) and i_{NaT} density at the AIS (from 0.02 to 1 S/cm², corresponding to a 0.2 to 10 fold difference in i_{NaT} density relative to the somatic i_{NaT} density of 0.1 S/cm²). The axo-somatic delay was then calculated as the delay between the time-points at which the slope of action potential rise in both compartments was maximal. A delay could also be derived from somatic voltage traces alone in our model, similar to the in vitro recordings. Derivations of simulated somatic voltage traces also revealed two distinct peaks under most conditions. The values of the axo-somatic delay obtained in this manner from the somatic recording alone showed a strong linear correlation to the values derived as a delay between AIS and somatic spikes ($R^2=0.9388$).

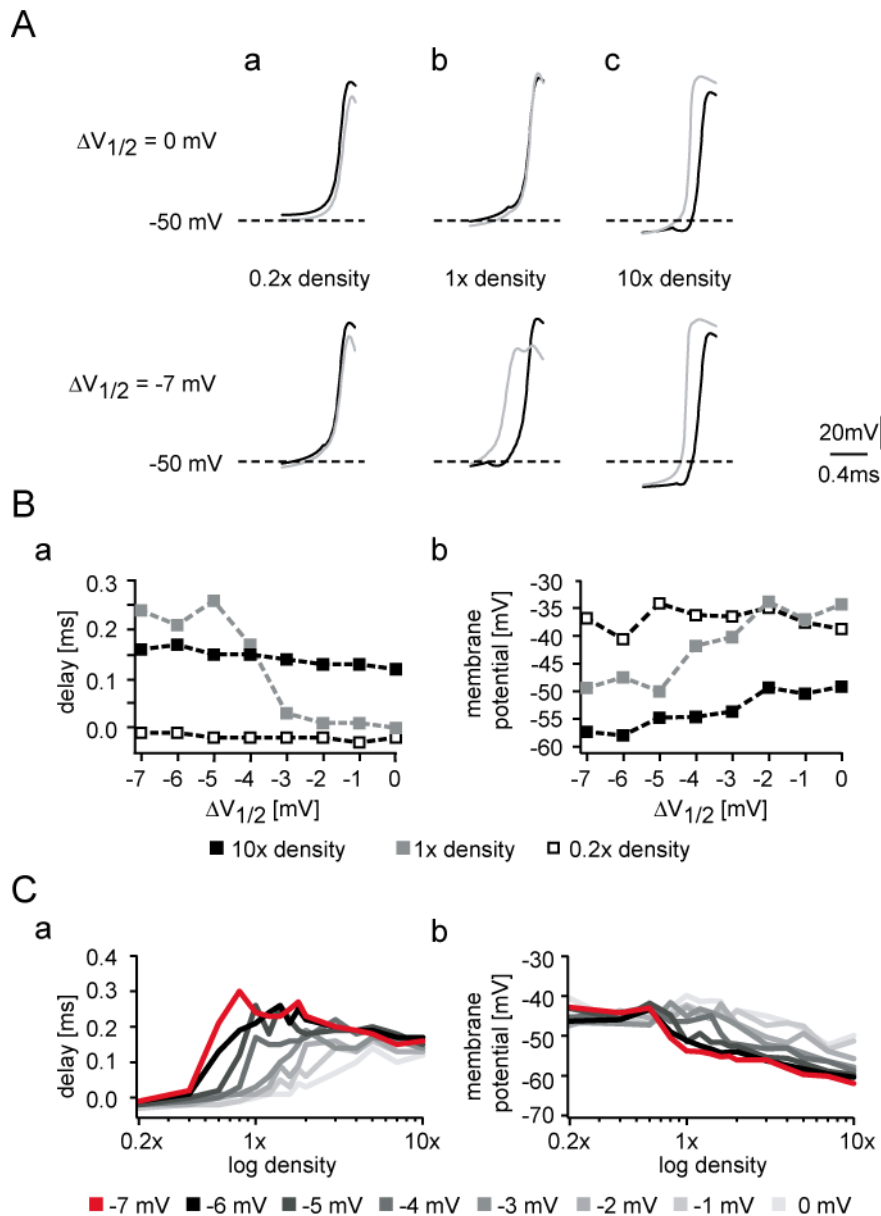


Figure 3-14: Influence of transient AIS Na^+ current density and voltage dependence on spike initiation.

(A), The rising phase of axonal (grey) and somatic (black) spikes are depicted at high resolution either with $\Delta V_{1/2}$ of 0 mV (upper traces) or -7 mV (lower traces), for AIS Na^+ current densities of 0.2, 1 and 10 fold somatic density (panels a-c, respectively). (B), Plot of the delay between time of maximal rise in the AIS and somatic spike over $\Delta V_{1/2}$ for different AIS Na^+ current densities (panel a). An equivalent graph is shown for the spike threshold (panel b). (C), Illustration of the dependence of the axo-somatic delay on the density of axonal Na^+ current for different values of $\Delta V_{1/2}$ (see legend, panel a). An equivalent diagram is shown for the spike threshold (panel b).

When i_{NaT} densities at both soma and AIS are equal, as suggested until recently [Colbert & Johnston, 1996, Colbert & Pan, 2002], spike initiation was strongly dependent on $\Delta V_{1/2}$. A pronounced delay from axonal to somatic spike initiation was observed at values of $\Delta V_{1/2}$ from -7 to -4 mV. When $\Delta V_{1/2}$ was reduced further, the axo-somatic delay showed a step reduction (examples for $\Delta V_{1/2}$ of 0 and -7 mV in figure 3-14 A, panel b, results for all values of $\Delta V_{1/2}$ in figure 3-14 B, panel a, grey data points). Higher i_{NaT} density at the AIS as suggested by Kole *et al.* [2008], always led to

a spike initiation at the AIS (*up to 10 fold increase relative to the soma implemented in our model*), and a stereotypical axo-somatic delay of ~ 0.15 ms, irrespective of $\Delta V_{1/2}$ (see *figure 3-14 Ac and figure 3-14 Ba, black symbols*). Conversely, a reduced i_{NaT} density at the AIS (*0.2 fold of somatic i_{NaT} density*) caused the spike to arise almost simultaneously in both compartments for all values of $\Delta V_{1/2}$ (see *figure 3-14 Aa and figure 3-14 B, panel a, open symbols*). Thus, a $\Delta V_{1/2}$ of more than -4 mV strongly promotes spike initiation at the AIS, even when the i_{NaT} densities at the AIS and soma are uniform. This phenomenon was also clearly apparent when we plotted the axo-somatic delay *versus* the relative i_{NaT} density at the AIS (see *figure 3-14 Ca*). This analysis revealed that for a $\Delta V_{1/2}$ of 0 mV the axo-somatic delay increased gradually with an increasing density of axonal i_{NaT} . When $\Delta V_{1/2}$ was decreased, this relation showed a steeper increase. As a consequence, a $\Delta V_{1/2}$ of -4 to -7 mV strongly affected the spike initiation site over a wide range of Na^+ channel density ratios (*from ~ 0.5 fold to 3 fold somatic density, see figure 3-14 Ca*).

The voltage dependence of activation of i_{NaT} at the AIS also influenced spike threshold, as observed experimentally. When i_{NaT} densities at the AIS and soma were equal, the firing threshold was dependent on $\Delta V_{1/2}$, such that an increase in $\Delta V_{1/2}$ led to a more hyperpolarized spike threshold (*examples for $\Delta V_{1/2}$ of 0 and -7 mV in figure 3-14 Ab, results for all values of $\Delta V_{1/2}$ in figure 3-14 Bb, grey data points*). At a very high i_{NaT} density at the AIS, spike threshold was always hyperpolarized, irrespective of $\Delta V_{1/2}$ (see *figure 3-14 Ac, and figure 3-14 Bb, black symbols*). Conversely, very low i_{NaT} density at the AIS led to a depolarized spike threshold without dependence on $\Delta V_{1/2}$ (*figure 3-14 Aa, and figure 3-14 Bb, open symbols*).

In *Scn8a^{med}* mice, we observed a significant reduction of I_{NaP} and I_{NaR} current [Royeck et al., 2008]. Of these two current components I_{NaP} might conceivably contribute to action potential initiation. We have therefore repeated the modeling experiment with i_{NaP} reduced to 60% in all compartments in which it was present (*soma: reduction to 0.6 mS/cm², AIS: 0.3 mS/cm², see figure 3-15*). In additional experiments, we reduced i_{NaP} only at the AIS (see *figure 3-16*). Under both conditions, the impact of varying i_{NaT} was similar to those depicted in *figure 3-14*. In both cases, changing the voltage dependence of activation of i_{NaT} at the AIS still influenced the axo-somatic delay (*figure 3-15 Aa and figure 3-16 Aa*) and spike threshold (*figure 3-15 Ab and figure 3-16 Ab*). Varying the density of i_{NaT} at the AIS also caused changes in axo-somatic delay and spike threshold that were well comparable to the data obtained without reduction in i_{NaP} (*compare figure 3-15 B and figure 3-16 B to figure 3-14 C*).

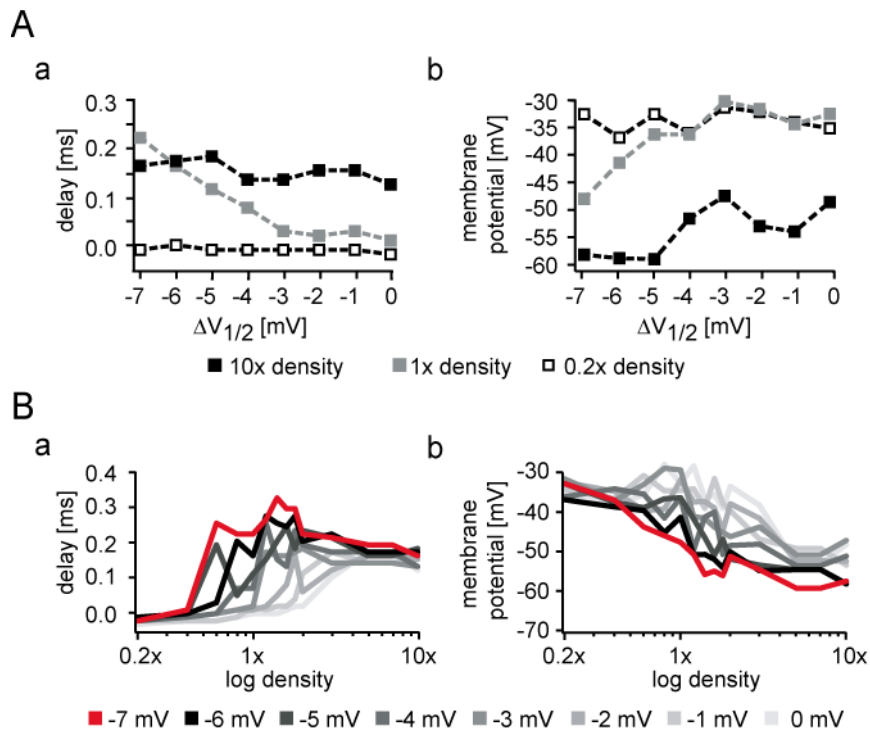


Figure 3-15: Influence of transient AIS Na^+ current density and voltage dependence on spike initiation with a 60% reduction of persistent Na^+ current.

(A), Plot of the delay between time of maximal rise in the AIS and somatic spike over $\Delta V_{1/2}$ for different AIS Na^+ current densities (*panel a*). An equivalent graph is shown for the spike threshold (*panel b*). (B) Illustration of the dependence of the axo-somatic delay on the density of axonal Na^+ current for different values of $\Delta V_{1/2}$ (see legend, *panel a*). An equivalent diagram is shown for the spike threshold (*panel b*).

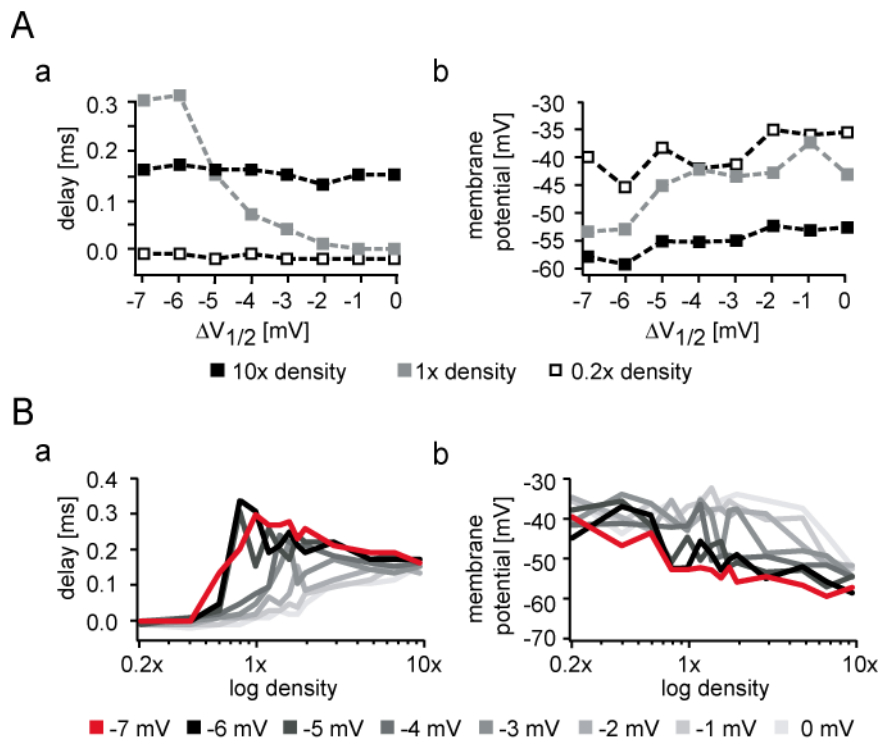


Figure 3-16: Influence of transient AIS Na⁺ current density and voltage dependence on spike initiation with a 60% reduction of persistent Na⁺ current only at the AIS..

(A), Plot of the delay between time of maximal rise in the AIS and somatic spike over $\Delta V_{1/2}$ for different AIS Na⁺ current densities (*panel a*). An equivalent graph is shown for the spike threshold (*panel b*). **(B)**, Illustration of the dependence of the axo-somatic delay on the density of axonal Na⁺ current for different values of $\Delta V_{1/2}$ (see *legend, panel a*). An equivalent diagram is shown for the spike threshold (*panel b*).

3.11 Na⁺ channel mRNA expression following status epilepticus

In the chronic phase of the pilocarpine model of epilepsy the hippocampus displays the hallmarks of Ammon's horn sclerosis. As in human patients sclerosis consists of astrogliosis, synaptic reorganization, and a loss of neurons in the hippocampus proper [for reviews see Cavalheiro, 1995 and Curia *et al.*, 2008]. In the CA1 region we quantified the loss of neurons in the pilocarpine model to be 40.3% 14 d after a 40 min status epilepticus [Kirschstein *et al.*, 2007]. Apart from these structural changes also physiological changes occur. The most prominent difference regarding discharge behavior is an increase in intrinsic bursting, that can be observed in CA1 pyramidal neurons of epileptic animals [Jensen *et al.*, 1994, Chen *et al.*, 2009]. Since Na_v1.6 has a strong influence on shaping neuronal discharge behavior (*see first part of this study*), we decided to investigate the regulation of this Na⁺ channel during epileptogenesis following status epilepticus. First, we performed a quantitative Taqman™ mRNA expression analysis (*see methods 2.4*) of the most prominently expressed Na⁺ channel α -subunits in the hippocampus: Na_v1.1, Na_v1.2, Na_v1.3, and Na_v1.6. We compared mRNA expression in hippocampal microslices of the CA1 region prepared at three time-points (6 h, 5 d, and 14 d) following status epilepticus to time-matched tissue acquired from sham control rats. As internal control we used expression data obtained for the neuron-specific protein synaptophysin (SYP). For better comparability between the individual subunits we normalized expression values for all Na⁺ channels to the ones obtained in controls. At the earliest time-point, in tissue collected 6 h after status epilepticus, Na_v1.1, Na_v1.2, Na_v1.3, and Na_v1.6 mRNA expression was not significantly different compared to expression in sham controls (Na_v1.1: 0.75 ± 0.08 fold, Na_v1.2: 1.10 ± 0.18 fold, Na_v1.3: 1.06 ± 0.14 fold, and Na_v1.6: 1.00 ± 0.17 fold; n = 5, *n.s.*). At the second time-point 5 d after status epilepticus during the latent period no significant differences in regulation of Na⁺ channel mRNA expression induced by the epileptogenesis could be detected (Na_v1.1: 0.94 ± 0.12 fold, Na_v1.2: 1.02 ± 0.13 fold, Na_v1.3: 1.28 ± 0.22 fold, and Na_v1.6: 1.04 ± 0.07 fold; n = 5, *n.s.*). The third time-point 14 d after status epilepticus is already in the chronic phase when rats suffer from spontaneous seizures and a significant cell loss has manifested [Kirschstein *et al.*, 2007]. At this time-point average ratios for all subunits were below one but failed to reach statistical significance (Na_v1.1: 0.88 ± 0.08 fold, Na_v1.2: 0.79 ± 0.07 fold, Na_v1.3: 0.78 ± 0.09 fold, and Na_v1.6: 0.63 ± 0.14 fold, n = 5; *n.s.*). In conclusion, this data shows that mRNA expression of Na⁺ channel α -subunits remains stable in the time following the pilocarpine induced status epilepticus.

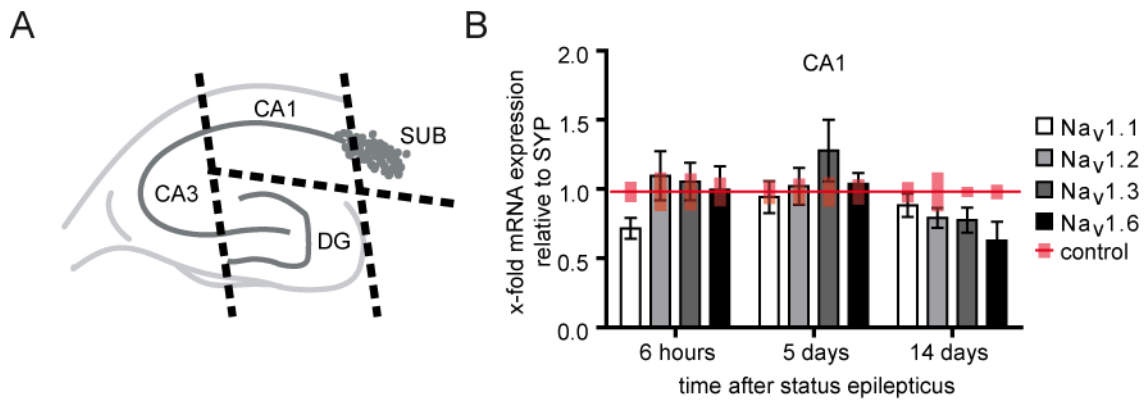


Figure 3-17: Na⁺ channel α -subunit mRNA expression in the CA1 region after status epilepticus

(A), Schematic drawing depicting the cuts (broken lines) to collect hippocampal CA1 micro-slices from 800 μ m thick horizontal slices in order to determine mRNA expression levels. (B), Relative mRNA expression levels of the main Na⁺ channel α -subunits Na_v1.1, Na_v1.2, Na_v1.3, and Na_v1.6 in CA1 micro-slices at three time-points following status epilepticus ($n = 5$ animals). Values shown were determined relative to synaptophysin mRNA expression (SYP) by the $\Delta\Delta$ -ct method and subsequently normalized to the mean mRNA expression in sham controls indicated by a red dotted line ($n = 5$ animals). The standard error of the expression values from sham control tissue is shown as opaque red bars extending from the red line. Changes in mRNA expression at each time-point were tested with a Mann Whitney U-test and the significance level adjusted for multiple comparisons to $p < 0.0125$. No significant changes in mRNA expression of Na⁺ channels were detected in these experiments.

3.12 Na⁺ channel protein expression following status epilepticus

In addition to the analysis of mRNA expression we also decided to determine the Na⁺ channel protein levels. We analyzed Western blots of CA1 micro-slices prepared at two time-points (5 d and 14 d) following status epilepticus. To quantify Na⁺ channel content we utilized a PanNa_v antibody directed against all Na⁺ channel α -subunits and two subunit specific antibodies against Na_v1.2 and Na_v1.6. As control we selected a monoclonal antibody directed against synaptophysin (SYP). In figure 3-18 (panel Aa and panel Ab) representative blots from both time-points are displayed. Quantification of the signals for the Na⁺ channels was always done relative to the synaptophysin signal from the same lane on the same blot membrane. At the early time-point we found a significant general decrease of Na⁺ channel protein content in CA1 micro-slices despite of the stable mRNA levels after status epilepticus (see chapter 3.11). The reduction in Na_v1.2 (0.31 ± 0.03 fold, $n = 5$, $p < 0.01$) and in Na_v1.6 (0.70 ± 0.06 fold, $n = 10$, $p < 0.01$) is consistent with the significant reduction seen in the PanNa_v signal (0.49 ± 0.05 fold, $n = 13$, $p < 0.01$). Two weeks after status epilepticus no downregulation of the Na_v1.2 protein content was detected (0.72 ± 0.09 fold, $n = 8$, *n.s.*). Even though less pronounced than 5 d after status epilepticus, Na_v1.6 protein content was significantly lowered in CA1 micro-slices from epileptic rats at 14 d (0.65 ± 0.07 fold, $n = 8$, $p < 0.01$). Total Na⁺ channel protein showed no change in expression in the PanNa_v antibody signal (0.87 ± 0.06 fold, $n = 4$, *n.s.*). This data is in good agreement with the findings from the mRNA experiments.

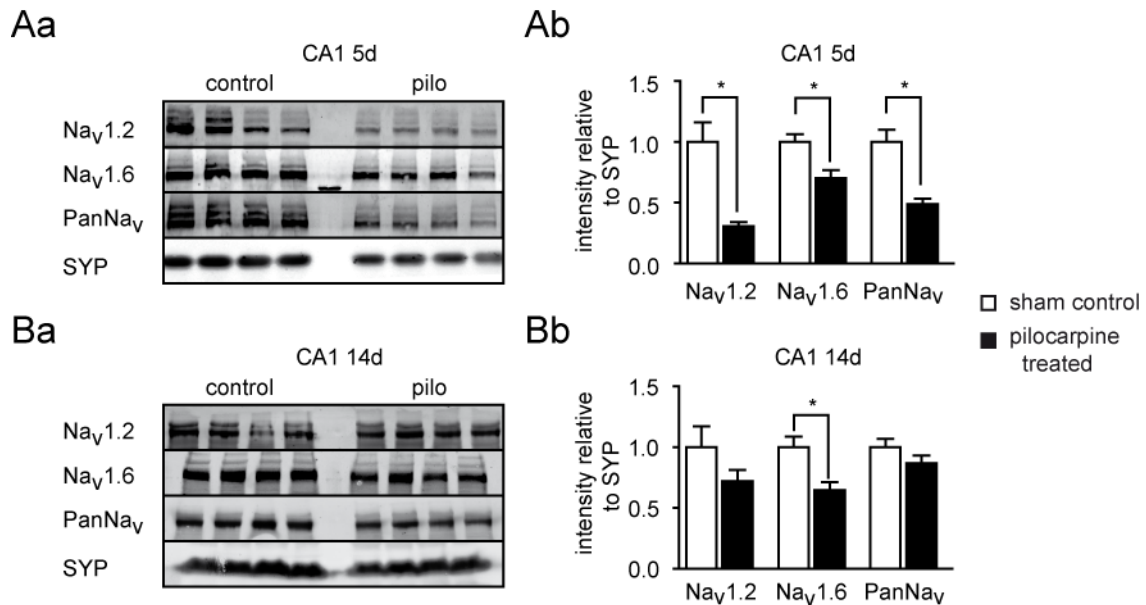


Figure 3-18: Na⁺ channel content in CA1 microslices after experienced status epilepticus.

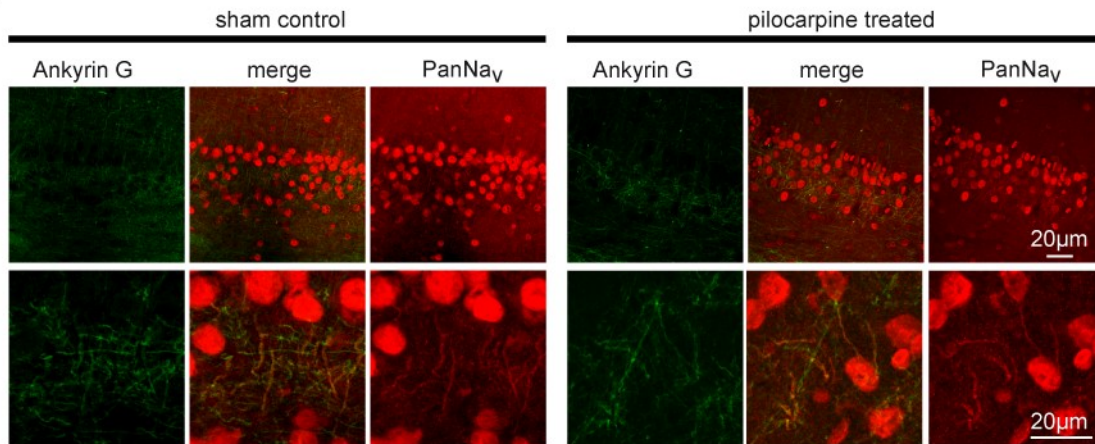
(Aa), Examples of Western blots for the Na⁺ channel α -subunits Na_v1.2 and Na_v1.6 together with PanNa_v and synaptophysin (SYP). Each lane was loaded with whole protein from CA1 microslices of one animal. **(Ab)**, Bar graph depicting average signal of Na⁺ channel antibody relative to the intensity of SYP acquired in the same lane on the same gel. 5 d after the pilocarpine treatment PanNa_v was significantly reduced (*rightmost black bar*, 0.49 ± 0.05 fold, $n = 13$, $p < 0.01$). This total Na⁺ channel reduction is consistent with the reduction of Na_v1.2 (*leftmost black bar*, 0.31 ± 0.03 fold, $n = 5$, $p < 0.01$) and Na_v1.6 (*middle black bar*, 0.70 ± 0.06 fold, $n = 10$, $p < 0.01$) For comparison normalized intensities from sham controls \pm SEM are shown as white bars next to the black bars. **(Ba)**, Examples of Western blots from tissue samples prepared 14 d after status using the same antibodies as in Aa. **(Bb)**, Quantitative Na⁺ channel content analyzed 14 d after status epilepticus. PanNa_v content is no longer reduced (*rightmost black bar*, 0.87 ± 0.06 fold, $n = 4$, *n.s.*). This was the same for Na_v1.2 protein content (*leftmost black bar*, 0.72 ± 0.09 fold, $n = 8$, *n.s.*). Na_v1.6 still showed a significant reduction compared to sham controls (*middle black bar*, 0.65 ± 0.07 fold, $n = 8$, $p < 0.01$). Statistical analysis was done using a Mann-Whitney U-test.

3.13 Axonal localization of Na⁺ channels and Na_v1.6 following status epilepticus

Subcellular localization of ion channels is important in determining neuronal discharge properties. The biochemical experiments we described above argue against a general increase in Na_v1.6 protein following the experience of status epilepticus. We hypothesized that changes in Na⁺ channel expression induced by the status epilepticus could substantially affect the subcellular distribution of Na⁺ channels. As a first step, we produced double immunolabellings, in the same manner as in the mouse experiments, using the PanNa_v and the Ank G antibody (*for comparison with the mouse data, see figure 3-2*). Comparing sections from epileptic rats 14 d after status epilepticus to sections from sham controls we found no apparent difference in axon initial segment fluorescence labelling. In addition, we tested for more specific alterations affecting Na_v1.6 aggregation at axon initial segments by performing double labellings for Ank G and Na_v1.6 in pilocarpine treated rats (*for comparison with the mouse data, see figure 3-1*). In these sections relative quantification of Na_v1.6 fluorescence intensity

relative to that of Ank G also yielded no difference between sham control and pilocarpine treated rats (see figure 3-20). Taken together, our biochemical data suggests that the hyperexcitability found in the epileptic hippocampus is not the result of an increase in Na^+ channel α -subunit expression. The most pronounced change were the cell loss and a reduction of Na^+ channel expression in the Western blots of CA1 microslices relative to the synaptic protein synaptophysin. However, Na^+ channel aggregation at the AIS persists in CA1 pyramidal cells from epileptic rats.

A



B

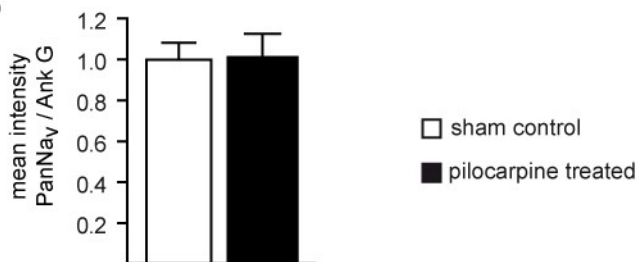


Figure 3-19: Unchanged axonal aggregation of Na^+ channel α -subunits in the hippocampus proper following status epilepticus.

(A), Representative immunohistochemical sections from both sham control rats (left) and pilocarpine treated animals (right) showing double labelling of a monoclonal Ankyrin G (Ank G) antibody, a marker for AIS (green, leftmost panels) that colocalizes with the labelling of polyclonal antibody directed against all Na^+ channel subunits (*PanNa_v*, green, right panels, merge in the middle panel). The *PanNa_v* antibody also produces a labelling of neuronal somata. **(B)**, Average AIS fluorescence intensity of $\text{Na}_v1.6$ relative to Ank G in sham controls (white bar, 10 AIS analyzed in each of 4 slices obtained from 4 animals) and pilocarpine treated rats (black bars, 10 AIS analyzed in each of 7 slices obtained from 7 animals, *n.s.*). For a detailed description of the semi-quantitative analysis see methods chapter 2.3.1.

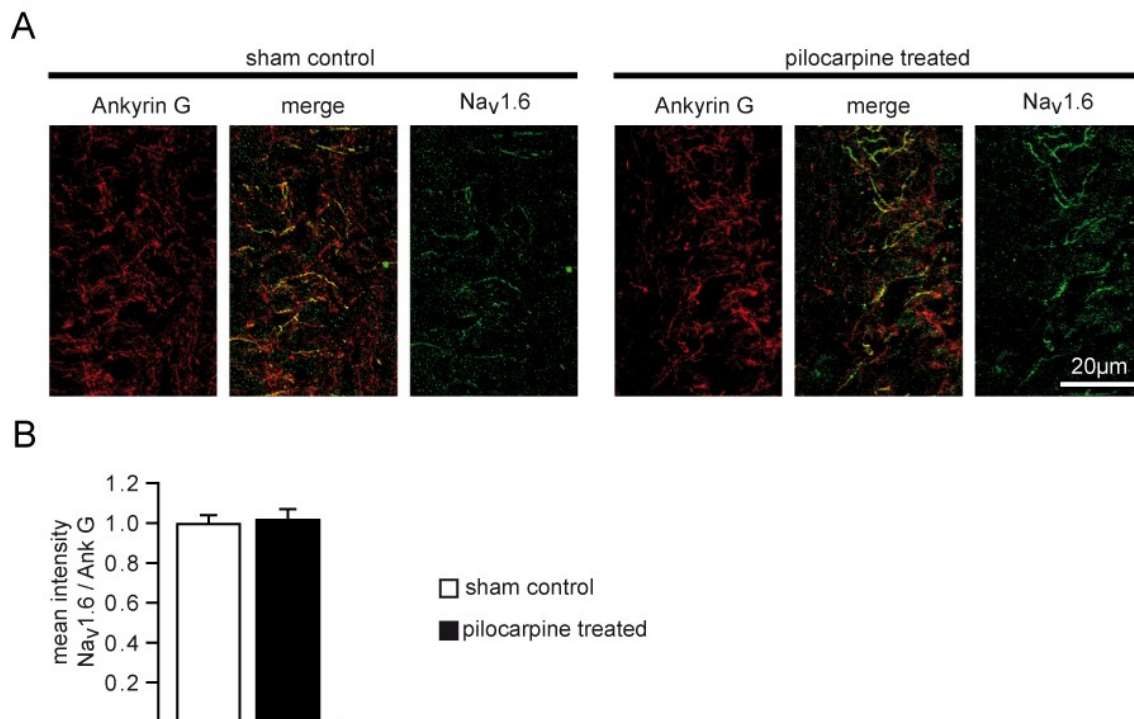


Figure 3-20: Axonal aggregation of $Na_v1.6$ in the hippocampus proper following status epilepticus.

(A), Representative immunohistochemical sections from both sham control (*left*) and pilocarpine treated rats (*right*). The labelling of a monoclonal Ankyrin G (Ank G) antibody, a marker for AIS (red, leftmost panels), colocalizes with the labelling of polyclonal antibody directed against $Na_v1.6$ (green, right panels, merge in the middle panel). **(B)**, Average AIS fluorescence intensity of $Na_v1.6$ relative to Ank G in sham controls (*white bar*, 10 AIS analyzed in each of 4 sections obtained from 4 animals) and pilocarpine treated rats (*black bars*, 10 AIS analyzed in each of 7 slices obtained from 7 animals, *n.s.*). For a detailed description of the semi-quantitative analysis of Pan Na_v staining at AIS see methods chapter 2.3.1. Axonal $Na_v1.6$ protein levels at the AIS of CA1 pyramidal neurons are not altered by epileptogenesis.

3.14 Changes in Na^+ currents of CA1 pyramidal neurons following status epilepticus

Are there specific alterations in Na^+ currents that affect intrinsic membrane properties and thereby contribute to the conversion of regular firing neurons to burst firing neurons [Sanabria et al. , 2001, Chen et al. , 2009]? Earlier studies, performed in electrical stimulation based models for epilepsy, found an increase in Na^+ current density and shifts in the voltage dependence of activation and inactivation [Vreugdenhil et al. , 1998, Ketelaars et al. , 2001]. In the pilocarpine model of epilepsy, the only difference found in a study performed in our laboratory analyzing transient Na^+ currents of CA1 pyramidal neurons was a slight increase in time-dependence of recovery from inactivation [Schaub et al. , 2007]. Interestingly, in this work neither the voltage dependence of activation nor the voltage dependence of inactivation was changed after status epilepticus. However, in another study from our group, various blockers of I_{NaP} were shown to also block the ADP in sharp microelectrode recordings performed in rats [Yue et al. , 2005]. Therefore, we decided to compare I_{NaP} between sham control and pilocarpine treated rats in the acute slice preparation (*see figure 3-21*). To do this we evoked I_{NaP} by applying the same protocols and analysis as in the mouse recordings (for compari-

son see figure 3-4). Our experiments revealed a significant increase of the maximal conductance of I_{NaP} in the epileptic rats (3.21 ± 0.42 nS, $n = 18$) compared to sham controls (2.07 ± 0.25 nS, $n = 19$, $p < 0.05$). This corresponds to a 55% increase in I_{NaP} amplitude. Comparing I_{NaP} kinetics, we found no differences in the averaged fit parameters for the voltage of half maximal activation ($V_{1/2}$) between pilocarpine treated rats ($V_{1/2} = -43.53 \pm 1.35$ mV) and sham controls ($V_{1/2} = -47.24 \pm 1.41$ mV, *n.s.*) as well as in the slope factor (km) (3.34 ± 0.21 mV and 3.74 ± 0.31 mV, *n.s.*, respectively). This increase in I_{NaP} amplitude could be an important factor which contributes to the increase number of burst firing neurons in sharp microelectrode recordings.

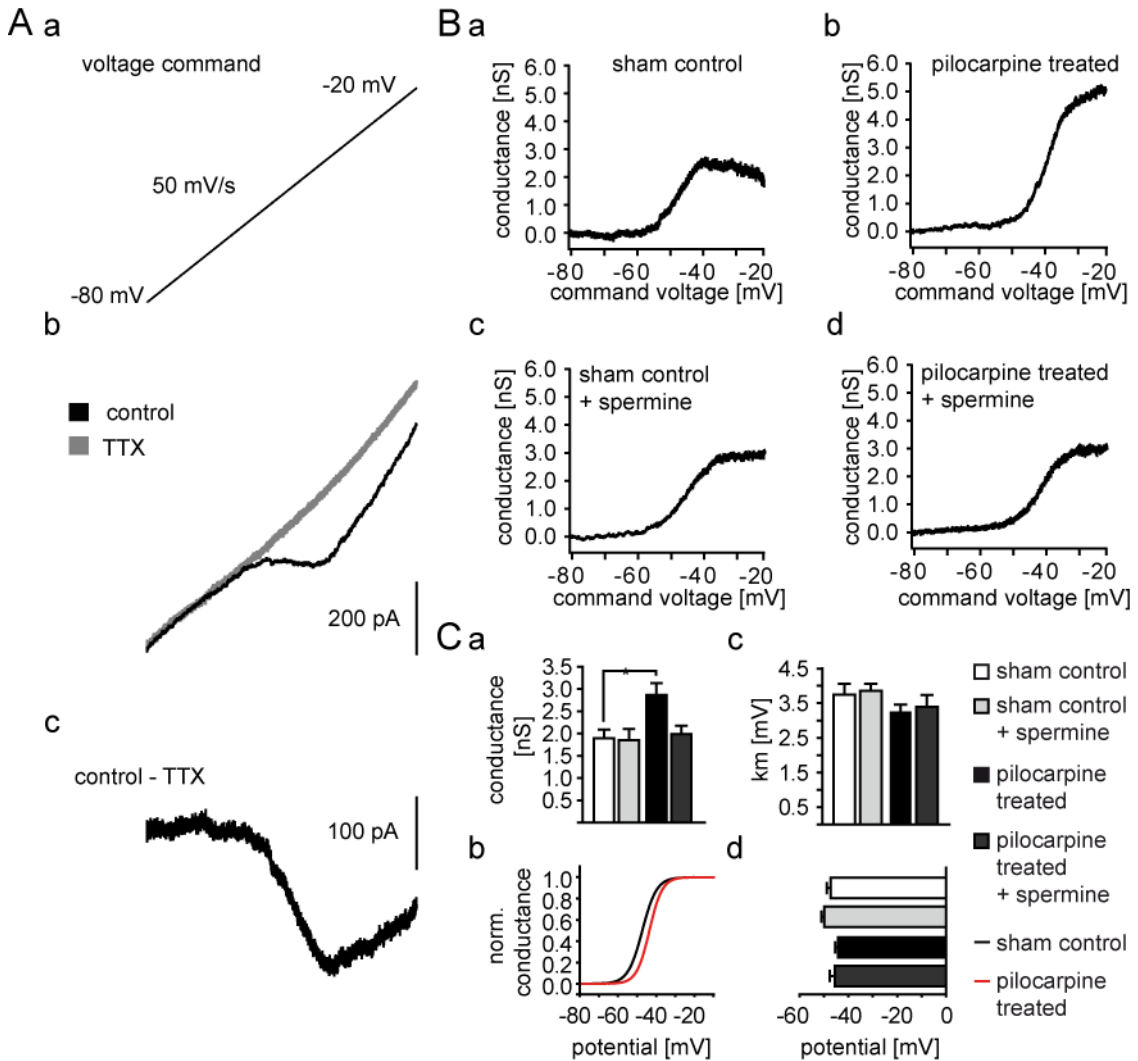


Figure 3-21: Increase in the persistent Na^+ current 12-20 d after status epilepticus

(A), In recording solutions designed to reduce other types of inward and outward currents (see methods 2.6.5), voltage ramps (50 mV/s, panel a) were applied to elicit I_{NaP} . Panel Ab depicts a representative current trace elicited under control conditions in an intact CA1 neuron in the slice preparation in a sham control rat in the absence (black trace) and presence of 0.5 μ M TTX (gray trace). The TTX-sensitive I_{NaP} was isolated by subtraction (subtracted trace in panel Ac). (Ba), Diagram depicting conductance versus voltage created from the exemplary current trace from panel Ac. (Bb), Conductance versus voltage plotted for a representative pyramidal neuron recorded from pilocarpine treated rat. (Bc) and (Bd), Conductance versus command voltage recorded from a sham control and pilocarpine treated rat with 1 mM spermine included in the pipette, respectively. (C), Bar graphs showing the 55% increase in averaged maximum conductance in pilocarpine treated rat compared to sham treated controls ($n = 18$, black bar and $n = 19$, white bar, respectively, panel Ca). Inclusion of spermine in the intracellular solution did not affect I_{NaP} amplitude in controls (light gray bar, $n = 12$) whereas the increase in I_{NaP} in pilo-

carpine treated rats (*dark gray bar*, $n = 11$) vanished. Voltage dependence of activation of I_{NaP} recorded in sham controls (*black curve*) and pilocarpine treated (*red curve*) constructed from the averaged fits parameters of the individual Boltzmann fits. Fit parameters for the slope factor (*panel Cc*) and the half maximal voltage of activation (*panel Cd*) of the Boltzmann curve fits were not different between the four groups.

3.15 Discharge behavior of CA1 pyramidal neurons following status epilepticus

The high threshold bursting persists after a pharmacological block of the low threshold bursting and can be blocked by application of TTX and riluzole [Chen et al. , 2009]. Since these studies were performed using sharp microelectrodes and in a different rat strain, we performed a series of current clamp recordings in Wistar rats 14 to 21 days following status epilepticus in whole-cell configuration (*see figure 3-22 A-F*) for better comparability with the experiments performed in *Scn8a^{med}* and *Scn8a^{wt}* mice (*see figure 3-07*). Most of the action potential parameters did not vary significantly between sham control and pilocarpine treated animals. Average membrane resistance ($91.40 \pm 14.34 \text{ M}\Omega$ and $84.81 \pm 7.39 \text{ M}\Omega$, *n.s.*) and membrane time constant ($18.06 \pm 1.14 \text{ ms}$ and $19.38 \pm 3.82 \text{ ms}$, *n.s.*) were not different between sham control ($n = 8$) and pilocarpine treated rats ($n = 7$), respectively. The action potential amplitude, measured from holding potential to peak potential ($102.50 \pm 3.01 \text{ mV}$ and $102.42 \pm 4.29 \text{ mV}$; *n.s.*), maximal rate of rise ($351.13 \pm 36.01 \text{ mV/s}$ and $330.71 \pm 23.59 \text{ mV/s}$; *n.s.*), and maximum rate of decay ($-83.92 \pm 6.10 \text{ mV/s}$ and $-84.20 \pm 7.67 \text{ mV/s}$; *n.s.*) were also found not to be altered following the pilocarpine induced epileptogenesis.

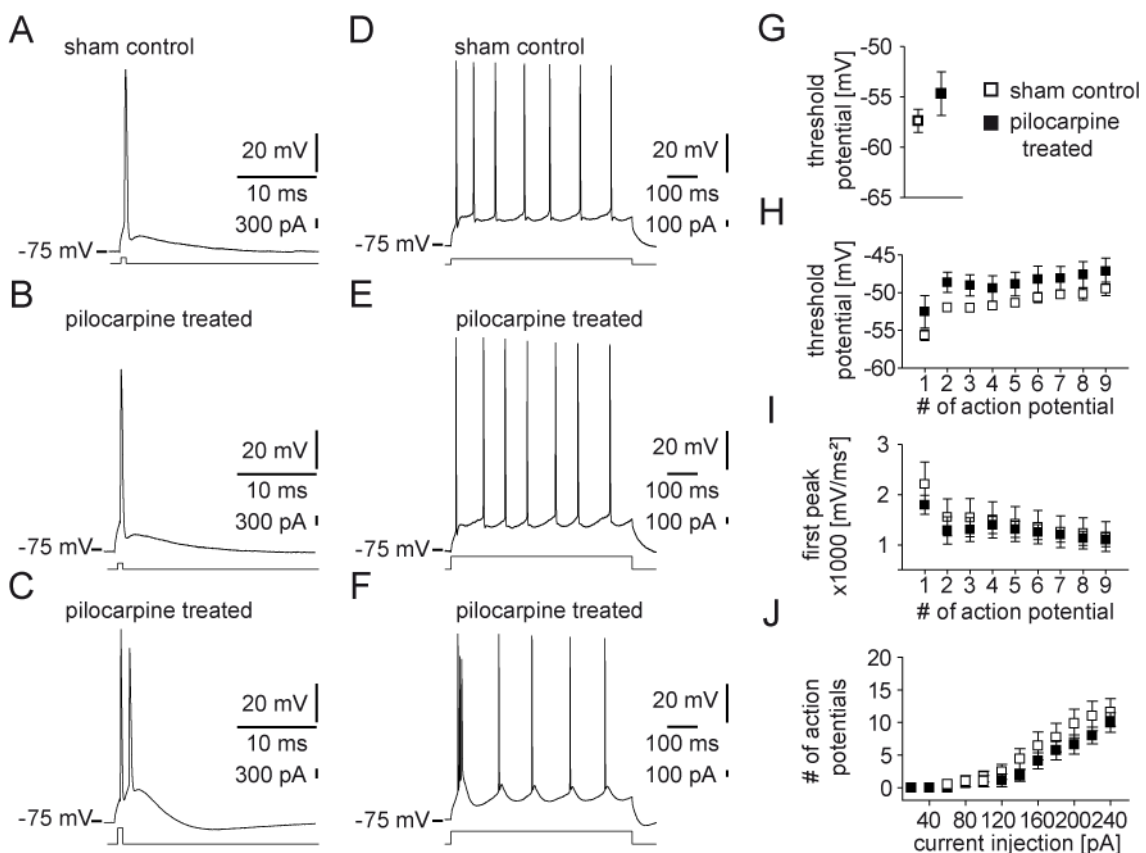


Figure 3-22: Discharge behavior of intact CA1 pyramidal neurons recorded in the slice preparation in whole-cell configuration in pilocarpine treated rats.

(A), (B), and (C), Example traces of single spikes elicited by brief (4 ms), just supra-threshold current injection recorded in a sham control (*panel A*) or pilocarpine treated rat (*panel B*). A burst discharge recorded in a pilocarpine treated rat (*panel C*). Lower traces depict the corresponding current injection. Steady state current injections were used to set the membrane potential to -75 mV. (D), (E), and (F), Responses to prolonged current injections (600 ms) from the same neurons shown in *panels A, B, and C*. Note the pronounced AHP following the initial burst discharge in *panel F*. (G), Average values obtained for the spike threshold with short current injections (*compare panels A, B, and C*) in sham control (*open symbols, n = 8*) and pilocarpine treated rats (*closed symbols, n = 7, n.s.*). (H), Average values for spike thresholds obtained during prolonged current injections (*compare panels D, E, and F*). The first nine spikes were analyzed binned according to their spike history. Spike thresholds were not significantly different between genotypes within all bins. (I), Amplitude of the first (*axonal*) peak in the second derivation of the voltage trace is not decreased between sham control and pilocarpine treated rats (*compare figure 3-11*). (J), Comparison of action potential gain of CA1 neurons by plotting the number of spikes during the 600 ms current injection versus the magnitude of the current injection (*sham control, n = 8 and pilocarpine treated rats, n = 7, n.s.*).

The occurrence of burst firing can also not be explained by a general increase in the input output relation of pyramidal CA1 neurons in epileptic animals. We found neither an increase in spike gain (*see figure 3-22 J*), nor a decrease of the action potential threshold. Average threshold of action potentials elicited with brief 4 ms just supra-threshold current injections was -57.38 ± 1.13 mV in sham controls and -54.67 ± 2.16 mV in pilocarpine treated rats (*n.s., action potentials triggered from -75 mV*). In addition, threshold for spikes evoked by prolonged 600 ms current injections was not significantly changed between both groups (*see figure 3-22 H*). Considering the initiation of action potentials (*see chapter 1.5*), in both epileptic and control group CA1 pyramidal neurons, action potentials were found to be reliably triggered in the AIS as apparent from two peaks visible in the second derivative of voltage traces (*data not shown*). Moreover, we did not find significant differences in the temporal separation of the two peaks (*data not shown*) or in the steepness of the onset phase ('kink') of the action potential (*see figure 3-22 I*). This stability of spike initiation is in good agreement with the lack of changes in axon initial segment morphology following status epilepticus (*see chapter 3.13*). In conclusion the shape of the fast spike seems to remain largely unaffected by the pilocarpine induced epileptogenesis.

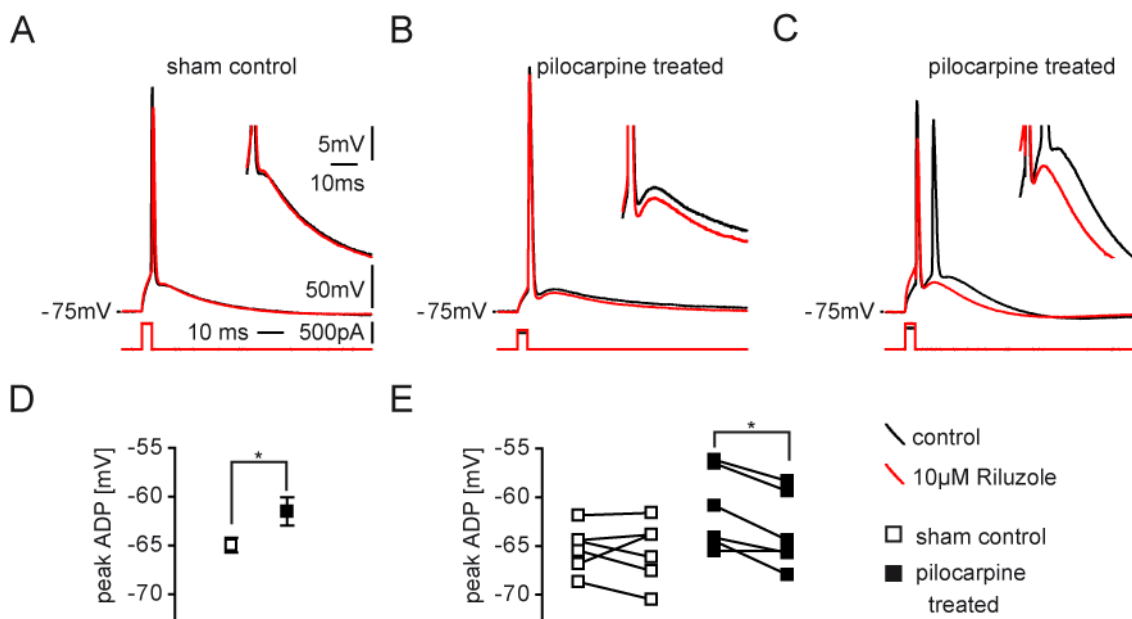


Figure 3-23: The spike afterdepolarization is increased in whole-cell recordings of CA1 pyramidal neurons in epileptic rats.

(A), (B), and (C), Example traces before (*black*) and after (*red*) the wash-in of 10 μM riluzole of spikes elicited by brief (4 ms) current injection recorded in a sham control (*panel A*) or pilocarpine treated rat (*panel B*). Notice the block of the spike doublet after the wash-in (*panel C*). Lower traces depict the corresponding current injection. Steady state current injections were used to keep the membrane potential to -75 mV. **(D)**, Mean ADP peak voltage is significantly increased in pilocarpine treated ($n = 7$) compared to sham control animals (*open symbols*, $n = 8$; $p < 0.05$) recorded in whole-cell configuration **(G)**, Plot of the in ADP peak voltage before (*left*) and after (*right*) the wash-in of 10 μM riluzole in sham control (*open symbols*, $n = 6$) and pilocarpine treated cells (*closed symbols*, $n = 6$). While in sham controls riluzole did not systematically affect the ADP (*n.s.*) in cells recorded from pilocarpine treated animals the ADP peak voltage was significantly reduced ($p < 0.01$, *paired t-test*).

In sharp microelectrode recordings from epileptic rats a large percentage of neurons respond to short current with a high frequency burst discharge [Chen et al. , 2009]. In these burst-firing neurons the first spike is followed by subsequent spikes that ride on the ADP of the first spike. Since this discharge behaviour is increased in epileptic animals we expected the ADP to be increased in CA1 pyramidal neurons from pilocarpine treated rats. Indeed, average peak ADP was significantly increased in pilocarpine treated rats (-61.51 ± 1.45 ; $n = 7$) when compared to sham controls (-64.96 ± 0.75 , $n = 8$, $p < 0.05$). Subtraction of the passive responses and thereby analysis of the active proportion of the ADP as we did in the mouse recordings (see *figure 3-8*) was not feasible, because the passive response recorded were in some cases larger than the ADP. This issue was already mentioned by Brown and Randall [2009], who performed whole-cell recordings of rat CA3 pyramidal neurons. In sharp microelectrode recordings high threshold bursting [Chen et al. , 2009] and the ADP [Yue et al. , 2005] are readily blocked by 10 μM riluzole, a substance known to block the persistent Na^+ current [Yue et al. , 2005]. We also tested how riluzole affects the ADP in whole-cell current clamp recordings. To our surprise 10 μM riluzole failed to reduce the ADP in CA1 cells from sham control animals (*difference before and after application* 0.28 ± 0.80 mV, $n = 6$, *n.s.*, *paired t-test*, *figure 3-23 A and E*). However, in epileptic neurons riluzole did reduce the peak amplitude of the ADP significantly (2.27 ± 0.55 mV, $n = 6$, $p < 0.01$, *paired t-test*, *figure 3-23 B, C, and E*). In particular in a neuron responding with a spike doublet to a brief 4 ms current injection the application of riluzole blocked the second action potential triggered by the ADP.

4. Discussion

4.1 Neuronal expression and subcellular localization of Na_v1.6

In our analysis of the mRNA levels of voltage gated Na⁺ channels in rat CA1 microslices (*see results, chapter 3.11*) we detected the Na⁺ channel α -subunits most prominently expressed in the central nervous system, namely Na_v1.1, Na_v1.2, Na_v1.3, and Na_v1.6 [Diss et al. , 2004, Vacher et al. , 2008]. Compared to humans expression of Na_v1.3 seems to be lower in rodents and is confined to the somatic and dendritic regions [Westenbroek et al. , 1992, Whitaker et al. , 2001]. Additionally, we also detected very low expression levels of Na_v1.5 mRNA (*data not shown*), which is in good agreement with data analyzing dentate gyrus microslices by Ellerkmann *et al.* [2001]. Neuronal expression of the Na_v1.5 mRNA at higher levels was already reported for the mouse limbic system [Hartmann et al. , 1999]. Until now, presence of Na_v1.5 protein was only detected by immunohistochemistry at axonal membranes of neurons in the cerebral cortex, hypothalamus, thalamus, basal ganglia and brainstem [Wu et al. , 2002].

On the protein level, we pronounced expression of Na_v1.2 and Na_v1.6 in Western blots of CA1 microslices (*see figure 3-18*). We investigated the subcellular distribution of Na⁺ channel α -subunits with immunohistochemical techniques. We utilized the PanNa_v antibody and found pronounced aggregation of Na⁺ channels at the axon initial segment of rat and mouse CA1 pyramidal neurons (*see figure 3-2 and figure 3-19*). To demarcate axon initial segments we chose an antibody directed against Ankyrin G [Jenkins & Bennett, 2001]. We also found that the Na_v1.6 subunit is present in high concentration at the axon initial segment in *Scn8a*^{wt} mice (*see figure 3-1, panels Aa and Ab*) and rats (*see figure 3-20*). In *Scn8a*^{med} mice, lacking Na_v1.6, the Ankyrin G aggregation was unaffected (*see figure 3-1B*).

Apart from Na⁺ channels, voltage gated K⁺ channels are aggregated at the axon initial segment [Garrido et al. , 2003a, Pan et al. , 2006, Lorincz & Nusser, 2008]. Among these the K_v7 K⁺ channels were shown to share the Ankyrin G binding motif with Na⁺ channels. This fact is suggestive of a competition between different ion channels for the binding to Ankyrin G and therefor localization at the axon initial segment. This hypothesis is strengthened by the possibility to experimentally direct dendritic K⁺ ion channels to the axon initial segment by including the Ankyrin G binding motif into its sequence [Garrido et al. , 2003a, Garrido et al. , 2003b]. Recently, the distribution of ion channels within a single axon initial segment was shown to be polarized with an increasing density of Na_v1.6 towards the distal part of the axon [Wart & Matthews, 2006a, Lorincz & Nusser, 2008]. The mechanism responsible for the generation of this gradient is still unknown.

4.2 The role of axonal Na_v1.6 channels in action potential initiation

Previous studies have shown that spike initiation occurs within the distal portion of the AIS in cortical neurons [Meeks & Mennerick, 2007, Palmer & Stuart, 2006] or the first node of Ranvier in Purkinje neurons [Clark et al. , 2005]. Several factors likely endow these subcellular compartments with a particularly low spike threshold. First, the passive electrical properties of axon *versus* soma may play an important role: modelling and physiological studies suggest that charging of the AIS capacitance by

inward current is rapid, with the much larger somatic capacitance being charged with a significant delay [McCormick et al. , 2007, Meeks & Mennerick, 2007, Shu et al. , 2007, Yu et al. , 2008]. Second, several studies have shown a high density of Na⁺ channel proteins at the AIS [Boiko et al. , 2001, Boiko et al. , 2003, Hossain et al. , 2005, Pan et al. , 2006, Wart & Matthews, 2006b], but how far this correlates with AIS Na⁺ current density is a matter of ongoing debate [Colbert & Pan, 2002, Palmer & Stuart, 2006, Kole et al. , 2008]. Last, more negative activation potentials of axon initial segment Na⁺ channels are thought to lower spike threshold [Colbert & Pan, 2002]. Clearly, these factors are not mutually exclusive; rather, it is likely that these factors in combination localize the spike trigger zone to the AIS.

Action potentials recorded in CA1 pyramidal neurons of mice and rats are reliably initiated at the axon initial segment (see *figure 3-11 and figure 3-22 I*). From this site of initiation the spike propagates in orthodromic direction along the axon. The action potential also back propagates into the soma, where it triggers the initiation of a somatic spike. This phenomenon becomes apparent in a biphasic shape of the upstroke of the action potential and a very high steepness of the initial increase in the spike [Coombs et al. , 1957, Meeks & Mennerick, 2007, Naundorf et al. , 2006, Yu et al. , 2008]. The biphasic shape of the initial part of the action potential is also apparent in the cell-attached recordings in *Scn8a^{med}* and *Scn8a^{wt}* mice, where spike discharges were elicited by synaptic activity and the intracellular milieu remained unperturbed (see *figure 3-6 A and B*). Initiation of the action potential remote from the soma causes the initial voltage increase of the action potential to appear step-like. This feature was termed 'kink' [Naundorf et al. , 2006]. Both 'kink' and temporal separation of the two biphasic components depend on the distance of the back propagation along the cylindrical axon and the subsequent entering of the larger soma [Yu et al. , 2008].

Regarding spike initiation, we found three major changes in *Scn8a^{med}* mice. Firstly, we observed a significant depolarizing shift in spike threshold in mice lacking Na_v1.6 channels (see *figure 3-7 D and G*). Secondly, absence of Na_v1.6 significantly reduced the temporal separation between axonal and somatic components of spike initiation during prolonged firing (see *figure 3-11 D*). The third characteristic affected by the mutation was a pronounced reduction in the 'kinkiness' of the action potentials initial phase (see *figure 3-10 Ab and Bb*). This feature was quantified by calculating the slope of the initial voltage rise of the action potential (see *figure 3-11 C*).

What are the reasons for the changes in spike initiation in mice lacking Na_v1.6?

Passive membrane properties, such as capacitance and input resistance were not different between *Scn8a^{med}* and *Scn8a^{wt}* mice (see *methods 2.6.3*). Furthermore, axon initial segment morphology appeared unaltered in the Ankyrin G immunolabellings (see *figure 3-2 A leftmost panels*). Therefore, the contributions of passive membrane properties and neuronal morphology to action potential initiation are unlikely to contribute to the changes observed in the absence of Na_v1.6.

The second factor localizing spike initiation to the axon initial segment is the high density of Na⁺ channels. In *Scn8a^{wt}* mice, Na_v1.6 strongly contributes to Na⁺ channels aggregation at the AIS (see *figure 3-1 A*, while in *Scn8a^{med}* mice aggregation of Na⁺ channels is not reduced (see *figure 3-2*). This is in good agreement with the finding that the amplitude of the transient Na⁺ current (I_{NaT}) in acutely isolated neurons is also not reduced in *Scn8a^{med}* mice (see *results 3.2*). However the exact contribution of axonal membranes to the currents recorded in this preparation might differ, but proximal parts of the axon are preserved [Yue et al. , 2005]. Due to incomplete voltage clamp, the determination of I_{NaT} amplitude in somatic recordings in the slice preparation, containing intact axons, is not feasible. Another way to assess I_{NaT} density at the axon initial segment would be by performing direct cell-attached recordings [Kole et al. , 2008]. However, we did not manage to establish electrophysiological recordings from axon initial segments of mouse CA1 pyramidal neurons. Therefore, we decided to analyze the impact of axonal Na⁺ currents on action potential initiation over a wide range I_{NaT}

densities by computational modeling (see *results chapter 3.10 and below for discussion*).

Even though we found transient Na^+ currents to be preserved in *Scn8a^{med}* mice, persistent Na^+ current (I_{NaP}) amplitudes were significantly reduced in the recordings performed in the slice preparation (see *figure 3-4*). The persistent Na^+ current is mainly generated at the proximal part of the axon [Yue et al. , 2005, Astman et al. , 2006] and rapidly activates at subthreshold membrane potentials [French et al. , 1990, Yue et al. , 2005]. Therefore a reduction in I_{NaP} is well suited to contribute to the changes observed in threshold and spike initiation in *Scn8a^{med}* mice. To analyze this we conducted our modeling experiments also with reduced I_{NaP} amplitudes (compare *figure 3-14 with figure 3-15 and figure 3-16*). These experiments show that I_{NaP} indeed influences spike threshold. This influence is particularly strong when I_{NaP} is reduced in both soma and axon initial segment and when I_{NaT} densities are low (compare *figure 3-14 Bb with figure 3-15 Ab, open symbols*). Changing I_{NaP} amplitude attenuates the influence of a shift in I_{NaT} activation on spike initiation as long as current densities are comparable between soma and axon initial segment (compare *figure 3-14 Ba with figure 3-15 Aa and figure 3-16 Aa, grey symbols*).

Finally, distinguished biophysical properties of Na^+ channels at the axon initial segment are thought to be important for the localization of spike initiation and setting of the action potential threshold [Colbert & Pan, 2002, Naundorf et al. , 2006]. In our recordings of I_{NaT} in *Scn8a^{med}* mice, we found a significant depolarizing shift in the voltage dependence of activation caused by the lack of functional $\text{Na}_v1.6$ (see *figure 3-3*). The biophysical properties of Na^+ channel α -subunits have been analyzed in great detail utilizing various expression systems. The results obtained in such experiments differ to a great extent dependent on the transfected cell-type and the presence of accessory subunits. Our findings are consistent with studies that have examined the properties of $\text{Na}_v1.2$ or $\text{Na}_v1.6$ in neurons by expressing them in mammalian DRG neurons that express accessory β -subunits. These experiments have indicated that the voltage dependence of activation and inactivation of $\text{Na}_v1.6$ channels is shifted in a hyperpolarized direction compared to $\text{Na}_v1.2$ [Rush et al. , 2005]. For unknown reasons, such a shift in voltage dependence was not observed when $\text{Na}_v1.2$ and $\text{Na}_v1.6$ were co-expressed with β -subunits $\beta1$ and $\beta2$ in *Xenopus laevis* oocytes [Smith et al. , 1998]. However, expression of the $\text{Na}_v1.6$ α -subunit in oocytes alone produced a voltage dependence of activation and inactivation that was shifted to unusually depolarized potentials.

Neurons from *Scn8a^{med}* mice were recorded previously in different regions of the CNS with varying results. A shift in the voltage dependence of activation was not observed in globus pallidus neurons [Mercer et al. , 2007], cerebellar neurons [Raman et al. , 1997], or mesencephalic trigeminal neurons [Enomoto et al. , 2007]. This feature of the transient Na^+ current, mediated by $\text{Na}_v1.6$, is exclusively described in CA1 pyramidal neurons in this work. Regarding the voltage dependence of inactivation of I_{NaT} however, we found no changes in *Scn8a^{med}* mice. This is in good agreement with observations from other cell types in mice [Enomoto et al. , 2007, Mercer et al. , 2007], but see [Raman et al. , 1997]. The reasons for these disparate findings are currently unknown but indicate the importance of cell-specific modulation of $\text{Na}_v1.6$ channels, as well as differences in potential compensatory changes following the loss of $\text{Na}_v1.6$ channels in *Scn8a^{med}* mice.

In our opinion, the observed depolarizing shift in the voltage dependence of Na^+ channel activation contributes strongly to the significant increase in the threshold for action potential generation in *Scn8a^{med}* mice. We also propose that activation at hyperpolarized potentials at the axon initial segment is well suited to localize spike initiation to this site. This hypothesis is supported by the fact, that action potential initiation was shown to occur at the most distal part of the axon initial segment [Palmer & Stuart, 2006, Meeks & Mennerick, 2007] and that this site displays the highest concentration of $\text{Na}_v1.6$ [Van Wart et al. , 2007, Lorincz & Nusser, 2008].

We systematically assessed the influence of a hyperpolarizing shift in the voltage dependence of activation at the axon initial segment over a range of Na^+ current densities in our computational model (see *figure 3-14*). In these experiments, we found that such a shift exerts a large influence on the threshold for action potentials (see *figure 3-14 Cb*). Additionally, localization of spike initiation to the axon initial segment was strongly augmented over a wide range of current densities tested (see *figure 3-14 Ca*). This important role of the voltage dependence of axonal Na^+ channels was also apparent when we adjusted the model to account for the reduced persistent Na^+ currents observed in *Scn8a^{med}* mice (see *figure 3-15 and figure 3-16*).

Taken together, we conclude that $\text{Na}_V1.6$ subunits expressed at the axon initial segment by their hyperpolarized voltage of activation localize action potential initiation to this subcellular compartment and also set the voltage threshold for action potential generation. Localization of spike initiation and a hyperpolarized spike threshold can also be achieved by higher densities of I_{NaT} at the axon initial segment compared to the soma (see *figure 3-14 Ba and Bb, closed symbols and figure 3-14, Ca and Cb, rightmost part*). Nevertheless, under conditions of prolonged depolarization and high frequency firing total Na^+ channel availability is reduced. Under such conditions the specialized biophysical properties of $\text{Na}_V1.6$ would show increased influence in determining spike threshold and initiation. This interpretation is in good agreement with the very low firing rates observed in *Scn8a^{med}* mice in cell-attached recordings (see *figure 3-6*).

4.3 The contribution of Na^+ currents to spike gain

In *Scn8a^{med}* mice we found a pronounced reduction in the spike gain, which is connected to the increased action potential threshold. The resurgent Na^+ current (I_{NaR}) and the persistent Na^+ current (I_{NaP}) have been shown to affect repetitive firing and spike gain [Levin et al. , 2006, Mercer et al. , 2007, Raman & Bean, 1997]. We showed that in CA1 neurons from *Scn8a^{med}* mice I_{NaP} is reduced by 42% and I_{NaR} by 71% [Royeck et al. , 2008]. It is already known that $\text{Na}_V1.6$ contributes to I_{NaP} and I_{NaR} in various neurons of the central nervous system. However, the extent and the relative proportion of the reduction in I_{NaP} and in I_{NaR} vary considerably in neurons recorded from *Scn8a^{med}* mice. This is similar to the results reported for mesencephalic trigeminal neurons in $\text{Na}_V1.6$ null mice (39% reduction in I_{NaP} , 76% reduction in I_{NaR} , [Enomoto et al. , 2007]), DRG neuron cultures (complete ablation of I_{NaR} , [Cummins et al. , 2005]), subthalamic nucleus neurons (63% reduction in I_{NaR} , 55% reduction in I_{NaP} , [Do & Bean, 2004]), or cerebellar neurons [Raman et al. , 1997]. Only in globus pallidus neurons of *Scn8a^{med}* mice I_{NaP} amplitude is independent of $\text{Na}_V1.6$, however I_{NaR} is still reduced [Mercer et al. , 2007]. The reasons for these differences are not very well understood, but suggest modulation of these currents.

What are the consequences of reductions in I_{NaP} and I_{NaR} on spike gain?

Most data suggest that I_{NaR} and I_{NaP} conspire to augment repetitive firing [Levin et al. , 2006, Mercer et al. , 2007, Raman & Bean, 1997]. The release of the open channel block following a spike that underlies I_{NaR} by itself depolarizes the cell, thus activating the subthreshold I_{NaP} . The depolarization mediated by these two currents help the cell to reach threshold again. In contrast to this, Vervaeke *et al.* [2008a] proposed an opposite effect of I_{NaP} on spike gain. From experiments that utilized dynamic clamp they conclude that the depolarization mediated by I_{NaP} depolarizes the cells in between two action potentials and thereby prevents inactivated Na^+ channels from recovery. The reduced availability of Na^+ channels would then attenuate spike gain.

This explanation is contrary to our experiments. We never observed an increase but a progressive reduction in the number of spikes evoked when we monitored the wash-in of 1 μM riluzole (a blocker of I_{NaP} , see *figure 3-23*) with 600 ms current

injections (*not shown*). We therefore propose that in the absence of Na_v1.6 the reduced amplitudes of I_{NaR} and I_{NaP} together with the shift in I_{NaT} activation together reduce reduce output gain in CA1 neurons. These results are also interesting because they imply that a substantial portion of I_{NaP} and I_{NaR} may be generated at the spike initiation zone at the AIS, as was shown in some types of neurons with physiological techniques [Astman et al. , 2006, Castelli et al. , 2007].

4.4 The contribution of Na⁺ currents to the spike afterdepolarization

We found that the increased amplitude of I_{NaP} in pilocarpine treated rats coincides with greater amplitudes of the spike afterdepolarization (*see figure 3-23*). This is in good agreement with experimental evidence that I_{NaP} contributes strongly to in adult rat CA1 pyramidal neurons [Yue et al. , 2005]. In contrast to the whole-cell current clamp data presented in this work, application of various blockers of I_{NaP} also reduced the spike ADP in non epileptic rats in sharp microelectrode recordings (*see figure 3-23 A and D*). Additionally to the difference in pharmacology of the ADP, burst discharges also seem to occur at higher frequency in sharp microelectrode recordings than in whole-cell configuration (*compare Chen et al. , [2009] with this study*). The reasons for this discrepancy are unclear but the contribution of I_{NaP} to the amplitude of the ADP might differ between sharp microelectrode and whole-cell patch clamp recordings. Another study published by Metz et al. [2005] proposed a pronounced contribution of voltage gated Ca²⁺ currents to the amplitude of the ADP in whole-cell patch clamp recordings. One hypothesis is that the substitution of the cytosol by the intracellular pipette solution disrupts or modulates currents affecting the amplitude of the ADP, whereas such a lysis is less pronounced in sharp microelectrode recordings.

In young rats of comparable age to the mice used in the first part of this study, not only I_{NaP} , but also dendritic voltage gated Ca²⁺ currents strongly amplify spike afterdepolarizations and cause the generation of spike bursts also in sharp microelectrode recordings [Chen et al. , 2005]. In this age range, region pharmacologically blocking either voltage gated Ca²⁺ currents at the dendrites or I_{NaP} in the perisomatic reduces spike afterdepolarizations and associated burst discharges. Surprisingly, spike afterdepolarizations were not reduced in *Scn8a^{med}* mice, despite a reduction of I_{NaP} by 42%. One explanation for this unexpected finding might be that a partial reduction of I_{NaP} in young animals, as used in this study, is not sufficient to affect the magnitude of the spike afterdepolarization, given the important contribution of voltage gated Ca²⁺ currents at this age [Chen et al. , 2005] and in whole-cell configuration [Metz et al. , 2005]. Another explanation for the stability of the ADP amplitude might be due to a compensatory mechanism. Indeed, the functional deletion of Na_v1.6 in *Scn8a^{med}* mice was shown to cause a compensatory upregulation of T-type Ca²⁺ currents in Purkinje neurons [Swensen & Bean, 2005]. In contrast, changes in K⁺ channels were subtle in *Scn8a^{med}* mice, with only small changes in the voltage dependence of K⁺ currents highly sensitive to tetraethylammonium [Khaliq et al. , 2003]. We did not find a compensatory upregulation of T-type Ca²⁺ currents in CA1 neurons (*see figure 3-5*), indicating that different compensatory changes may be invoked in different neuron types.

4.5 Compensatory or homeostatic changes in mice lacking functional Na_v1.6 channels

Interestingly Na⁺ channel α -subunit aggregation persisted in *Scn8a*^{med} mice, thus indicating compensation (see figure 3-2). The most probable candidate countervailing for the loss of Na_v1.6 in *Scn8a*^{med} mice is Na_v1.2. This subunit has been already reported to colocalize with Ankyrin G (Ank G) in retinal ganglion cells [Boiko et al. , 2003] and share the Ank G binding motif with Na_v1.6. A developmental shift from Na_v1.2 to Na_v1.6 expression in the postnatal mouse development was recently described [Wart & Matthews, 2006a]. Therefore the compensation by Na_v1.2 could occur due to a delayed reduction of Na_v1.2 expression in *Scn8a*^{med} mice. This hypothesis is supported by Western blot analysis of heterozygous *Scn8a*^{wt/med} mice, which had reduced Na_v1.6 expression paired with increased Na_v1.2 expression compared to *Scn8a*^{wt} mice [Vega et al. , 2008]. Finally, aggregation of Na_v1.2 at axon initial segments was shown in cortical, retinal, and cerebellar neurons of *Scn8a*^{med} mice [Wart & Matthews, 2006b].

In this context it might also be interesting to look at K⁺ channels expressed at the axon initial segment. So far, K_v1.1, K_v1.2 [Inda et al. , 2006, Lorincz & Nusser, 2008], as well as K_v7.2 and K_v7.3 [Pan et al. , 2006] have been reported to be concentrated at the axon initial segment of CA1 pyramidal neurons. Application of the two specific K_v7 channel blockers XE991 and linopirdine failed to significantly affect spike threshold for single action potentials [Yue & Yaari, 2004, Peters et al. , 2005], whereas both blockers drastically increased the amplitude of the ADP and induced burst firing in CA1 pyramidal neurons [Yue & Yaari, 2004]. This observation is in good agreement with the stability of the ADP and with the increased action potential threshold in *Scn8a*^{med} mice. Additionally, the K_v7 channels are candidates for homeostatic regulations occurring in the absence of Na_v1.6 since they share the motif for Ank G interaction [Pan et al. , 2006]. However, also other currents could be regulated in the absence of Na_v1.6, such as Na⁺- and Ca²⁺-dependent K⁺ currents, as well as the A- and D-type voltage gated K⁺ currents [Swensen & Bean, 2005, Khaliq et al. , 2003].

4.6 Na⁺ channels in chronic epilepsy

There is a tight connection between Na⁺ channels and epilepsy. On one hand, several antiepileptic drugs used in the treatment of epilepsy influence the biophysical properties of Na⁺ currents [Reckziegel et al. , 1999, Köhling, 2002, Remy et al. , 2003, Schaub et al. , 2007]. Therefore, investigating the contribution of individual Na⁺ channel α -subunits to neuronal discharge properties in the healthy and diseased nervous system can help in the development of drugs with a more selective mode of action. On the other hand, there is evidence for causal relation of mutations in Na⁺ channel genes with genetic epilepsies [Köhling, 2002, Meisler & Kearney, 2005, Yu et al. , 2006]. For example, Na_v1.1 mutations are found in more than 70 % of patients with severe myoclonic epilepsy of infancy (SMEI) [Fukuma et al. , 2004]. Generalized epilepsy with febrile seizures plus (GEFS+) has been associated with mutations in the accessory β 1-subunit [Wallace et al. , 1998, Moulard et al. , 1999, Wallace et al. , 2001, Spanpanato et al. , 2004] and the α -subunit Na_v1.2 [Haug et al. , 2001, Baulac et al. , 1999]. Mutations in the Na_v1.2 gene are also detected in Benign Familial Neonatal-Infantile Seizures (BFNIS) [Heron et al. , 2002]. Recently, also mutations in the Na_v1.3 gene were detected in patients suffering from genetic epilepsy [Holland et al. , 2008]. So far, no mutations in the gene encoding Na_v1.6 have been found in epileptic patients. A recent work in genetic mouse models of GEFS+ and SMEI reported that mutations in Na_v1.6 can act as a modifier of disease severity [Martin et al. , 2007]. However, mutations in Na_v1.6 have been causally related with other genetic diseases in humans, such as

cognitive impairment, cerebellar atrophy, and ataxia [Meisler & Kearney, 2005, Trudeau et al. , 2006].

Interestingly, several epileptogenic mutations in Na⁺ channels mediate an increased persistent Na⁺ current (I_{NaP}) in expression systems when compared to wild-type channels. Increases in I_{NaP} amplitude were reported to be caused by mutations of genes encoding Na_v1.1 [Lossin et al. , 2002, Lossin et al. , 2003, Rhodes et al. , 2004] and Na_v1.3 [Holland et al. , 2008], while mutations affecting Na_v1.2 [Kamiya et al. , 2004, Scalmani et al. , 2006] or the accessory β 1-subunit [Wallace et al. , 1998, Meadows et al. , 2002] rather modulate transient Na⁺ currents leading to hyperexcitability. However, an epileptogenic mutation affecting the β 1-subunit was recently shown to increase I_{NaP} amplitude through an interaction involving the β 4-subunit [Aman et al. , 2009]. Furthermore, a mutation affecting Na_v1.2 in mice increased I_{NaP} amplitude and led to the development of epileptic seizures in conjunction with gliosis and hippocampal cell loss.

In the pilocarpine model of epilepsy we found a significant upregulation of the amplitude of I_{NaP} in CA1 pyramidal neurons (*see figure 3-21*). What underlies this upregulation of I_{NaP} ? Analysis of mRNA expression of the Na⁺ channel α -subunits Na_v1.1, Na_v1.2, Na_v1.3, and Na_v1.6 failed to detect any upregulation (*see figure 3-17 B*). Our Western blot analysis also points to stable expression of Na⁺ channel α -subunits (*see figure 3-18 Bb, rightmost bars*) and rather a downregulation of Na_v1.6 (*see figure 3-18 Bb*). Our immunohistochemical experiments argue for stable expression of Na_v1.6 Na⁺ channels in general at the axon initial segment following status epilepticus (*see figure 3-19 and figure 3-20, respectively*). Hence, we propose that a simple increase in one of the Na⁺ channel α -subunits cannot be responsible for the increase in I_{NaP} amplitude.

Accessory Na⁺ channel β -subunits might be regulated following pilocarpine induced epileptogenesis, as well. Such a regulation could affect biophysical properties or subcellular targeting of Na⁺ channels [Isom, 2002]. Changes in β -subunit expression following status epilepticus were already investigated in the dentate gyrus, where early downregulation of β 2-subunits was followed by downregulation of β 1-subunits in the chronic phase of epilepsy [Ellerkmann et al. , 2003]. The authors suggest that this downregulation could mediate the depolarizing shift in voltage dependence of inactivation, which they report to occur in dentate gyrus granule cells. This shift is not observed in CA1 pyramidal cells [Schaub et al. , 2007]. Despite of this, regulation of β -subunit expression in CA1 in epilepsy might still occur mediating other changes dependent on the associated Na⁺ channel α -subunit isoform or subcellular location of the β -subunit. In this context it might be interesting to analyze the expression of the β 4-subunit, which was shown to influence I_{NaP} [Aman et al. , 2009] and is expressed at low levels in the healthy hippocampus [Yu et al. , 2003].

What else might lead to the increase in I_{NaP} amplitude? One reason could be changes in the expression of alternatively spliced Na⁺ channel isoforms. Some of these Na⁺ channel isoforms are normally expressed during development. Na⁺ channel splicing, including that of Na_v1.6, often leads to the generation of a truncated mRNA of unknown functionality [Plummer et al. , 1997, Diss et al. , 2004]. Another kind of splicing leads to functional isoforms, which sometimes only differ in a single amino acid [Diss et al. , 2004, Kerr et al. , 2004]. Such a variant of Na_v1.2 displays a hyperpolarized shift in the voltage dependence of activation and inactivation [Auld et al. , 1990]. There is already some evidence that upregulation of Na⁺ channel splice variants occurs both in humans suffering from epilepsy [Heinzen et al. , 2007] and in animal models of epilepsy [Gastaldi et al. , 1997]. Our experiments analyzing Na⁺ channel mRNA and protein expression in epileptic rats were not suited to distinguish between Na⁺ channel splice variants. Therefore, changes in the ratio of Na⁺ channel splice variant expression could in principle contribute to the increase in I_{NaP} amplitude.

4.7 Modulation of persistent Na⁺ currents by intracellular spermine

Including 1 mM of the polyamine spermine into the pipette solution completely blocked the upregulated portion of I_{NaP} in epileptic rats (see figure 3-21). Modulation of I_{NaP} by cytosolic polyamines was recently described in cortical neurons by Fleidervish *et al.* [2008]. Spermine is a derivative of the amino acid ornithine. Ornithine is decarboxylated by the ornithine decarboxylase. This enzyme is considered to be rate limiting in the metabolism of polyamine production and can be irreversibly inhibited by the ornithine analogon α -difluoromethylornithine (DFMO) [Gilad & Gilad, 2003, Wallace *et al.*, 2003]. Fleidervish *et al.* [2008] showed that preincubation of slices with DFMO lead to an increase in the amplitude of I_{NaP} which was then sensitive to spermine.

What could be responsible for the *de novo* appearance of a spermine sensitive portion of I_{NaP} in epilepsy? One hypothesis would be a reduction in spermine levels within neurons, possibly by regulation of enzymes involved in polyamine metabolism, such as ornithine decarboxylase (ODC), spermine synthase (SS), S-adenosylmethionine decarboxylase (SAM-DC), or the catabolic enzyme spermidine/spermine N1-acetyltransferase (SSAT). Such regulations were reported to occur in ischemia, Alzheimer's disease, as well as in electrical and chemical animal models of epilepsy [for review see Bernstein & Müller, 1999]. Transcription of these enzymes and polyamine levels, particularly those of putrescine, show a transient increase shortly after seizures or ischemia. This phenomenon is termed the polyamine stress response [Gilad & Gilad, 2003]. Interestingly, a reduction in spermine content was observed in human hippocampal tissue from patients with temporal lobe epilepsy [Laschet *et al.*, 1992, Laschet *et al.*, 1999]. However, it has to be considered that polyamines and related metabolic enzymes are present in all cells of the brain including endothelial, neuronal and glial cells [Fujiwara *et al.*, 1997, Laube & Veh, 1997, Krauss *et al.*, 2007, Laube *et al.*, 2002, Bernstein & Müller, 1999]. This is especially important in epilepsy where neuronal cell death is paired with a proliferation of glial cells. Furthermore, polyamines were shown to modulate voltage gated Ca²⁺ and Na⁺ channels [Scott *et al.*, 1993, Huang & Moczydlowski, 2001, Chen *et al.*, 2007], as well as inward rectifier K⁺ channels and glutamate receptors [for review see Tagliatela *et al.* 1995 and Williams, 1997]. Therefore, any interpretation connecting physiological effects with data from compound polyamine measurements or analysis of changes in enzyme regulation has to be done carefully. In fact, differences in polyamine content might be important on the subcellular level, because of the high metabolic turnover of polyamines could result in differential subcellular distribution of polyamines, thus exerting local effects on ion channels [Bernstein & Müller, 1999, Krauss *et al.*, 2007]. However, the molecular reasons underlying the occurrence of the spermine sensitive I_{NaP} require further investigation.

4.8 Changes in intrinsic firing properties in chronic epilepsy

Is the upregulation of the persistent Na⁺ current (I_{NaP}) in epilepsy reflected in altered CA1 pyramidal cell discharge properties? Utilizing whole-cell patch clamp recordings in current clamp mode we found an increase in burst firing of CA1 neurons in pilocarpine treated rats (see figure 3-22). The occurrence of burst firing was accompanied by an increase in the amplitude of the spike afterdepolarization (ADP, see figure 3-23 D). All other spike properties analyzed were unaffected by the pilocarpine treatment (see figure 3-22 G-J). Application of the I_{NaP} blocker riluzole significantly reduced the ADP amplitude in epileptic rats without affecting the ADP in sham control rats. We thus conclude that the upregulation of I_{NaP} in epilepsy is associated with an increase in the ADP amplitude and contributes to the occurrence of burst firing. However, this data is partly in contrast to findings by Yue *et al.* [2005] who show utilizing sharp microelectrodes, that the I_{NaP} mediates the ADP also in CA1 neurons from healthy animals. The most

probable explanation for this discrepancy is that the contribution of I_{NaP} to the ADP is sensitive to the dilution of the cytosol in whole-cell configuration.

The increased intrinsic burst firing in epilepsy and the underlying mechanisms have been investigated previously. A study published by Becker et al. [2008] shows that an upregulation of $Ca_v3.2$ Ca^{2+} channels mediating T-type Ca^{2+} currents contributes to increased excitability. Using sharp microelectrode recordings they show that application of low concentrations of Ni^{2+} blocks the ADP and attenuates burst firing in epileptic animals.

More recently, a submitted study provides evidence that also alterations in Na^+ currents contribute to the increased excitability in epilepsy [Chen et al. , 2009]. The authors of that study show that two distinct mechanisms conspire in order to generate the pathologic increase in burst firing observed in CA1 pyramidal cells. One burst mechanism, termed low threshold bursting, is sensitive to low concentrations of Ni^{2+} and attributed to the upregulation of T-type Ca^{2+} currents mentioned above. After blocking of this low threshold bursting, most neurons still displayed burst discharges upon stronger and prolonged depolarization. This high threshold bursting was sensitive to somatic applications of blockers acting on persistent Na^+ currents [Chen et al. , 2009] and is therefore probably mediated by the *de novo* I_{NaP} component appearing in epileptic rats, which is described in this study (*see figure 3-21*).

In conclusion, we propose that an epilepsy induced spermine sensitive I_{NaP} contributes to the augmented intrinsic excitability and increases high threshold bursting propensity in CA1 pyramidal neurons. Furthermore, we propose that this additional portion of I_{NaP} is not associated with an upregulation of Na^+ channel α -subunits but rather caused by posttranscriptional or posttranslational modifications.

5. References

- [Alzheimer *et al.*, 1993] Alzheimer, C., Schwindt, P. C., & Crill, W. E. 1993. Modal gating of Na⁺ channels as a mechanism of persistent Na⁺ current in pyramidal neurons from rat and cat sensorimotor cortex. *J Neurosci*, **13**(2), 660–673.
- [Aman *et al.*, 2009] Aman, Teresa K, Grieco-Calub, Tina M, Chen, Chunling, Rusconi, Raffaella, Slat, Emily A, Isom, Lori L, & Raman, Indira M. 2009. Regulation of persistent Na current by interactions between beta subunits of voltage-gated Na channels. *J Neurosci*, **29**(7), 2027–2042.
- [Amaral & Witter, 1989] Amaral, D. G., & Witter, M. P. 1989. The three-dimensional organization of the hippocampal formation: a review of anatomical data. *Neuroscience*, **31**(3), 571–591.
- [Amaral *et al.*, 1991] Amaral, D. G., Dolorfo, C., & Alvarez-Royo, P. 1991. Organization of CA1 projections to the subiculum: a pha-I analysis in the rat. *Hippocampus*, **1**(4), 415–435.
- [Andersen *et al.*, 1971] Andersen, P., Bliss, T. V., & Skrede, K. K. 1971. Lamellar organization of hippocampal pathways. *Exp Brain Res*, **13**(2), 222–238.
- [Astman *et al.*, 2006] Astman, Nadav, Gutnick, Michael J, & Fleidervish, Ilya A. 2006. Persistent sodium current in layer 5 neocortical neurons is primarily generated in the proximal axon. *J Neurosci*, **26**(13), 3465–3473.
- [Auld *et al.*, 1990] Auld, V. J., Goldin, A. L., Krafte, D. S., Catterall, W. A., Lester, H. A., Davidson, N., & Dunn, R. J. 1990. A neutral amino acid change in segment IIS4 dramatically alters the gating properties of the voltage-dependent sodium channel. *Proc Natl Acad Sci U.S.A.*, **87**(1), 323–327.
- [Bannister & Larkman, 1995a] Bannister, N. J., & Larkman, A. U. 1995a. Dendritic morphology of CA1 pyramidal neurones from the rat hippocampus: I. branching patterns. *J Comp Neurol*, **360**(1), 150–160.
- [Bannister & Larkman, 1995b] Bannister, N. J., & Larkman, A. U. 1995b. Dendritic morphology of CA1 pyramidal neurones from the rat hippocampus: II. spine distributions. *J Comp Neurol*, **360**(1), 161–171.
- [Baulac *et al.*, 1999] Baulac, S., Gourfinkel-An, I., Picard, F., Rosenberg-Bourgin, M., Prud'homme, J. F., Baulac, M., Brice, A., & LeGuern, E. 1999. A second locus for familial generalized epilepsy with febrile seizures plus maps to chromosome 2q21-q33. *Am J Hum Genet*, **65**(4), 1078–1085.
- [Bean, 2007] Bean, Bruce P. 2007. The action potential in mammalian central neurons. *Nat Rev Neurosci*, **8**(6), 451–465.
- [Beck & Yaari, 2008] Beck, Heinz, & Yaari, Yoel. 2008. Plasticity of intrinsic neuronal properties in CNS disorders. *Nat Rev Neurosci*, **9**(5), 357–369.
- [Becker *et al.*, 2008] Becker, Albert J, Pitsch, Julika, Sochivko, Dmitry, Opitz, Thoralf, Staniek, Matthäus, Chen, Chien-Chang, Campbell, Kevin P, Schoch, Susanne, Yaari, Yoel, & Beck, Heinz. 2008. Transcriptional upregulation of Ca_v3.2 mediates epileptogenesis in the pilocarpine model of epilepsy. *J Neurosci*, **28**(49), 13341–13353.
- [Bekenstein & Lothman, 1993] Bekenstein, J. W., & Lothman, E. W. 1993. Dormancy of inhibitory interneurons in a model of temporal lobe epilepsy. *Science*, **259**(5091), 97–100.
- [Bell & Sander, 2001] Bell, G. S., & Sander, J. W. 2001. The epidemiology of epilepsy: the size of the problem. *Seizure*, **10**(4), 306–315.
- [Bender & Trussell, 2009] Bender, Kevin J, & Trussell, Laurence O. 2009. Axon initial segment Ca²⁺ channels influence action potential generation and timing. *Neuron*, **61**(2), 259–271.

- [Bennett, 2001] Bennett, E. S. 2001. Channel cytoplasmic loops alter voltage-dependent sodium channel activation in an isoform-specific manner. *J Physiol*, **535**(Pt 2), 371–381.
- [Bennett, 2002] Bennett, Eric S. 2002. Isoform-specific effects of sialic acid on voltage-dependent Na⁺ channel gating: functional sialic acids are localized to the S5-S6 loop of domain I. *J Physiol*, **538**(Pt 3), 675–690.
- [Bernard *et al.*, 2004] Bernard, Christophe, Anderson, Anne, Becker, Albert, Poolos, Nicholas P, Beck, Heinz, & Johnston, Daniel. 2004. Acquired dendritic channelopathy in temporal lobe epilepsy. *Science*, **305**(5683), 532–535.
- [Bernstein & Müller, 1999] Bernstein, H. G., & Müller, M. 1999. The cellular localization of the L-ornithine decarboxylase/polyamine system in normal and diseased central nervous systems. *Prog Neurobiol*, **57**(5), 485–505.
- [Bevan & Storey, 2002] Bevan, Stuart, & Storey, Nina. 2002. Modulation of sodium channels in primary afferent neurons. *Novartis Found Symp*, **241**, 144–53; 153–8, 226–32.
- [Bird & Burgess, 2008] Bird, Chris M, & Burgess, Neil. 2008. The hippocampus and memory: insights from spatial processing. *Nat Rev Neurosci*, **9**(3), 182–194.
- [Blackstad, 1958] Blackstad, T. W. 1958. On the termination of some afferents to the hippocampus and fascia dentata; an experimental study in the rat. *Acta Anat (Basel)*, **35**(3), 202–214.
- [Bliss & Lomo, 1973] Bliss, T. V., & Lomo, T. 1973. Long-lasting potentiation of synaptic transmission in the dentate area of the anaesthetized rabbit following stimulation of the perforant path. *J Physiol*, **232**(2), 331–356.
- [Blümcke *et al.*, 1999] Blümcke, I., Beck, H., Lie, A. A., & Wiestler, O. D. 1999. Molecular neuropathology of human mesial temporal lobe epilepsy. *Epilepsy Res*, **36**(2-3), 205–223.
- [Blümcke *et al.*, 2002] Blümcke, I., Thom, M., & Wiestler, O.D. 2002. Ammon's horn sclerosis: a maldevelopmental disorder associated with temporal lobe epilepsy. *Brain Pathol*, **12**(2), 199–211.
- [Boiko *et al.*, 2001] Boiko, T., Rasband, M. N., Levinson, S. R., Caldwell, J. H., Mandel, G., Trimmer, J. S., & Matthews, G. 2001. Compact myelin dictates the differential targeting of two sodium channel isoforms in the same axon. *Neuron*, **30**(1), 91–104.
- [Boiko *et al.*, 2003] Boiko, Tatiana, Wart, Audra Van, Caldwell, John H, Levinson, S. Rock, Trimmer, James S, & Matthews, Gary. 2003. Functional specialization of the axon initial segment by isoform-specific sodium channel targeting. *J Neurosci*, **23**(6), 2306–2313.
- [Bowden *et al.*, 2001] Bowden, S. E., Fletcher, S., Loane, D. J., & Marrion, N. V. 2001. Somatic colocalization of rat SK1 and D class (Ca(v)1.2) L-type calcium channels in rat CA1 hippocampal pyramidal neurons. *J Neurosci*, **21**(20), RC175.
- [Brown & Randall, 2009] Brown, Jon T, & Randall, Andrew D. 2009. Activity-dependent depression of the spike after-depolarization generates long-lasting intrinsic plasticity in hippocampal CA3 pyramidal neurons. *J Physiol*, **587**(Pt 6), 1265–1281.
- [Burgess *et al.*, 1995] Burgess, D. L., Kohrman, D. C., Galt, J., Plummer, N. W., Jones, J. M., Spear, B., & Meisler, M. H. 1995. Mutation of a new sodium channel gene, *Scn8a*, in the mouse mutant 'motor endplate disease'. *Nat Genet*, **10**(4), 461–465.
- [Cantrell & Catterall, 2001] Cantrell, A. R., & Catterall, W. A. 2001. Neuromodulation of Na⁺ channels: an unexpected form of cellular plasticity. *Nat Rev Neurosci*, **2**(6), 397–407.
- [Carnevale & Hines, 2006] Carnevale, N.T., & Hines, M. 2006. *The Neuron Book*. Cambridge, UK.
- [Carr *et al.*, 2003] Carr, David B, Day, Michelle, Cantrell, Angela R, Held, Joshua, Scheuer, Todd, Catterall, William A, & Surmeier, D. James. 2003. Transmitter modulation of slow, activity-dependent alterations in sodium channel availability endows neurons with a novel form of cellular plasticity. *Neuron*, **39**(5), 793–806.
- [Castelli *et al.*, 2007] Castelli, Loretta, Nigro, Maximiliano J, & Magistretti, Jacopo. 2007. Analysis of resurgent sodium-current expression in rat parahippocampal cortices and hippocampal formation. *Brain Res*, **1163**(Aug), 44–55.

- [Catterall, 1981] Catterall, W. A. 1981. Localization of sodium channels in cultured neural cells. *J Neurosci*, **1**(7), 777–783.
- [Catterall, 1986] Catterall, W. A. 1986. Molecular properties of voltage-sensitive sodium channels. *Annu Rev Biochem*, **55**, 953–985.
- [Catterall, 2000] Catterall, W. A. 2000. From ionic currents to molecular mechanisms: the structure and function of voltage-gated sodium channels. *Neuron*, **26**(1), 13–25.
- [Catterall *et al.*, 2005] Catterall, William A, Goldin, Alan L, & Waxman, Stephen G. 2005. International union of pharmacology. XLVII. nomenclature and structure-function relationships of voltage-gated sodium channels. *Pharmacol Rev*, **57**(4), 397–409.
- [Cavalheiro, 1995] Cavalheiro, E. A. 1995. The pilocarpine model of epilepsy. *Ital J Neurol Sci*, **16**(1-2), 33–37.
- [Chen *et al.*, 2004] Chen, C., Westenbroek, R. E., Xu, X., Edwards, C. A., Sorenson, D. R., Chen, Y., McEwen, D. P., O'Malley, H. A., Bharucha, V., Meadows, L. S., Knudsen, G. A., Vilaythong, A., Noebels, J. L., Saunders, T. L., Scheuer, T., Shrager, P., Catterall, W. A., & Isom, L. L. 2004. Mice lacking sodium channel beta1 subunits display defects in neuronal excitability, sodium channel expression, and nodal architecture. *J Neurosci*, **24**(16), 4030–4042.
- [Chen *et al.*, 2001] Chen, J., Sochivko, D., Beck, H., Marechal, D., Wiestler, O. D., & Becker, A. J. 2001. Activity-induced expression of common reference genes in individual CNS neurons. *Lab Invest*, **81**(6), 913–916.
- [Chen *et al.*, 2005] Chen, S., Yue, C., & Yaari, Y. 2005. A transitional period of Ca²⁺-dependent spike afterdepolarization and bursting in developing rat CA1 pyramidal cells. *J Physiol*, **567**(Pt 1), 79–93.
- [Chen *et al.*, 2009] Chen, S, Su, H, Remy, S, Yue, C, Sochivko, D, Beck, H, & Yaari, Y. 2009. Two distinct mechanisms generating aberrant intrinsic bursting in acquired temporal lobe epilepsy. *Submitted*.
- [Chen & Yaari, 2008] Chen, Shmuel, & Yaari, Yoel. 2008. Spike Ca²⁺ influx upmodulates the spike afterdepolarization and bursting via intracellular inhibition of K_v7 / M channels. *J Physiol*, **586**(5), 1351–1363.
- [Chen *et al.*, 2007] Chen, Wenyan, Harnett, Mark T, & Smith, Stephen M. 2007. Modulation of neuronal voltage-activated calcium and sodium channels by polyamines and pH. *Channels (Austin)*, **1**(4), 281–290.
- [Chen *et al.*, 2008] Chen, Yuan, Yu, Frank H, Sharp, Elizabeth M, Beacham, Daniel, Scheuer, Todd, & Catterall, William A. 2008. Functional properties and differential neuromodulation of Na(v)1.6 channels. *Mol Cell Neurosci*, **38**(4), 607–615.
- [Chiu *et al.*, 1984] Chiu, S. Y., Shrager, P., & Ritchie, J. M. 1984. Neuronal-type Na⁺ and K⁺ channels in rabbit cultured Schwann cells. *Nature*, **311**(5982), 156–157.
- [Clark *et al.*, 2005] Clark, R. E., Broadbent, N. J., & Squire, L. R. 2005. Hippocampus and remote spatial memory in rats. *Hippocampus*, **15**(2), 260–272.
- [Colbert & Johnston, 1996] Colbert, C. M., & Johnston, D. 1996. Axonal action-potential initiation and Na⁺ channel densities in the soma and axon initial segment of subicular pyramidal neurons. *J Neurosci*, **16**(21), 6676–6686.
- [Colbert & Pan, 2002] Colbert, C. M., & Pan, E. 2002. Ion channel properties underlying axonal action potential initiation in pyramidal neurons. *Nat Neurosci*, **5**(6), 533–538.
- [Coombs *et al.*, 1957] Coombs, J. S., Curtis, D. R., & Eccles, J. C. 1957. The generation of impulses in motoneurons. *J Physiol*, **139**(2), 232–249.
- [Crill, 1996] Crill, W. E. 1996. Persistent sodium current in mammalian central neurons. *Annu Rev Physiol*, **58**, 349–362.
- [Cummins *et al.*, 2005] Cummins, Theodore R, Dib-Hajj, Sulayman D, Herzog, Raimund I, & Waxman, Stephen G. 2005. Na_v1.6 channels generate resurgent sodium currents in spinal sensory neurons. *Febs Lett*, **579**(10), 2166–2170.

- [Curia *et al.*, 2008] Curia, Giulia, Longo, Daniela, Biagini, Giuseppe, Jones, Roland S G, & Avoli, Massimo. 2008. The pilocarpine model of temporal lobe epilepsy. *J Neurosci Methods*, **172**(2), 143–157.
- [DeLorenzo *et al.*, 1996] DeLorenzo, R. J., Hauser, W. A., Towne, A. R., Boggs, J. G., Pellock, J. M., Penberthy, L., Garnett, L., Fortner, C. A., & Ko, D. 1996. A prospective, population-based epidemiologic study of status epilepticus in Richmond, Virginia. *Neurology*, **46**(4), 1029–1035.
- [der Weel *et al.*, 1997] der Weel, M. J. Dolleman-Van, da Silva, F. H. Lopes, & Witter, M. P. 1997. Nucleus reuniens thalami modulates activity in hippocampal field CA1 through excitatory and inhibitory mechanisms. *J Neurosci*, **17**(14), 5640–5650.
- [Deuchars & Thomson, 1996] Deuchars, J., & Thomson, A. M. 1996. Ca1 pyramid-pyramid connections in rat hippocampus *in vitro*: dual intracellular recordings with biocytin filling. *Neuroscience*, **74**(4), 1009–1018.
- [Devaux *et al.*, 2004] Devaux, Jérôme J, Kleopa, Kleopas A, Cooper, Edward C, & Scherer, Steven S. 2004. *KCNQ2* is a nodal K⁺ channel. *J Neurosci*, **24**(5), 1236–1244.
- [Diss *et al.*, 2004] Diss, J. K J, Fraser, S. P., & Djamgoz, M. B A. 2004. Voltage-gated Na⁺ channels: multiplicity of expression, plasticity, functional implications and pathophysiological aspects. *Eur Biophys j*, **33**(3), 180–193.
- [Do & Bean, 2004] Do, M. T., & Bean, B. P. 2004. Sodium currents in subthalamic nucleus neurons from Na_v1.6-null mice. *J Neurophysiol*, **92**(2), 726–733.
- [Drews *et al.*, 2005] Drews, V. L., Lieberman, A. P., & Meisler, M. H. 2005. Multiple transcripts of sodium channel *Scn8a* (Na(v)1.6) with alternative 5'- and 3'-untranslated regions and initial characterization of the *Scn8a* promoter. *Genomics*, **85**(2), 245–257.
- [Duchen, 1970] Duchen, L. W. 1970. Hereditary motor end-plate disease in the mouse: light and electron microscopic studies. *J Neurol Neurosurg Psychiatry*, **33**(2), 238–250.
- [Duchen & Stefani, 1971] Duchen, L. W., & Stefani, E. 1971. Electrophysiological studies of neuromuscular transmission in hereditary 'motor end-plate disease' of the mouse. *J Physiol*, **212**(2), 535–548.
- [Ellerkmann *et al.*, 2001] Ellerkmann, R. K., Riazanski, V., Elger, C. E., Urban, B. W., & Beck, H. 2001. Slow recovery from inactivation regulates the availability of voltage-dependent Na(+) channels in hippocampal granule cells, hilar neurons and basket cells. *J Physiol*, **532**(Pt 2), 385–397.
- [Ellerkmann *et al.*, 2003] Ellerkmann, R. K., Remy, S., Chen, J., Sochivko, D., Elger, C. E., Urban, B. W., Becker, A., & Beck, H. 2003. Molecular and functional changes in voltage-dependent Na(+) channels following pilocarpine-induced status epilepticus in rat dentate granule cells. *Neuroscience*, **119**(2), 323–333.
- [Engel, 1996] Engel, J. 1996. Introduction to temporal lobe epilepsy. *Epilepsy Res*, **26**(1), 141–150.
- [Engel, 2001] Engel, J. 2001. Intractable epilepsy: definition and neurobiology. *Epilepsia*, **42** Suppl 6, 3.
- [Enomoto *et al.*, 2007] Enomoto, Akifumi, Han, Juliette M, Hsiao, Chie-Fang, & Chandler, Scott H. 2007. Sodium currents in mesencephalic trigeminal neurons from Na_v1.6 null mice. *J Neurophysiol*, **98**(2), 710–719.
- [Finch & Babb, 1981] Finch, D. M., & Babb, T. L. 1981. Demonstration of caudally directed hippocampal efferents in the rat by intracellular injection of horseradish peroxidase. *Brain Res*, **214**(2), 405–410.
- [Fink *et al.*, 1998] Fink, L., Seeger, W., Ermert, L., Hänze, J., Stahl, U., Grimminger, F., Kummer, W., & Bohle, R. M. 1998. Real-time quantitative RT-PCR after laser-assisted cell picking. *Nat Med*, **4**(11), 1329–1333.
- [Fleiderovich *et al.*, 2008] Fleiderovich, Ilya A, Libman, Lior, Katz, Efrat, & Gutnick, Michael J. 2008. Endogenous polyamines regulate cortical neuronal excitability by blocking voltage-gated Na⁺ channels. *Proc Natl Acad Sci U.S.A.*, **105**(48), 18994–18999.

- [Frank *et al.* , 2001] Frank, L. M., Brown, E. N., & Wilson, M. A. 2001. A comparison of the firing properties of putative excitatory and inhibitory neurons from CA1 and the entorhinal cortex. *J Neurophysiol*, **86**(4), 2029–2040.
- [French *et al.* , 1990] French, C. R., Sah, P., Buckett, K. J., & Gage, P. W. 1990. A voltage-dependent persistent sodium current in mammalian hippocampal neurons. *J Gen Physiol*, **95**(6), 1139–1157.
- [Freund & Buzsáki, 1996] Freund, T. F., & Buzsáki, G. 1996. Interneurons of the hippocampus. *Hippocampus*, **6**(4), 347–470.
- [Fujiwara *et al.* , 1997] Fujiwara, K., Bai, G., & Kitagawa, T. 1997. Polyamine-like immunoreactivity in rat neurons. *Brain Res*, **767**(1), 166–171.
- [Fukuma *et al.* , 2004] Fukuma, Goryu, Oguni, Hirokazu, Shirasaka, Yukiyo, Watanabe, Kazuyoshi, Miyajima, Tasuku, Yasumoto, Sawa, Ohfu, Masaharu, Inoue, Takahito, Watanachai, Aruchalean, Kira, Ryutaro, Matsuo, Muneaki, Muranaka, Hideki, Sofue, Fumiko, Zhang, Bo, Kaneko, Sunao, Mitsudome, Akihisa, & Hirose, Shinichi. 2004. Mutations of neuronal voltage-gated Na⁺ channel alpha 1 subunit gene *Scn1a* in core severe myoclonic epilepsy in infancy (SMEI) and in borderline SMEI (SMEB). *Epilepsia*, **45**(2), 140–148.
- [Garrido *et al.* , 2003a] Garrido, J. J., Giraud, P., Carlier, E., Fernandes, F., Moussif, A., Fache, M. P., Debanne, D., & Dargent, B. 2003a. A targeting motif involved in sodium channel clustering at the axonal initial segment. *Science*, **300**(5628), 2091–2094.
- [Garrido *et al.* , 2003b] Garrido, Juan José, Fernandes, Fanny, Moussif, Anissa, Fache, Marie-Pierre, Giraud, Pierre, & Dargent, Bénédicte. 2003b. Dynamic compartmentalization of the voltage-gated sodium channels in axons. *Biol Cell*, **95**(7), 437–445.
- [Gastaldi *et al.* , 1997] Gastaldi, M., Bartolomei, F., Massacrier, A., Planells, R., Robaglia-Schlupp, A., & Cau, P. 1997. Increase in mRNAs encoding neonatal II and III sodium channel alpha-isoforms during kainate-induced seizures in adult rat hippocampus. *Brain Res Mol Brain Res*, **44**(2), 179–190.
- [Gilad & Gilad, 2003] Gilad, Gad M., & Gilad, Varda H. 2003. Overview of the brain polyamine-stress-response: regulation, development, and modulation by lithium and role in cell survival. *Cell Mol Neurobiol*, **23**(4-5), 637–649.
- [Goldberg *et al.* , 2008] Goldberg, Ethan M, Clark, Brian D, Zagha, Edward, Nahmani, Mark, Erisir, Alev, & Rudy, Bernardo. 2008. K⁺ channels at the axon initial segment dampen near-threshold excitability of neocortical fast-spiking GABAergic interneurons. *Neuron*, **58**(3), 387–400.
- [Golomb *et al.* , 2006] Golomb, David, Yue, Cuiyong, & Yaari, Yoel. 2006. Contribution of persistent Na⁺ current and M-type K⁺ current to somatic bursting in CA1 pyramidal cells: combined experimental and modeling study. *J Neurophysiol*, **96**(4), 1912–1926.
- [Gordienko & Tsukahara, 1994] Gordienko, D. V., & Tsukahara, H. 1994. Tetrodotoxin-blockable depolarization-activated Na⁺ currents in a cultured endothelial cell line derived from rat interlobar artery and human umbilical vein. *Pflügers Arch*, **428**(1), 91–93.
- [Gray, 1959] Gray, E. G. 1959. Electron microscopy of synaptic contacts on dendrite spines of the cerebral cortex. *Nature*, **183**(4675), 1592–1593.
- [Grieco *et al.* , 2005] Grieco, T. M., Malhotra, J. D., Chen, C., Isom, L. L., & Raman, I. M. 2005. Open-channel block by the cytoplasmic tail of sodium channel *beta4* as a mechanism for resurgent sodium current. *Neuron*, **45**(2), 233–244.
- [Grieco *et al.* , 2002] Grieco, Tina M, Afshari, Fatemeh S, & Raman, Indira M. 2002. A role for phosphorylation in the maintenance of resurgent sodium current in cerebellar purkinje neurons. *J Neurosci*, **22**(8), 3100–3107.
- [Gu *et al.* , 2007] Gu, N., Vervaeke, K., & Storm, J. F. 2007. BK potassium channels facilitate high-frequency firing and cause early spike frequency adaptation in rat CA1 hippocampal pyramidal cells. *J Physiol*, **580**(Pt.3), 859–882.

- [Gulyás *et al.*, 1999] Gulyás, A. I., Megias, M., Emri, Z., & Freund, T. F. 1999. Total number and ratio of excitatory and inhibitory synapses converging onto single interneurons of different types in the CA1 area of the rat hippocampus. *J Neurosci*, **19**(22), 10082–10097.
- [Gustafson *et al.*, 1993] Gustafson, T. A., Clevinger, E. C., O'Neill, T. J., Yarowsky, P. J., & Krueger, B. K. 1993. Mutually exclusive exon splicing of type III brain sodium channel alpha subunit RNA generates developmentally regulated isoforms in rat brain. *J Biol Chem*, **268**(25), 18648–18653.
- [Guy & Seetharamulu, 1986] Guy, H. R., & Seetharamulu, H. R. 1986. Molecular model of the action potential sodium channel. *Proc Natl Acad Sci U.S.A.*, **83**(2), 508–512.
- [Hamlyn, 1962] Hamlyn, L. H. 1962. The fine structure of the mossy fibre endings in the hippocampus of the rabbit. *J Anat*, **96**(Jan), 112–120.
- [Harris & Cotman, 1986] Harris, E. W., & Cotman, C. W. 1986. Long-term potentiation of guinea pig mossy fiber responses is not blocked by N-methyl D-aspartate antagonists. *Neurosci Lett*, **70**(1), 132–137.
- [Hartmann *et al.*, 1999] Hartmann, H. A., Colom, L. V., Sutherland, M. L., & Noebels, J. L. 1999. Selective localization of cardiac *Scn5a* sodium channels in limbic regions of rat brain. *Nat Neurosci*, **2**(7), 593–595.
- [Haug *et al.*, 2001] Haug, K., Hallmann, K., Rebstock, J., Dullinger, J., Muth, S., Haverkamp, F., Pfeiffer, H., Rau, B., Elger, C. E., Propping, P., & Heils, A. 2001. The voltage-gated sodium channel gene *Scn2a* and idiopathic generalized epilepsy. *Epilepsy res*, **47**(3), 243–246.
- [Heinzen *et al.*, 2007] Heinzen, Erin L, Yoon, Woohyun, Weale, Michael E, Sen, Arjune, Wood, Nicholas W, Burke, James R, Welsh-Bohmer, Kathleen A, Hulette, Christine M, Sisodiya, Sanjay M, & Goldstein, David B. 2007. Alternative ion channel splicing in mesial temporal lobe epilepsy and Alzheimer's disease. *Genome Biol*, **8**(3), R32.
- [Heron *et al.*, 2002] Heron, Sarah E, Crossland, Kathryn M, Andermann, Eva, Phillips, Hilary A, Hall, Allison J, Bleasel, Andrew, Shevell, Michael, Mercho, Suha, Seni, Marie-Helene, Guiot, Marie-Christine, Mulley, John C, Berkovic, Samuel F, & Scheffer, Ingrid E. 2002. Sodium-channel defects in benign familial neonatal-infantile seizures. *Lancet*, **360**(9336), 851–852.
- [Herzog *et al.*, 2003] Herzog, Raimund I, Liu, Chuanju, Waxman, Stephen G, & Cummins, Theodore R. 2003. Calmodulin binds to the c terminus of sodium channels Nav1.4 and Nav1.6 and differentially modulates their functional properties. *J Neurosci*, **23**(23), 8261–8270.
- [Hesdorffer *et al.*, 1998] Hesdorffer, D. C., Logroscino, G., Cascino, G., Annegers, J. F., & Hauser, W. A. 1998. Risk of unprovoked seizure after acute symptomatic seizure: effect of status epilepticus. *Ann Neurol*, **44**(6), 908–912.
- [Hille, 2001] Hille, B. 2001. *Ion channels of excitable membranes*. 3rd edition. *Sinauer Associates*.
- [Hodgkin & Huxley, 1952] Hodgkin, A. L., & Huxley, A. F. 1952. A quantitative description of membrane current and its application to conduction and excitation in nerve. *J Physiol*, **117**(4), 500–544.
- [Holland *et al.*, 2008] Holland, Katherine D, Kearney, Jennifer A, Glauser, Tracy A, Buck, Gerri, Keddache, Mehdi, Blankston, John R, Glaaser, Ian W, Kass, Robert S, & Meisler, Miriam H. 2008. Mutation of sodium channel *Scn3a* in a patient with cryptogenic pediatric partial epilepsy. *Neurosci Lett*, **433**(1), 65–70.
- [Hossain *et al.*, 2005] Hossain, Waheeda A, Antic, Srdjan D, Yang, Yang, Rasband, Matthew N, & Morest, D. Kent. 2005. Where is the spike generator of the cochlear nerve? Voltage-gated sodium channels in the mouse cochlea. *J Neurosci*, **25**(29), 6857–6868.
- [Hu *et al.*, 2007] Hu, H., Vervaeke, K., & Storm, J. F. 2007. M-channels (K_v7/KCNQ channels) that regulate synaptic integration, excitability, and spike pattern of CA1 pyramidal cells are located in the perisomatic region. *J Neurosci*, **27**(8), 1853–1867.
- [Huang & Moczydlowski, 2001] Huang, C. J., & Moczydlowski, E. 2001. Cytoplasmic polyamines as permeant blockers and modulators of the voltage-gated sodium channel. *Biophys J*, **80**(3), 1262–1279.

- [Inda *et al.*, 2006] Inda, Maria Carmen, DeFelipe, Javier, & Muñoz, Alberto. 2006. Voltage-gated ion channels in the axon initial segment of human cortical pyramidal cells and their relationship with chandelier cells. *Proc Natl Acad Sci U.S.A.*, **103**(8), 2920–2925.
- [Isom, 2001] Isom, L. L. 2001. Sodium channel beta subunits: anything but auxiliary. *Neuroscientist*, **7**(1), 42–54.
- [Isom *et al.*, 1995] Isom, L. L., Scheuer, T., Brownstein, A. B., Ragsdale, D. S., Murphy, B. J., & Catterall, W. A. 1995. Functional co-expression of the beta 1 and type IIa alpha subunits of sodium channels in a mammalian cell line. *J Biol Chem*, **270**(7), 3306–3312.
- [Isom, 2002] Isom, Lori L. 2002. Beta subunits: players in neuronal hyperexcitability? *Novartis Found Symp*, **241**, 124–38; discussion 138–43, 226–32.
- [Jenkins & Bennett, 2001] Jenkins, S. M., & Bennett, V. 2001. Ankyrin-G coordinates assembly of the spectrin-based membrane skeleton, voltage-gated sodium channels, and L1 CAMs at purkinje neuron initial segments. *J Cell Biol*, **155**(5), 739–746.
- [Jensen *et al.*, 1994] Jensen, M. S., Azouz, R., & Yaari, Y. 1994. Variant firing patterns in rat hippocampal pyramidal cells modulated by extracellular potassium. *J Neurophysiol*, **71**(3), 831–839.
- [Jensen *et al.*, 1996] Jensen, M. S., Azouz, R., & Yaari, Y. 1996. Spike after-depolarization and burst generation in adult rat hippocampal CA1 pyramidal cells. *J physiol*, **492**(Pt 1), 199–210.
- [Johnston & Amaral, 2003] Johnston, D., & Amaral, D. G. 2003. The synaptic organization of the brain. 5th edition. *Oxford University Press*.
- [Jung *et al.*, 2007] Jung, Sangwook, Jones, Terrance D, Lugo, Joaquin N, Sheerin, Aaron H, Miller, John W, D'Ambrosio, Raimondo, Anderson, Anne E, & Poolos, Nicholas P. 2007. Progressive dendritic HCN channelopathy during epileptogenesis in the rat pilocarpine model of epilepsy. *J Neurosci*, **27**(47), 13012–13021.
- [Kado & Baud, 1981] Kado, R. T., & Baud, C. 1981. The rise and fall of electrical excitability in the oocyte of *Xenopus laevis*. *J Physiol (paris)*, **77**(9), 1113–1117.
- [Kamiya *et al.*, 2004] Kamiya, Kazusaku, Kaneda, Makoto, Sugawara, Takashi, Mazaki, Emi, Okamura, Nami, Montal, Mauricio, Makita, Naomasa, Tanaka, Masaki, Fukushima, Katsuyuki, Fujiwara, Tateki, Inoue, Yushi, & Yamakawa, Kazuhiro. 2004. A nonsense mutation of the sodium channel gene *Scn2a* in a patient with intractable epilepsy and mental decline. *J Neurosci*, **24**(11), 2690–2698.
- [Kandel & Spencer, 1961] Kandel, E. R., & Spencer, W. A. 1961. Electrophysiology of hippocampal neurons. II. after-potentials and repetitive firing. *J Neurophysiol*, **24**(May), 243–259.
- [Kandel *et al.*, 1961] Kandel, E. R., W. A. Spencer, W. A., & Brinley, F. J. 1961. Electrophysiology of hippocampal neurons. I. sequential invasion and synaptic organization. *J Neurophysiol*, **24**(May), 225–242.
- [Kazen-Gillespie *et al.*, 2000] Kazen-Gillespie, K. A., Ragsdale, D. S., D'Andrea, M. R., Mattei, L. N., Rogers, K. E., & Isom, L. L. 2000. Cloning, localization, and functional expression of sodium channel beta1a subunits. *J Biol Chem*, **275**(2), 1079–1088.
- [Kemppainen *et al.*, 2002] Kemppainen, Samuli, Jolkkonen, Esa, & Pitkänen, Asla. 2002. Projections from the posterior cortical nucleus of the amygdala to the hippocampal formation and parahippocampal region in rat. *Hippocampus*, **12**(6), 735–755.
- [Kerr *et al.*, 2004] Kerr, Niall C H, Holmes, Fiona E, & Wynn, David. 2004. Novel isoforms of the sodium channels Na_v1.8 and Na_v1.5 are produced by a conserved mechanism in mouse and rat. *J Biol Chem*, **279**(23), 24826–24833.
- [Ketelaars *et al.*, 2001] Ketelaars, S. O., Gorter, J. A., van Vliet, E. A., da Silva, F. H. Lopes, & Wadman, W. J. 2001. Sodium currents in isolated rat CA1 pyramidal and dentate granule neurons in the post-status epilepticus model of epilepsy. *Neuroscience*, **105**(1), 109–120.
- [Khaliq & Raman, 2005] Khaliq, Zayd M, & Raman, Indira M. 2005. Axonal propagation of simple and complex spikes in cerebellar purkinje neurons. *J Neurosci*, **25**(2), 454–463.

- [Khaliq & Raman, 2006] Khaliq, Zayd M, & Raman, Indira M. 2006. Relative contributions of axonal and somatic Na channels to action potential initiation in cerebellar purkinje neurons. *J Neurosci*, **26**(7), 1935–1944.
- [Khaliq *et al.* , 2003] Khaliq, Zayd M, Gouwens, Nathan W, & Raman, Indira M. 2003. The contribution of resurgent sodium current to high-frequency firing in purkinje neurons: an experimental and modeling study. *J Neurosci*, **23**(12), 4899–4912.
- [Köhling, 2002] Köhling, Rüdiger. 2002. Voltage-gated sodium channels in epilepsy. *Epilepsia*, **43**(11), 1278–1295.
- [Kim *et al.* , 2007] Kim, Doo Yeon, Carey, Bryce W, Wang, Haibin, Ingano, Laura A M, Binshtok, Alexander M, Wertz, Mary H, Pettingell, Warren H, He, Ping, Lee, Virginia M-Y, Woolf, Clifford J, & Kovacs, Dora M. 2007. BACE1 regulates voltage-gated sodium channels and neuronal activity. *Nat Cell Biol*, **9**(7), 755–764.
- [Kirschstein *et al.* , 2007] Kirschstein, T., Bauer, M., Muller, L., Ruschenschmidt, C., Reitze, M., Becker, A. J., Schoch, S., & Beck, H. 2007. Loss of metabotropic glutamate receptor-dependent long-term depression via downregulation of mGLUR5 after status epilepticus. *J Neurosci*, **27**(29), 7696–7704.
- [Kohrman *et al.* , 1996] Kohrman, D. C., Harris, J. B., & Meisler, M. H. 1996. Mutation detection in the med and medj alleles of the sodium channel *Scn8a*. unusual splicing due to a minor class AT-AC intron. *J Biol Chem*, **271**(29), 17576–17581.
- [Kole *et al.* , 2007] Kole, M. H., Letzkus, J. J., & Stuart, G. J. 2007. Axon initial segment K_v1 channels control axonal action potential waveform and synaptic efficacy. *Neuron*, **55**(4), 633–647.
- [Kole *et al.* , 2008] Kole, Maarten H P, Ilschner, Susanne U, Kampa, Björn M, Williams, Stephen R, Ruben, Peter C, & Stuart, Greg J. 2008. Action potential generation requires a high sodium channel density in the axon initial segment. *Nat Neurosci*, **11**(2), 178–186.
- [Koticha *et al.* , 2006] Koticha, D., Maurel, P., Zanazzi, G., Kane-Goldsmith, N., Basak, S., Babiarz, J., Salzer, J., & Grumet, M. 2006. Neurofascin interactions play a critical role in clustering sodium channels, Ankyrin G and beta IV spectrin at peripheral nodes of ranvier. *Dev Biol*, **293**(1), 1–12.
- [Krauss *et al.* , 2007] Krauss, M., Weiss, T., Langnaese, K., Richter, K., Kowski, A., Veh, R. W., & Laube, G. 2007. Cellular and subcellular rat brain spermidine synthase expression patterns suggest region-specific roles for polyamines, including cerebellar pre-synaptic function. *J Neurochem*, **103**(2), 679–693.
- [Krettek & Price, 1977] Krettek, J. E., & Price, J. L. 1977. The cortical projections of the mediadorsal nucleus and adjacent thalamic nuclei in the rat. *J Comp Neurol*, **171**(2), 157–191.
- [Lancaster & Adams, 1986] Lancaster, B., & Adams, P. R. 1986. Calcium-dependent current generating the afterhyperpolarization of hippocampal neurons. *J Neurophysiol*, **55**(6), 1268–1282.
- [Lancaster & Nicoll, 1987] Lancaster, B., & Nicoll, R. A. 1987. Properties of two calcium-activated hyperpolarizations in rat hippocampal neurones. *J Physiol*, **389**(Aug), 187–203.
- [Laschet *et al.* , 1992] Laschet, J., Trottier, S., Grisar, T., & Leviel, V. 1992. Polyamine metabolism in epileptic cortex. *Epilepsy Res*, **12**(2), 151–156.
- [Laschet *et al.* , 1999] Laschet, J., Trottier, S., Leviel, V., Guibert, B., Bansard, J. Y., Chauvel, P., & Bureau, M. 1999. Heterogeneous distribution of polyamines in temporal lobe epilepsy. *Epilepsy Res*, **35**(2), 161–172.
- [Laube & Veh, 1997] Laube, G., & Veh, R. W. 1997. Astrocytes, not neurons, show most prominent staining for spermidine/spermine-like immunoreactivity in adult rat brain. *Glia*, **19**(2), 171–179.
- [Laube *et al.* , 2002] Laube, Gregor, Bernstein, Hans-Gert, Wolf, Gerald, & Veh, Rüdiger W. 2002. Differential distribution of spermidine/spermine-like immunoreactivity in neurons of the adult rat brain. *J Comp Neurol*, **444**(4), 369–386.
- [Lee *et al.* , 1993] Lee, L. G., Connell, C. R., & Bloch, W. 1993. Allelic discrimination by nick-translation PCR with fluorogenic probes. *Nucleic Acids Res*, **21**(16), 3761–3766.

- [Levin *et al.*, 2006] Levin, Stephen I, Khaliq, Zayd M, Aman, Teresa K, Grieco, Tina M, Kearney, Jennifer A, Raman, Indira M, & Meisler, Miriam H. 2006. Impaired motor function in mice with cell-specific knockout of sodium channel *Scn8a* (Na_v1.6) in cerebellar purkinje neurons and granule cells. *J Neurophysiol*, **96**(2), 785–793.
- [Lorente de No, 1934] Lorente de No, R. 1934. Studies on the structure of the cerebral cortex. II. continuation of the study of the ammonic system. *J Psychol Neurol*, **46**, 225–242.
- [Lorincz & Nusser, 2008] Lorincz, Andrea, & Nusser, Zoltan. 2008. Cell-type-dependent molecular composition of the axon initial segment. *J Neurosci*, **28**(53), 14329–14340.
- [Lossin *et al.*, 2002] Lossin, Christoph, Wang, Dao W, Rhodes, Thomas H, Vanoye, Carlos G, & George, Alfred L. 2002. Molecular basis of an inherited epilepsy. *Neuron*, **34**(6), 877–884.
- [Lossin *et al.*, 2003] Lossin, Christoph, Rhodes, Thomas H, Desai, Reshma R, Vanoye, Carlos G, Wang, Dao, Carniciu, Sanda, Devinsky, Orrin, & George, Alfred L. 2003. Epilepsy-associated dysfunction in the voltage-gated neuronal sodium channel *Scn1a*. *J Neurosci*, **23**(36), 11289–11295.
- [Ma *et al.*, 1997] Ma, J. Y., Catterall, W. A., & Scheuer, T. 1997. Persistent sodium currents through brain sodium channels induced by g protein betagamma subunits. *Neuron*, **19**(2), 443–452.
- [Madison & Nicoll, 1984] Madison, D. V., & Nicoll, R. A. 1984. Control of the repetitive discharge of rat CA 1 pyramidal neurones in vitro. *J Physiol*, **354**(Sep), 319–331.
- [Magee & Carruth, 1999] Magee, J. C., & Carruth, M. 1999. Dendritic voltage-gated ion channels regulate the action potential firing mode of hippocampal CA1 pyramidal neurons. *J Neurophysiol*, **82**(4), 1895–1901.
- [Magistretti & Alonso, 1999] Magistretti, J., & Alonso, A. 1999. Biophysical properties and slow voltage-dependent inactivation of a sustained sodium current in entorhinal cortex layer-II principal neurons: a whole-cell and single-channel study. *J Gen Physiol*, **114**(4), 491–509.
- [Magistretti *et al.*, 1999] Magistretti, J., Ragsdale, D. S., & Alonso, A. 1999. High conductance sustained single-channel activity responsible for the low-threshold persistent Na⁺ current in entorhinal cortex neurons. *J Neurosci*, **19**(17), 7334–7341.
- [Magloczky & Freund, 2005] Magloczky, Z., & Freund, T. F. 2005. Impaired and repaired inhibitory circuits in the epileptic human hippocampus. *Trends Neurosci*, **28**(6), 334–340.
- [Malenka & Bear, 2004] Malenka, R. C., & Bear, M. F. 2004. LTP and LTD: an embarrassment of riches. *Neuron*, **44**(1), 5–21.
- [Malik-Hall *et al.*, 2003] Malik-Hall, Misbah, Poon, W-Y. Louisa, Baker, Mark D, Wood, John N, & Okuse, Kenji. 2003. Sensory neuron proteins interact with the intracellular domains of sodium channel Na_v1.8. *Brain Res Mol Brain Res*, **110**(2), 298–304.
- [Marcelin *et al.*, 2008] Marcelin, Béatrice, Chauvière, Laëtitia, Becker, Albert, Migliore, Michele, Esclapez, Monique, & Bernard, Christophe. 2008. H channel-dependent deficit of theta oscillation resonance and phase shift in temporal lobe epilepsy. *Neurobiol Dis*.
- [Marrion & Tavalin, 1998] Marrion, N. V., & Tavalin, S. J. 1998. Selective activation of Ca²⁺-activated K⁺ channels by co-localized Ca²⁺ channels in hippocampal neurons. *Nature*, **395**(6705), 900–905.
- [Martin *et al.*, 2007] Martin, Melinda S, Tang, Bin, Papale, Ligia A, Yu, Frank H, Catterall, William A, & Escayg, Andrew. 2007. The voltage-gated sodium channel *Scn8a* is a genetic modifier of severe myoclonic epilepsy of infancy. *Hum mol genet*, **16**(23), 2892–2899.
- [Martin & Morris, 2002] Martin, S. J., & Morris, R. G M. 2002. New life in an old idea: the synaptic plasticity and memory hypothesis revisited. *Hippocampus*, **12**(5), 609–636.
- [Masukawa *et al.*, 1982] Masukawa, L. M., Benardo, L. S., & Prince, D. A. 1982. Variations in electrophysiological properties of hippocampal neurons in different subfields. *Brain Res*, **242**(2), 341–344.

- [Matthews *et al.*, 2008] Matthews, Elizabeth A, Weible, Aldis P, Shah, Samit, & Disterhoft, John F. 2008. The BK-mediated fAHP is modulated by learning a hippocampus-dependent task. *Proc Natl Acad Sci U.S.A.*, **105**(39), 15154–15159.
- [Maurice *et al.*, 2001] Maurice, N., Tkatch, T., Meisler, M., Sprunger, L. K., & Surmeier, D. J. 2001. D1/D5 dopamine receptor activation differentially modulates rapidly inactivating and persistent sodium currents in prefrontal cortex pyramidal neurons. *J Neurosci*, **21**(7), 2268–2277.
- [McCormick *et al.*, 2007] McCormick, D. A., Shu, Y., & Yu, Y. 2007. Neurophysiology: Hodgkin and Huxley model—still standing? *Nature*, **445**(7123), E1–2; discussion E2–3.
- [Meadows *et al.*, 2002] Meadows, L. S., Malhotra, J., Loukas, A., Thyagarajan, V., Kazen-Gillespie, K. A., Koopman, M. C., Kriegler, S., Isom, L. L., & Ragsdale, D. S. 2002. Functional and biochemical analysis of a sodium channel beta1 subunit mutation responsible for generalized epilepsy with febrile seizures plus type 1. *J Neurosci*, **22**(24), 10699–10709.
- [Meeks & Mennerick, 2007] Meeks, J. P., & Mennerick, S. 2007. Action potential initiation and propagation in CA3 pyramidal axons. *J Neurophysiol*, **97**(5), 3460–3472.
- [Megías *et al.*, 2001] Megías, M., Emri, Z., Freund, T. F., & Gulyás, A. I. 2001. Total number and distribution of inhibitory and excitatory synapses on hippocampal CA1 pyramidal cells. *Neuroscience*, **102**(3), 527–540.
- [Meisler & Kearney, 2005] Meisler, Miriam H, & Kearney, Jennifer A. 2005. Sodium channel mutations in epilepsy and other neurological disorders. *J Clin Invest*, **115**(8), 2010–2017.
- [Mercer *et al.*, 2007] Mercer, Jeff N, Chan, C. Savio, Tkatch, Tatiana, Held, Joshua, & Surmeier, D. James. 2007. Na_v1.6 sodium channels are critical to pacemaking and fast spiking in globus pallidus neurons. *J Neurosci*, **27**(49), 13552–13566.
- [Metz *et al.*, 2005] Metz, A. E., Jarsky, T., Martina, M., & Spruston, N. 2005. R-type calcium channels contribute to afterdepolarization and bursting in hippocampal CA1 pyramidal neurons. *J Neurosci*, **25**(24), 5763–5773.
- [Metz *et al.*, 2007] Metz, A. E., Spruston, N., & Martina, M. 2007. Dendritic D-type potassium currents inhibit the spike afterdepolarization in rat hippocampal CA1 pyramidal neurons. *J Physiol*, **581**(Pt 1), 175–187.
- [Mittmann *et al.*, 1997] Mittmann, T., Linton, S. M., Schwandt, P., & Crill, W. 1997. Evidence for persistent Na⁺ current in apical dendrites of rat neocortical neurons from imaging of Na⁺-sensitive dye. *J neurophysiol*, **78**(2), 1188–1192.
- [Moulard *et al.*, 1999] Moulard, B., Guipponi, M., Chaigne, D., Mouthon, D., Buresi, C., & Malafosse, A. 1999. Identification of a new locus for generalized epilepsy with febrile seizures plus (GEFS+) on chromosome 2q24–q33. *Am J Hum Genet*, **65**(5), 1396–1400.
- [Naundorf *et al.*, 2006] Naundorf, Björn, Wolf, Fred, & Volgushev, Maxim. 2006. Unique features of action potential initiation in cortical neurons. *Nature*, **440**(7087), 1060–1063.
- [Neves *et al.*, 2008] Neves, Guilherme, Cooke, Sam F, & Bliss, Tim V P. 2008. Synaptic plasticity, memory and the hippocampus: a neural network approach to causality. *Nat Rev Neurosci*, **9**(1), 65–75.
- [Noda *et al.*, 1986] Noda, M., Ikeda, T., Suzuki, H., Takeshima, H., Takahashi, T., Kuno, M., & Numa, S. 1986. Expression of functional sodium channels from cloned cDNA. *Nature*, **322**(6082), 826–828.
- [Ogiwara *et al.*, 2007] Ogiwara, I., Miyamoto, H., Morita, N., Atapour, N., Mazaki, E., Inoue, I., Takeuchi, T., Itohara, S., Yanagawa, Y., Obata, K., Furuichi, T., Hensch, T. K., & Yamakawa, K. 2007. Na(v)1.1 localizes to axons of parvalbumin-positive inhibitory interneurons: a circuit basis for epileptic seizures in mice carrying an *Scn1a* gene mutation. *J Neurosci*, **27**(22), 5903–5914.
- [O’Keefe & Dostrovsky, 1971] O’Keefe, J., & Dostrovsky, J. 1971. The hippocampus as a spatial map. preliminary evidence from unit activity in the freely-moving rat. *Brain Res*, **34**(1), 171–175.
- [Otto *et al.*, 2006] Otto, James F, Yang, Yan, Frankel, Wayne N, White, H. Steve, & Wilcox, Karen S. 2006. A spontaneous mutation involving *KCNQ2* (K_v7.2) reduces m-current density and spike frequency adaptation in mouse CA1 neurons. *J Neurosci*, **26**(7), 2053–2059.

- [Palmer & Stuart, 2006] Palmer, L. M., & Stuart, G. J. 2006. Site of action potential initiation in layer 5 pyramidal neurons. *J Neurosci*, **26**(6), 1854–1863.
- [Pan *et al.* , 2006] Pan, Z., Kao, T., Horvath, Z., Lemos, J., Sul, J. Y., Cranstoun, S. D., Bennett, V., Scherer, S. S., & Cooper, E. C. 2006. A common Ankyrin-G-based mechanism retains KCNQ and Na_v channels at electrically active domains of the axon. *J Neurosci*, **26**(10), 2599–2613.
- [Perkins, 2006] Perkins, Katherine L. 2006. Cell-attached voltage-clamp and current-clamp recording and stimulation techniques in brain slices. *J Neurosci Methods*, **154**(1-2), 1–18.
- [Peters *et al.* , 2005] Peters, H. C., Hu, H., Pongs, O., Storm, J. F., & Isbrandt, D. 2005. Conditional transgenic suppression of M channels in mouse brain reveals functions in neuronal excitability, resonance and behavior. *Nat Neurosci*, **8**(1), 51–60.
- [Plummer *et al.* , 1997] Plummer, N. W., McBurney, M. W., & Meisler, M. H. 1997. Alternative splicing of the sodium channel *Scn8a* predicts a truncated two-domain protein in fetal brain and non-neuronal cells. *J Biol Chem*, **272**(38), 24008–24015.
- [Pyapali *et al.* , 1998] Pyapali, G. K., Sik, A., Penttonen, M., Buzsaki, G., & Turner, D. A. 1998. Dendritic properties of hippocampal CA1 pyramidal neurons in the rat: intracellular staining *in vivo* and *in vitro*. *J Comp Neurol*, **391**(3), 335–352.
- [Qin *et al.* , 2003] Qin, Ning, D'Andrea, Michael R, Lubin, Mary-Lou, Shafae, Navid, Codd, Ellen E, & Correa, Ana M. 2003. Molecular cloning and functional expression of the human sodium channel beta1b subunit, a novel splicing variant of the beta1 subunit. *Eur J Biochem*, **270**(23), 4762–4770.
- [Qu *et al.* , 2001] Qu, Y., Curtis, R., Lawson, D., Gilbride, K., Ge, P., DiStefano, P. S., Silos-Santiago, I., Catterall, W. A., & Scheuer, T. 2001. Differential modulation of sodium channel gating and persistent sodium currents by the beta1, beta2, and beta3 subunits. *Mol cell neurosci*, **18**(5), 570–580.
- [Raman & Bean, 1997] Raman, I. M., & Bean, B. P. 1997. Resurgent sodium current and action potential formation in dissociated cerebellar purkinje neurons. *J Neurosci*, **17**(12), 4517–4526.
- [Raman *et al.* , 1997] Raman, I. M., Sprunger, L. K., Meisler, M. H., & Bean, B. P. 1997. Altered subthreshold sodium currents and disrupted firing patterns in purkinje neurons of *Scn8a* mutant mice. *Neuron*, **19**(4), 881–891.
- [Ramon y Cajal, 1893] Ramon y Cajal, S. 1893. Estructura del asta de Ammon y fascia dentata. *Ann Soc Esp Hist Nat*, **22**.
- [Ratcliffe *et al.* , 2000] Ratcliffe, C. F., Qu, Y., McCormick, K. A., Tibbs, V. C., Dixon, J. E., Scheuer, T., & Catterall, W. A. 2000. A sodium channel signaling complex: modulation by associated receptor protein tyrosine phosphatase beta. *Nat Neurosci*, **3**(5), 437–444.
- [Ratcliffe *et al.* , 2001] Ratcliffe, C. F., Westenbroek, R. E., Curtis, R., & Catterall, W. A. 2001. Sodium channel beta1 and beta3 subunits associate with neurofascin through their extracellular immunoglobulin-like domain. *J Cell Biol*, **154**(2), 427–434.
- [Reckziegel *et al.* , 1999] Reckziegel, G., Beck, H., Schramm, J., Urban, B. W., & Elger, C. E. 1999. Carbamazepine effects on Na⁺ currents in human dentate granule cells from epileptogenic tissue. *Epilepsia*, **40**(4), 401–407.
- [Regesta & Tanganelli, 1999] Regesta, G., & Tanganelli, P. 1999. Clinical aspects and biological bases of drug-resistant epilepsies. *Epilepsy res*, **34**(2-3), 109–122.
- [Rempel-Clower *et al.* , 1996] Rempel-Clower, N. L., Zola, S. M., Squire, L. R., & Amaral, D. G. 1996. Three cases of enduring memory impairment after bilateral damage limited to the hippocampal formation. *J Neurosci*, **16**(16), 5233–5255.
- [Remy *et al.* , 2003] Remy, Stefan, Urban, Bernd W, Elger, Christian E, & Beck, Heinz. 2003. Anticonvulsant pharmacology of voltage-gated Na⁺ channels in hippocampal neurons of control and chronically epileptic rats. *Eur J Neurosci*, **17**(12), 2648–2658.
- [Rhodes *et al.* , 2004] Rhodes, Thomas H, Lossin, Christoph, Vanoye, Carlos G, Wang, Dao W, & George, Alfred L. 2004. Noninactivating voltage-gated sodium channels in severe myoclonic epilepsy of infancy. *Proc Natl Acad Sci U.S.A.*, **101**(30), 11147–11152.

- [Royeck *et al.*, 2008] Royeck, Michel, Horstmann, Marie-Therese, Remy, Stefan, Reitze, Margit, Yaari, Yoel, & Beck, Heinz. 2008. Role of axonal Na_v1.6 sodium channels in action potential initiation of CA1 pyramidal neurons. *J Neurophysiol*, **100**(4), 2361–2380.
- [Rush *et al.*, 2005] Rush, A. M., Dib-Hajj, S. D., & Waxman, S. G. 2005. Electrophysiological properties of two axonal sodium channels, Na_v1.2 and Na_v1.6, expressed in mouse spinal sensory neurones. *J Physiol*, **564**(Pt 3), 803–815.
- [Salin *et al.*, 1996] Salin, P. A., Scanziani, M., Malenka, R. C., & Nicoll, R. A. 1996. Distinct short-term plasticity at two excitatory synapses in the hippocampus. *Proc Natl Acad Sci U.S.A.*, **93**(23), 13304–13309.
- [Sanabria *et al.*, 2001] Sanabria, E. R., Su, H., & Yaari, Y. 2001. Initiation of network bursts by Ca²⁺-dependent intrinsic bursting in the rat pilocarpine model of temporal lobe epilepsy. *J Physiol*, **532**(Pt 1), 205–216.
- [Sander & Shorvon, 1996] Sander, J. W., & Shorvon, S. D. 1996. Epidemiology of the epilepsies. *J Neurol Neurosurg Psychiatry*, **61**(5), 433–443.
- [Sarao *et al.*, 1991] Sarao, R., Gupta, S. K., Auld, V. J., & Dunn, R. J. 1991. Developmentally regulated alternative RNA splicing of rat brain sodium channel mRNAs. *Nucleic Acids Res*, **19**(20), 5673–5679.
- [Scalmani *et al.*, 2006] Scalmani, Paolo, Rusconi, Raffaella, Armatura, Elena, Zara, Federico, Avanzini, Giuliano, Franceschetti, Silvana, & Mantegazza, Massimo. 2006. Effects in neocortical neurons of mutations of the Na(v)1.2 Na⁺ channel causing benign familial neonatal-infantile seizures. *J Neurosci*, **26**(40), 10100–10109.
- [Schaub *et al.*, 2007] Schaub, C., Uebachs, M., & Beck, H. 2007. Diminished response of CA1 neurons to antiepileptic drugs in chronic epilepsy. *Epilepsia*, **48**(7), 1339–1350.
- [Scheibel *et al.*, 1974] Scheibel, M. E., Crandall, P. H., & Scheibel, A. B. 1974. The hippocampal-dentate complex in temporal lobe epilepsy. a golgi study. *Epilepsia*, **15**(1), 55–80.
- [Scott *et al.*, 1993] Scott, R. H., Sutton, K. G., & Dolphin, A. C. 1993. Interactions of polyamines with neuronal ion channels. *Trends Neurosci*, **16**(4), 153–160.
- [Scoville & Milner, 1957] Scoville, W. B., & Milner, B. 1957. Loss of recent memory after bilateral hippocampal lesions. *J Neurol Neurosurg Psychiatry*, **20**(1), 11–21.
- [Searle, 1962] Searle, A. G. 1962. Provisional 'seal' (med). *Mouse News Lett.*, **27**, 34–5.
- [Shah *et al.*, 2008] Shah, Mala M, Migliore, Michele, Valencia, Ignacio, Cooper, Edward C, & Brown, David A. 2008. Functional significance of axonal K_v7 channels in hippocampal pyramidal neurons. *Proc Natl Acad Sci U.S.A.*, **105**(22), 7869–7874.
- [Shu *et al.*, 2007] Shu, Y., Duque, A., Yu, Y., Haider, B., & McCormick, D. A. 2007. Properties of action-potential initiation in neocortical pyramidal cells: evidence from whole cell axon recordings. *J Neurophysiol*, **97**(1), 746–760.
- [Smith *et al.*, 1998] Smith, M. R., Smith, R. D., Plummer, N. W., Meisler, M. H., & Goldin, A. L. 1998. Functional analysis of the mouse *Scn8a* sodium channel. *J Neurosci*, **18**(16), 6093–6102.
- [Sochivko *et al.*, 2002] Sochivko, D., Pereverzev, A., Smyth, N., Gissel, C., Schneider, T., & Beck, H. 2002. The Ca(v)2.3 Ca(2+) channel subunit contributes to R-type ca(2+) currents in murine hippocampal and neocortical neurones. *J Physiol*, **542**(Pt 3), 699–710.
- [Spampanato *et al.*, 2004] Spampanato, J., Kearney, J. A., de Haan, G., McEwen, D. P., Escayg, A., Aradi, I., MacDonald, B. T., Levin, S. I., Soltesz, I., Benna, P., Montalenti, E., Isom, L. L., Goldin, A. L., & Meisler, M. H. 2004. A novel epilepsy mutation in the sodium channel *Scn1a* identifies a cytoplasmic domain for beta subunit interaction. *J Neurosci*, **24**(44), 10022–10034.
- [Squire *et al.*, 2004] Squire, Larry R, Stark, Craig E L, & Clark, Robert E. 2004. The medial temporal lobe. *Annu Rev Neurosci*, **27**, 279–306.
- [Stühmer *et al.*, 1989] Stühmer, W., Conti, F., Suzuki, H., Wang, X. D., Noda, M., Yahagi, N., Kubo, H., & Numa, S. 1989. Structural parts involved in activation and inactivation of the sodium channel. *Nature*, **339**(6226), 597–603.

- [Storm, 1987a] Storm, J. F. 1987a. Action potential repolarization and a fast after-hyperpolarization in rat hippocampal pyramidal cells. *J Physiol*, **385**(Apr), 733–759.
- [Storm, 1987b] Storm, J. F. 1987b. Intracellular injection of a Ca^{2+} chelator inhibits spike repolarization in hippocampal neurons. *Brain Res*, **435**(1-2), 387–392.
- [Storm, 1989] Storm, J. F. 1989. An after-hyperpolarization of medium duration in rat hippocampal pyramidal cells. *J Physiol*, **409**(Feb), 171–190.
- [Stuart & Häusser, 1994] Stuart, G., & Häusser, M. 1994. Initiation and spread of sodium action potentials in cerebellar purkinje cells. *Neuron*, **13**(3), 703–712.
- [Stuart *et al.*, 1997] Stuart, G., Schiller, J., & Sakmann, B. 1997. Action potential initiation and propagation in rat neocortical pyramidal neurons. *J Physiol*, **505**(Pt 3), 617–632.
- [Stuart & Sakmann, 1994] Stuart, G. J., & Sakmann, B. 1994. Active propagation of somatic action potentials into neocortical pyramidal cell dendrites. *Nature*, **367**(6458), 69–72.
- [Su *et al.*, 2001] Su, H., Alroy, G., Kirson, E. D., & Yaari, Y. 2001. Extracellular calcium modulates persistent sodium current-dependent burst-firing in hippocampal pyramidal neurons. *J Neurosci*, **21**(12), 4173–4182.
- [Su *et al.*, 2002] Su, H., Sochivko, D., Becker, A., Chen, J., Jiang, Y., Yaari, Y., & Beck, H. 2002. Upregulation of a T-type Ca^{2+} channel causes a long-lasting modification of neuronal firing mode after status epilepticus. *J Neurosci*, **22**(9), 3645–3655.
- [Suzuki & Smith, 1985] Suzuki, S. S., & Smith, G. K. 1985. Burst characteristics of hippocampal complex spike cells in the awake rat. *Exp Neurol*, **89**(1), 90–95.
- [Swanson & Cowan, 1977] Swanson, L. W., & Cowan, W. M. 1977. An autoradiographic study of the organization of the efferent connections of the hippocampal formation in the rat. *J Comp Neurol*, **172**(1), 49–84.
- [Swensen & Bean, 2005] Swensen, A. M., & Bean, B. P. 2005. Robustness of burst firing in dissociated purkinje neurons with acute or long-term reductions in sodium conductance. *J Neurosci*, **25**(14), 3509–3520.
- [Tagliatalata *et al.*, 1995] Tagliatalata, M., Ficker, E., Wible, B., & Brown, A. M. 1995. Pharmacological implications of inward rectifier K^+ channels regulation by cytoplasmic polyamines. *Pharmacol Res*, **32**(6), 335–344.
- [Tamamaki *et al.*, 1987] Tamamaki, N., Abe, K., & Nojyo, Y. 1987. Columnar organization in the subiculum formed by axon branches originating from single CA1 pyramidal neurons in the rat hippocampus. *Brain Res*, **412**(1), 156–160.
- [Terlau & Stühmer, 1998] Terlau, H., & Stühmer, W. 1998. Structure and function of voltage-gated ion channels. *Naturwissenschaften*, **85**(9), 437–444.
- [Trudeau *et al.*, 2006] Trudeau, M. M., Dalton, J. C., Day, J. W., Ranum, L. P W., & Meisler, M. H. 2006. Heterozygosity for a protein truncation mutation of sodium channel *Scn8a* in a patient with cerebellar atrophy, ataxia, and mental retardation. *J Med Genet*, **43**(6), 527–530.
- [Turski *et al.*, 1984] Turski, W. A., Cavalheiro, E. A., Bortolotto, Z. A., Mello, L. M., Schwarz, M., & Turski, L. 1984. Seizures produced by pilocarpine in mice: a behavioral, electroencephalographic and morphological analysis. *Brain Res*, **321**(2), 237–253.
- [Vacher *et al.*, 2008] Vacher, Helene, Mohapatra, Durga P., & Trimmer, James S. 2008. Localization and targeting of voltage-dependent ion channels in mammalian central neurons. *Physiol Rev*, **88**(4), 1407–1447.
- [van Groen & Wyss, 1990] van Groen, T., & Wyss, J. M. 1990. Extrinsic projections from area CA1 of the rat hippocampus: olfactory, cortical, subcortical, and bilateral hippocampal formation projections. *J Comp Neurol*, **302**(3), 515–528.
- [Van Wart *et al.*, 2007] Van Wart, A., Trimmer, J. S., & Matthews, G. 2007. Polarized distribution of ion channels within microdomains of the axon initial segment. *J Comp Neurol*, **500**(2), 339–352.
- [Varona *et al.*, 2000] Varona, P., Ibarz, J. M., López-Aguado, L., & Herreras, O. 2000. Macroscopic and subcellular factors shaping population spikes. *J Neurophysiol*, **83**(4), 2192–2208.

- [Vega *et al.*, 2008] Vega, Ana V, Henry, Diane L, & Matthews, Gary. 2008. Reduced expression of Na(v)1.6 sodium channels and compensation by Na(v)1.2 channels in mice heterozygous for a null mutation in *Scn8a*. *Neurosci Lett*, **442**(1), 69–73.
- [Vervaeke *et al.*, 2006a] Vervaeke, K., Hu, H., Graham, L. J., & Storm, J. F. 2006a. Contrasting effects of the persistent Na⁺ current on neuronal excitability and spike timing. *Neuron*, **49**(2), 257–270.
- [Vervaeke *et al.*, 2006b] Vervaeke, K., Gu, N., Agdestein, C., Hu, H., & Storm, J. F. 2006b. Kv7/KCNQ/M-channels in rat glutamatergic hippocampal axons and their role in regulation of excitability and transmitter release. *J Physiol*, **576**(Pt 1), 235–256.
- [Vreugdenhil *et al.*, 1998] Vreugdenhil, M., Faas, G. C., & Wadman, W. J. 1998. Sodium currents in isolated rat CA1 neurons after kindling epileptogenesis. *Neuroscience*, **86**(1), 99–107.
- [Wallace *et al.*, 2003] Wallace, Heather M, Fraser, Alison V, & Hughes, Alun. 2003. A perspective of polyamine metabolism. *Biochem J*, **376**(Pt 1), 1–14.
- [Wallace *et al.*, 1998] Wallace, R. H., Wang, D. W., Singh, R., Scheffer, I. E., George, A. L., Phillips, H. A., Saar, K., Reis, A., Johnson, E. W., Sutherland, G. R., Berkovic, S. F., & Mulley, J. C. 1998. Febrile seizures and generalized epilepsy associated with a mutation in the Na⁺-channel beta1 subunit gene *Scn1b*. *Nat Genet*, **19**(4), 366–370.
- [Wallace *et al.*, 2001] Wallace, R. H., Scheffer, I. E., Barnett, S., Richards, M., Dibbens, L., Desai, R. R., Lerman-Sagie, T., Lev, D., Mazarib, A., Brand, N., Ben-Zeev, B., Goikhman, I., Singh, R., Kremmidiotis, G., Gardner, A., Sutherland, G. R., George, A. L., Mulley, J. C., & Berkovic, S. F. 2001. Neuronal sodium-channel alpha1-subunit mutations in generalized epilepsy with febrile seizures plus. *Am J Hum Genet*, **68**(4), 859–865.
- [Wart & Matthews, 2006a] Wart, Audra Van, & Matthews, Gary. 2006a. Expression of sodium channels Na_v1.2 and Na_v1.6 during postnatal development of the retina. *Neurosci Lett*, **403**(3), 315–317.
- [Wart & Matthews, 2006b] Wart, Audra Van, & Matthews, Gary. 2006b. Impaired firing and cell-specific compensation in neurons lacking Na_v1.6 sodium channels. *J Neurosci*, **26**(27), 7172–7180.
- [Westenbroek *et al.*, 1992] Westenbroek, R. E., Noebels, J. L., & Catterall, W. A. 1992. Elevated expression of type II Na⁺ channels in hypomyelinated axons of shiverer mouse brain. *J Neurosci*, **12**(6), 2259–2267.
- [Whitaker *et al.*, 2001] Whitaker, W. R., Faull, R. L., Waldvogel, H. J., Plumpton, C. J., Emson, P. C., & Clare, J. J. 2001. Comparative distribution of voltage-gated sodium channel proteins in human brain. *Brain Res Mol Brain Res*, **88**(1-2), 37–53.
- [Williams, 1997] Williams, K. 1997. Modulation and block of ion channels: a new biology of polyamines. *Cell Signal*, **9**(1), 1–13.
- [Wilson & McNaughton, 1993] Wilson, M. A., & McNaughton, B. L. 1993. Dynamics of the hippocampal ensemble code for space. *Science*, **261**(5124), 1055–1058.
- [Wollner & Catterall, 1986] Wollner, D. A., & Catterall, W. A. 1986. Localization of sodium channels in axon hillocks and initial segments of retinal ganglion cells. *Proc Natl Acad Sci U.S.A.*, **83**(21), 8424–8428.
- [Wouterlood *et al.*, 1990] Wouterlood, F. G., Saldana, E., & Witter, M. P. 1990. Projection from the nucleus reuniens thalami to the hippocampal region: light and electron microscopic tracing study in the rat with the anterograde tracer phaseolus vulgaris-leucoagglutinin. *J Comp Neurol*, **296**(2), 179–203.
- [Wu *et al.*, 2002] Wu, Ling, Nishiyama, Kazutoshi, Hollyfield, Joe G, & Wang, Qing. 2002. Localization of Na_v1.5 sodium channel protein in the mouse brain. *Neuroreport*, **13**(18), 2547–2551.
- [Xu *et al.*, 2005] Xu, J., Kang, N., Jiang, L., Nedergaard, M., & Kang, J. 2005. Activity-dependent long-term potentiation of intrinsic excitability in hippocampal CA1 pyramidal neurons. *J Neurosci*, **25**(7), 1750–1760.
- [Yaari & Beck, 2002] Yaari, Y., & Beck, H. 2002. "epileptic neurons" in temporal lobe epilepsy. *Brain Pathol*, **12**(2), 234–239.

- [Yaari *et al.*, 2007] Yaari, Y., Yue, C., & Su, H. 2007. Recruitment of apical dendritic T-type Ca^{2+} channels by backpropagating spikes underlies *de novo* intrinsic bursting in hippocampal epileptogenesis. *J Physiol*, **580**(Pt. 2), 435–450.
- [Yu & Catterall, 2003] Yu, F. H., & Catterall, W. A. 2003. Overview of the voltage-gated sodium channel family. *Genome Biol*, **4**(3), 207.
- [Yu *et al.*, 2006] Yu, F. H., Mantegazza, M., Westenbroek, R. E., Robbins, C. A., Kalume, F., Burton, K. A., Spain, W. J., McKnight, G. S., Scheuer, T., & Catterall, W. A. 2006. Reduced sodium current in GABAergic interneurons in a mouse model of severe myoclonic epilepsy in infancy. *Nat Neurosci*, **9**(9), 1142–1149.
- [Yu *et al.*, 2003] Yu, Frank H, Westenbroek, Ruth E, Silos-Santiago, Inmaculada, McCormick, Kimberly A, Lawson, Deborah, Ge, Pei, Ferriera, Holly, Lilly, Jeremiah, DiStefano, Peter S, Catterall, William A, Scheuer, Todd, & Curtis, Rory. 2003. Sodium channel beta4, a new disulfide-linked auxiliary subunit with similarity to beta2. *J Neurosci*, **23**(20), 7577–7585.
- [Yu *et al.*, 2008] Yu, Yuguo, Shu, Yousheng, & McCormick, David A. 2008. Cortical action potential backpropagation explains spike threshold variability and rapid-onset kinetics. *J Neurosci*, **28**(29), 7260–7272.
- [Yue & Yaari, 2004] Yue, C., & Yaari, Y. 2004. *KCNQ/M* channels control spike afterdepolarization and burst generation in hippocampal neurons. *J Neurosci*, **24**(19), 4614–4624.
- [Yue *et al.*, 2005] Yue, C., Remy, S., Su, H., Beck, H., & Yaari, Y. 2005. Proximal persistent Na^+ channels drive spike afterdepolarizations and associated bursting in adult *ca1* pyramidal cells. *J Neurosci*, **25**(42), 9704–9720.
- [Zalutsky & Nicoll, 1990] Zalutsky, R. A., & Nicoll, R. A. 1990. Comparison of two forms of long-term potentiation in single hippocampal neurons. *Science*, **248**(4963), 1619–1624.
- [Zhang & McBain, 1995] Zhang, L., & McBain, C. J. 1995. Potassium conductances underlying repolarization and after-hyperpolarization in rat CA1 hippocampal interneurons. *J physiol*, **488** (Pt 3)(Nov), 661–672.
- [Zhang & Linden, 2003] Zhang, W., & Linden, D. J. 2003. The other side of the engram: experience-driven changes in neuronal intrinsic excitability. *Nat Rev Neurosci*, **4**(11), 885–900.

6. Contributions

Immunohistochemistry was done together with Margit Reitze. I took the confocal images and performed the quantitative analysis.

Taqman mRNA analysis was done together with Sandra Bauerkämper. I did the analysis of the data.

The computational model was created by Marie-Therese Horstmann and Dr. Heinz Beck. We planned the modelling experiments together. I performed the analysis of the computational data.

Electrophysiological experiments on rats were done in parallel with Dr. Thoralf Opitz. We both contributed equally to the data. I did the analysis of the data.

7. Curriculum vitae

Name: Michael Winfried Royeck
Pseudonym: Michel Royeck
Date of birth: 23.07.1977
Place of birth: Germany, Püttlingen
Birth name: Michael Winfried Bauer

8. Erklärung

Hiermit erkläre ich, dass ich die vorliegende Dissertation selbständig angefertigt habe. Es wurden nur die in der Arbeit ausdrücklich benannten Quellen und Hilfsmittel benutzt. Wörtlich oder sinngemäß übernommenes Gedankengut habe ich als solches kenntlich gemacht.

Ort, Datum

Unterschrift